



UNIVERSIDAD DE INVESTIGACIÓN DE TECNOLOGÍA EXPERIMENTAL YACHAY

Escuela de Ciencias Químicas e Ingeniería

**TÍTULO: Breaking New Grounds in Zinc-Air Battery Research:
Studying the Effects of Innovative Drying Techniques on the
Structural and Electrochemical Properties of
Carboxymethylcellulose-Chitosan-Citric Acid Hydrogels as Next-
Generation Electrolytes.**

Trabajo de integración curricular presentado como requisito para la
obtención del título de Químico

Autor:

María Fernanda Bósquez Cáceres

Tutor:

Juan Pablo Tafur PhD.

Co-Tutor:

Lorena Álvarez Contreras PhD.

Urcuquí, mayo 2023

AUTORÍA

Yo, **María Fernanda Bósquez Cáceres**, con cédula de identidad 0202412151, declaro que las ideas, juicios, valoraciones, interpretaciones, consultas bibliográficas, definiciones y conceptualizaciones expuestas en el presente trabajo; así cómo, los procedimientos y herramientas utilizadas en la investigación, son de absoluta responsabilidad de la autora del trabajo de integración curricular. Así mismo, me acojo a los reglamentos internos de la Universidad de Investigación de Tecnología Experimental Yachay.

Urcuquí, mayo 2023.

María Fernanda Bósquez Cáceres
CI: 0202412151

AUTORIZACIÓN DE PUBLICACIÓN

Yo, **María Fernanda Bósquez Cáceres**, con cédula de identidad 0202412151, cedo a la Universidad de Tecnología Experimental Yachay, los derechos de publicación de la presente obra, sin que deba haber un reconocimiento económico por este concepto. Declaro además que el texto del presente trabajo de titulación no podrá ser cedido a ninguna empresa editorial para su publicación u otros fines, sin contar previamente con la autorización escrita de la Universidad.

Asimismo, autorizo a la Universidad que realice la digitalización y publicación de este trabajo de integración curricular en el repositorio virtual, de conformidad a lo dispuesto en el Art. 144 de la Ley Orgánica de Educación Superior

Urcuquí, mayo 2023.

María Fernanda Bósquez Cáceres
CI: 0202412151

Dedicatoria

A Dios, forjador de mi camino y mi padre celestial, y a la Virgen María, mi madre espiritual, que siempre están conmigo y no me abandonan ante las dificultades. Por otorgarme la sabiduría y fortaleza para continuar por este camino.

A mis padres, que sin ellos nada habría sido posible, por creer en mí, por confiar en mis decisiones y por apoyarme incondicionalmente a perseguir mis sueños.

A mi hermano Miguel, para que en su camino de aprender a vivir sepa que, aunque haya dificultades, dudas y miedos, el atreverse a ir más allá será siempre bien recompensado. Siempre tendrá a su hermana en toda su travesía, sin importar la distancia.

María Fernanda Bósquez Cáceres



Este trabajo fue realizado en la Universidad de Investigación de Tecnología Experimental Yachay, y el Centro de Investigación en Materiales Avanzados S. C. (CIMAV), bajo la dirección del Dr. Juan Pablo Tafur y la Dra. Lorena Álvarez Contreras, con el apoyo financiero del Consejo Mexicano de Ciencia y Tecnología (CONACYT) a través del proyecto Ciencia de Frontera grant#CF-2019-39569, y a CIMAV a través del proyecto interno grant # PI-22-05 y # PI-23-10.

Agradecimientos

Quiero expresar mi más sincera gratitud a Dios y a la Virgen María por brindarme la fortaleza, sabiduría y guía a lo largo de mi trayecto académico y durante toda mi vida. Estoy agradecida por su amor y misericordia que me han sostenido en los momentos difíciles y me han inspirado a buscar la excelencia. También estoy agradecida por las innumerables personas que ha puesto en mi vida para ofrecerme su orientación y asistencia. Sus contribuciones han sido invaluable para mi éxito.

Mi más profundo amor y gratitud a mis padres, quienes han sido mi sistema de apoyo fundamental. Su amor, contención y sacrificios han sido la fuerza impulsora detrás de cada éxito que pueda llegar a tener en mi vida. Siempre han creído en mí, incluso cuando ni yo misma lo hacía, a pesar de que todos les decían que no estaba bien que me fuera lejos de ustedes. Aun así, me han empujado a alcanzar mi máximo potencial. Ni todas las líneas de este trabajo de tesis pueden hacer justicia a todo por lo cual les puedo agradecer. Ni toda mi vida podrá honrarlos como se debe. Gracias mami y daddy, por todo.

Gracias a mi hermanito Miguel, quien ha sido una fuente constante de alegría e inspiración para mí. Estoy verdaderamente agradecida de tenerte en mi vida, porque llegaste a impactar en ella y sacarme de mi zona de confort. Gracias Melito por estar ahí para mí.

Mi gratitud y amor infinito a mi abuelita Choli, por estar siempre pendiente de mi bienestar, necesidades y por toda su comprensión. Gracias por acompañarme todos estos años. Gracias a mi abuelita Angélica, por todo su cariño y apoyo siempre que lo he necesitado. A mi familia (Mel, Fausto, Katy, Daniel, Valentina y Wilger) por el soporte que me han dado durante todo mi proceso, por tratar de entender en lo que he estado trabajando, y todos los años que he tenido que alejarme por ello. Gracias por estar ahí y apoyar mis sueños. Siempre los llevo en mi corazón.

Mi más sincera gratitud y aprecio a mi tutor de investigación, Dr. Juan Pablo Tafur, por su apoyo, confianza, paciencia, orientación y por ser mi mentor a lo largo de toda mi trayectoria de investigación. Su experiencia, conocimiento y acompañamiento han sido fundamentales para darle forma a mi perfil profesional. Gracias por empujarme a dar siempre lo mejor. Le agradezco por haberme dado la confianza de trabajar con usted. Espero no haberlo decepcionado.

Mi eterno agradecimiento a la Dra. Lorena Álvarez Contreras, que creyó en mí, mi trabajo, ideas e investigación desde el primer día. Sin conocerme personalmente me brindó su confianza y hasta el día de hoy recibo su apoyo incondicional. Su enorme compromiso con la excelencia y su gran calidad humana me han desafiado a esforzarme por alcanzar los niveles más altos, me han empujado a lograr mis objetivos y plantearme metas aún más ambiciosas. Espero nunca decepcionarla y continuar aportando positivamente a usted y a Iaredcito, que tiene ganado mi corazón.

Mi cariño y reconocimiento enorme hacia la profesora Vivian Morera, que ha sido un pilar fundamental en el desarrollo de todo mi trabajo y durante mi vida universitaria. Gracias por ser ese hombro en el cual apoyarme, por escucharme y por sus palabras cuando más lo he necesitado. Gracias por sus infinitos consejos y correcciones durante el desarrollo de mis trabajos. Ha sido un honor para mí tenerla como coautora y como amiga.

A los profesores Antonio Diaz y Manuel Caetano, por aceptar ser los jurados de mi tribunal de titulación. Los elegí porque quería honrar de alguna manera el gran impacto que han tenido en mi camino profesional. Gracias por haberme permitido ser su ayudante de investigación y/o cátedra. Las oportunidades que me brindaron me han enriquecido mucho como estudiante y como persona, por lo cual tienen mi cariño y gratitud eterna.

A las profesoras Sandra Hidalgo, Lola De Lima y Rose Mary Michell, por el aporte que tuvieron en mis trabajos como coautoras. Sus ideas, guía y correcciones mejoraron mi trabajo y lo potenciaron magníficamente.

A Guille, Danny, y Zaillmar, por su gran colaboración en cada una de las actividades que realicé en el laboratorio, y su paciencia en permitirme estar todo el tiempo posible en las instalaciones. Igualmente, a los técnicos de la ECFN y ECBI, por facilitarme el acceso a sus respectivos equipos de caracterización.

Para el GIAMP y el NanoMat Lab, porque con sus diversas perspectivas y experiencias han enriquecido la comprensión de mi campo, han puesto en tela de juicio mis suposiciones y me han inspirado para buscar soluciones innovadoras. Gracias por permitirme ser parte de sus grupos de investigación. En especial, muchas gracias al Dr. Eduardo García y la Dra. Anabel De La Cruz, por toda la paciencia, comprensión y dedicación que me brindaron durante la estancia de investigación que aportó enormemente a este trabajo.

Gracias a cada uno de los profesores que he tenido a lo largo de mi carrera por ser tan excelentes profesionales y seres humanos. Todas las enseñanzas que me dieron me hacen ser la profesional que soy hoy, cada uno de ustedes tiene un espacio en mi corazón. A Yachay Tech, mi alma mater, por brindarme las mejores y más bellas experiencias y por reafirmar mi amor por la ciencia y la investigación.

Mi más sincera gratitud y cariño a León, por su inquebrantable apoyo, amor y comprensión a lo largo de todo este tiempo. Tu presencia en mi vida me ha aportado alegría, equilibrio, inspiración, contención y ha hecho que esta etapa sea más satisfactoria y gratificante. Gracias por el ser humano increíble que eres, y por haber sido mi roca durante los altos y bajos que he tenido. Espero haber incidido positivamente en ti.

A las extraordinarias personas que la Universidad me permitió tener en mi vida. A Isabel, mi gran amiga y compañera de investigación, por las incontables horas trabajando juntas, complicidades, amanecidas y hasta lágrimas compartidas en el proceso. Gracias por tu apoyo y comprensión en cada momento, por aceptar el reto que fue este año de trabajo y por no rendirte ni en los momentos más oscuros de nuestro camino. Gracias a Dani y Ana por haber sido mis mejores amigas, confidentes y compañeras de grupo de trabajo durante estos últimos años. Gracias por elegir tenerme en su vida y lidiar con lo complicada que puedo llegar a ser. A Mike y Jean Carlo por estar para mí, brindarme su cariño, compañía y soporte en estos años de amistad. A L.R., por haberme ofrecido su amistad cuando más perdida me encontraba, haber aportado enormemente a que sea la persona que soy hoy y hacer que me dé cuenta de todo el potencial que tengo.

Me gustaría dedicar este último párrafo a agradecerme a mí misma el duro trabajo, la dedicación y la perseverancia que me han llevado a cumplir esta meta. A lo largo de este viaje, me he enfrentado a numerosos retos, dudas y contratiempos, pero nunca me he rendido a pesar de haberlo considerado innumerables veces. Me he esforzado más allá de mis límites, he explorado nuevos campos y he aprendido de mis errores. He crecido como persona, como profesional e investigadora, y estoy orgullosa del trabajo que he realizado. Me doy las gracias a mí misma por la disciplina, la concentración y el compromiso que he demostrado. Sin mi propio trabajo y esfuerzo, esta tesis no habría sido posible. Me dedico estas palabras para que mi yo del futuro, en sus momentos más bajos, tenga un recordatorio de mi propia fuerza, resistencia y potencial.

María Fernanda Bósquez Cáceres

Resumen

En tiempos actuales, los electrolitos basados en materiales poliméricos han generado un gran interés debido a su posible uso como sustitutos de los electrolitos líquidos o en otras aplicaciones de dispositivos de almacenamiento de energía. En concreto, el uso de biopolímeros con un enfoque en la sostenibilidad lleva a una amplia investigación en esta área que todavía tiene mucho trabajo por hacer.

Esta tesis de licenciatura recoge el trabajo incluido en tres artículos publicados en prestigiosas revistas científicas. En ellos se refleja la revisión del estado del arte en el área de electrolitos poliméricos para baterías de zinc y magnesio. Además, se presenta la síntesis y caracterización de nuevos hidrogeles como electrolitos basados en quitosano, carboximetilcelulosa, y distintas concentraciones de entrecruzante químico de ácido cítrico. Posteriormente, se propone una modificación en el proceso de síntesis de los hidrogeles anteriormente realizados, para utilizar estrategias de congelamiento que potencien las propiedades requeridas en las membranas para ser aplicables como electrolitos de baterías zinc-aire.

Los materiales resultantes han demostrado propiedades estructurales y térmicas adecuadas. Además, han obtenido notables valores de conductividad iónica de hasta $0.39 \text{ S}\cdot\text{cm}^{-1}$, y de capacidad de descarga en batería de $1899 \text{ mA}\cdot\text{h g}^{-1}$, sentando un precedente para la próxima generación de biomateriales con aplicaciones energéticas.

Palabras Clave:

Electrolitos poliméricos, biopolímeros, técnicas de entrecruzamiento, baterías zinc-aire.

Abstract

In current times, electrolytes based on polymeric materials have generated great interest due to their possible use as substitutes for liquid electrolytes or in other energy storage device applications. In particular, the use of biopolymers with a focus on sustainability leads to extensive research in this area that still has a lot of work to do.

This thesis collects the work included in three articles published in prestigious scientific journals. They reflect the review of the state-of-the-art in the area of polymer electrolytes for zinc and magnesium batteries. In addition, the synthesis and characterization of new hydrogels as electrolytes based on chitosan, carboxymethylcellulose, and different concentrations of citric acid chemical crosslinker is presented. Subsequently, a modification in the synthesis process of the previously prepared hydrogels is proposed to use freezing strategies that enhance the properties required in the membranes to be applicable as electrolytes for zinc-air batteries.

The resulting materials have demonstrated adequate structural and thermal properties. In addition, they have obtained remarkable ionic conductivity values of up to $0.39 \text{ S}\cdot\text{cm}^{-1}$, and battery discharge capacity of $1899 \text{ mA}\cdot\text{h g}^{-1}$, setting a precedent for the next generation of biomaterials with energy applications.

Key Words:

Polymer electrolytes, biopolymers, crosslinking techniques, zinc-air batteries.

Table of Contents

Chapter 1.....	1
1. Introduction.....	1
1.1. General Introduction	1
1.2. General and Specific Objectives	4
1.2.1. General Objective	4
1.2.2. Specific Objectives	4
Chapter 2.....	5
2. Methodology and Results.....	5
2.1. Article published in the Journal <i>Polymers</i> “Nanocomposite Polymer Electrolytes for Zinc and Magnesium Batteries: From Synthetic to Biopolymers”	5
2.2. Article published in the Journal <i>Batteries</i> “Chitosan-Carboxymethylcellulose Hydrogels as Electrolytes for Zinc–Air Batteries: An Approach to the Transition towards Renewable Energy Storage Devices.”	46
2.3. Article published in the <i>Journal of the Electrochemical Society</i> “Enhancing Electrochemical Performance of Zinc-Air Batteries using Freeze Crosslinked Carboxymethylcellulose-Chitosan Hydrogels as Electrolytes.”	68
3. Conclusions.....	82
4. References.....	85
5. Appendixes	88
5.1. Notifications of acceptance of the articles.	88
5.1.1. Article published in the Journal <i>Polymers</i>	88
5.1.2. Article published in the Journal <i>Batteries</i>	89
5.1.3. Article published in the <i>Journal of the Electrochemical Society</i>	90
5.2. Impact Factors of Publications.....	90

Chapter 1

1. Introduction

1.1. General Introduction

The current efforts of designing new ways to obtain energy from environmentally friendly materials are directly related to the need of designing environmentally friendly devices capable of storing the energy generated. Among these devices, the most widely used in everyday life around the world are batteries. The main problem generated from batteries is that the ones currently used, for example, lithium-ion batteries (LIBs), can suffer thermal runaway, have low energy density, and low cycling efficiency¹⁻³. In addition, they are highly reactive, costly, unsafe, and environmentally polluting⁴⁻⁷.

A key point for the development of environmentally friendly batteries is the physical state of the electrolyte. Currently, batteries use the electrolyte in a liquid state, which presents safety, toxicity, flammability, and leakage problems. In addition, electrode corrosion that occurs at the interfaces and the growth of dendrites on the metal electrode, reduce the capacity and life cycle of the battery⁸⁻¹⁰. Besides, they can cause problems such as preferential nucleation and uneven currents during charging causing fires^{11,12}. Therefore, current battery development strategies focus on the use of solid or gel electrolytes, as a possible replacement for the current aqueous systems.

Among the existing types of electrolytes, polymer electrolytes (PEs) present far-reaching advantages such as high flexibility and good electrochemical performance¹³⁻¹⁵. However, the main problem with these electrolytes is that they present low battery efficiency, insufficient ionic conductivities for practical applications, poor electrochemical stabilities, deficient mechanical resistance, and huge interfacial resistance⁷. These electrolytes must be defined for a specific cathode type. In the present project, zinc is the main focus, since it has key characteristics for battery performance such as high volumetric capacity, and low redox potential^{16,17}. In addition, it possesses some fundamental characteristics for this application area, such as lower reactivity, high abundance, low cost, low toxicity, and intrinsic safety¹⁸⁻²², necessary for the development of sustainable energy storage options. Therefore, the first part of this project focuses on the review of the state-of-the-art of nanocomposite polymer electrolytes (NCPEs) for batteries designed with zinc or magnesium.

Biopolymers are the work's main focus, in order to develop the PEs with nature-friendly raw materials, which can be extracted from plants, microbes, animals, and marine sources, and recognized for their abundant availability. From the biopolymer options, chitosan (CS) and carboxymethylcellulose (CMC) are

herein used as the matrix elements in the synthesis of hydrogel PEs. Chitosan (CS) is a cationic biopolymeric material, known to be good membrane-forming, non-toxic, biodegradable, and biocompatible, which makes it a good solution for various electrochemical applications that can be modified to obtain electrolytes^{23,24}. CS is produced from the deacetylation reaction of chitin, which; is a natural polysaccharide normally found in the exoskeleton of arthropods and various fungi²⁵. CS is widely applied in many fields, such as biotechnology and biomedicine²⁶. Its molecule presents several polar groups, such as hydroxyl and amino groups, which can form complexes with inorganic salts. However, pristine CS has a very low ionic conductivity (10^{-9} S cm⁻¹)²⁷, a fact that is aimed to be enhanced by the combination of another biopolymer and doping with ionic salts.

Carboxymethyl cellulose (CMC) is a water-soluble derivative of cellulose, an anionic polymer, linear polysaccharide of anhydro-glucose. Its composition provides the subsequent structure with high mechanical strength, viscosity, and tunable hydrophilicity²⁸. CMC is widely used in textile, food, paper, drug applications, biomedical and energy production. Both CS and CMC are polysaccharides that have several functional groups, such as amino, hydroxyl, and carboxyl groups. It has been documented that CS and CMC can form an inter macromolecular complex through strong electrostatic and hydrogen bonding interactions between these groups^{29,30}. Hydrogels can be modified through chemical and physical crosslinking techniques. In the case of "chemical" hydrogels, there is evidence of the use of epichlorohydrin (ECH), glutaraldehyde (GA), genipin, and diglycidyl ethers of ethylene glycol or polyethylene glycol³¹⁻³³, as crosslinking agents.

Particularly, citric acid (CA) is an effective chemical crosslinker that forms amide and ester bonds between CMC and CS, leading to a structure with good mechanical stability and porous networks³⁴. Hence, the second part of this work is centered in the synthesis of hydrogels made of CS and CMC with the addition of different amounts of CA, to form a host matrix capable of swell ionic salts. The achieved crosslinking in the membranes provides a superior structural stability, along with a higher thermal stability and enhanced ionic conductivity and current values.

On the other hand, physically crosslinked hydrogels are synthesized by ionic interactions, crystallization (freezing strategies), the formation of hydrophobic polysaccharide stereocomplexes, protein interaction, hydrogen bonding, among others³⁵. "Physical" hydrogels can be obtained by repeated freeze-thaw (F-T) cycles, method based on performing repetitive freeze-thaw cycles in an aqueous solution of water-soluble polymers. During the freezing part, the ice crystals that are formed organize the polymer chains around themselves. Subsequently, during the thawing part of the cycle, the ice crystals melt, leading to the formation of a porous structure³⁷. It is reported that the stability of hydrogels obtained by this method

increases with the number of (F-T) cycles³⁸. From the works reported so far where chitosan hydrogels are synthesized by this technique, a decrease in pore size and an increase in the elastic modulus and tensile strength are obtained^{39–41}. On that account, the third part of this project modifies the hydrogels reported in the second part through the implementation of freezing-thawing cycles, in addition to a final freezing-drying cycle.

From the preliminary revision and research work, the following hypothesis is presented:

The addition of carboxymethylcellulose to chitosan, in addition to chemical crosslinking with citric acid and novel drying strategies improve the structural and electrochemical properties of hydrogel membranes for their use as electrolyte in zinc-air batteries.

After the literature review, synthesis and characterization of both crosslinking approaches and final materials, the most relevant findings and results are presented as three scientific papers in the thesis, published in high impact journals, to set an important precedent in the development of solid-state electrolytes for the next new generations of batteries.

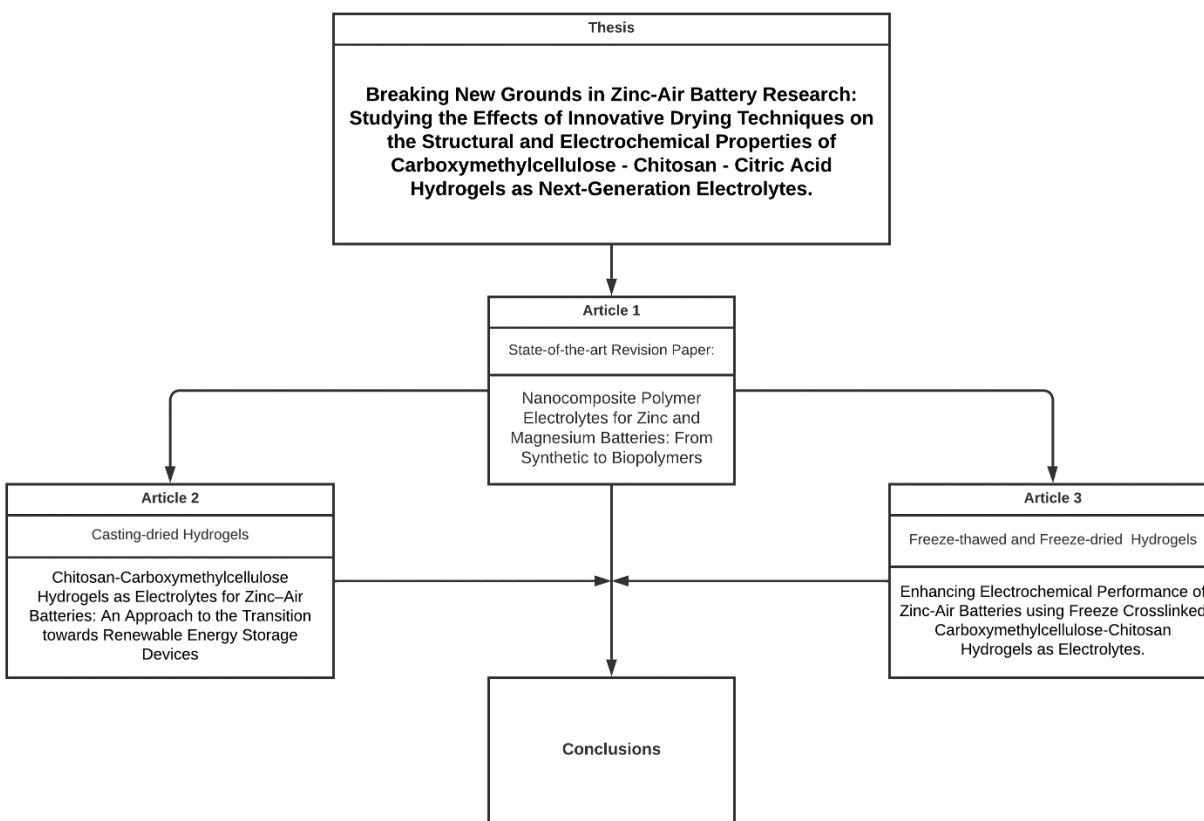


Figure 1. Flowchart of the articles that make up this integration curricular work.

1.2. General and Specific Objectives

1.2.1. General Objective

- To develop novel hydrogels made of biopolymers with different crosslinking strategies to be applied as electrolytes in Zinc-air Batteries.

1.2.2. Specific Objectives

- To compile and analyze the state-of-the-art about the development of nanocomposite polymer electrolytes applied in the field of Zn-ion and Mg-ion batteries.
- To synthesize composite polymeric hydrogels based on chitosan and carboxymethylcellulose through different crosslinking approaches: citric acid as chemical crosslinking, and freeze-thawing freeze-drying physical crosslinking strategies.
- To characterize the designed hydrogels in terms of their structural, thermal, and electrochemical properties.
- To apply and evaluate the synthesized hydrogels in Zinc-air battery prototypes.

Chapter 2

2. Methodology and Results

2.1. **Article published in the Journal *Polymers* “Nanocomposite Polymer Electrolytes for Zinc and Magnesium Batteries: From Synthetic to Biopolymers”**

In the first article of this thesis, a review of the state of the art of the published works that report the development of nanocomposite polymer electrolytes (NCPEs) in zinc or magnesium batteries is carried out. This effort is put in response to the problems related to the use of aqueous electrolytes that direct the current strategies to the use of solid or gel-based electrolytes as a possible solution. In addition, the incorporation of inorganic phases in PEs is a variable to be considered since these hybrid systems have a higher ionic conductivity and better mechanical properties for the desired applications. From this approach, nanocomposite polymer electrolytes are proposed, showing how the combination of both phases reduces the drawbacks of polymer electrolytes in pure state. The discussion centers its attention on comparing and analyzing the results regarding ionic conductivities, electrochemical stabilities, and overall performances in battery systems.

Biopolymers are in the main scope of this review, on the development of electrolytes that can be obtained from abundant and bio-sustainable sources, considered environmentally friendly, and biocompatible. These are characterized by their natural abundance, cost-effectiveness, high solvent compatibility, and high film-forming ability. The coverage of the review was divided into four sections, Poly(vinylidene fluoride-co-hexafluoropropylene, (PVDF-HFP), polyethylene oxide (PEO) based electrolytes, as these two have been the most reported to date, followed by a section about other synthetic polymers, and the final section involving biopolymers.

Abundance, low cost, and simple processability make it expected that biopolymer electrolytes bring a better future to green technologies compared to non-biodegradable, toxic, and harmful materials used in commercial batteries today. It has been evidenced that the role of nanofillers is of great importance in the transport system. These nanoparticles can form space-charge regions and induce a local electric field. The electric charge and the area associated with the nanoparticle interact with the liquid electrolyte structure, causing the space-charge region. It can be described as a region containing free electrons on the nanocomposite surface, and cations together with dipoles in the adjacent double layer balance the surface electronic charge. The addition of nanoparticles has been shown to improve the conductivity, in the smallest case, by an order of magnitude. In addition, the electrochemical properties, mechanical strength, and transport properties of cationic species are also improved. On the other hand, it is found that excessive

fillers can cause a decrease in conductivity in NCPE, which can trigger ion pair formation and ion aggregation, as a non-conductive phase, being an electrically inert component blocking ion transport.

Finally, these studies should be further developed to achieve practical applications for the large-scale industry of polymer-based electrolytic batteries, as well as other electrochemical devices, such as biobatteries, offering an innovative solution to the problems currently faced by biomedical applications, generating positive impacts for the welfare of humans and the environment.



Review

Nanocomposite Polymer Electrolytes for Zinc and Magnesium Batteries: From Synthetic to Biopolymers

María Fernanda Bósquez-Cáceres, Sandra Hidalgo-Bonilla, Vivian Morera Córdova, Rose M. Michell and Juan P. Tafur

Special Issue

Advanced Polymer Nanocomposites II

Edited by


Dr. Ting-Yu Liu and Dr. Yu-Wei Cheng



<https://doi.org/10.3390/polym13244284>

Review

Nanocomposite Polymer Electrolytes for Zinc and Magnesium Batteries: From Synthetic to Biopolymers

María Fernanda Bósquez-Cáceres , Sandra Hidalgo-Bonilla , Vivian Morera Córdova, Rose M. Michell 
and Juan P. Tafur *

School of Chemical Sciences & Engineering, Yachay Tech University, Urcuquí 100119, Ecuador; maria.bosquez@yachaytech.edu.ec (M.F.B.-C.); sahidalgo@yachaytech.edu.ec (S.H.-B.); vmorera@yachaytech.edu.ec (V.M.C.); rmichell@yachaytech.edu.ec (R.M.M.)

* Correspondence: jtafur@yachaytech.edu.ec



Citation: Bósquez-Cáceres, M.F.; Hidalgo-Bonilla, S.; Morera Córdova, V.; Michell, R.M.; Tafur, J.P. Nanocomposite Polymer Electrolytes for Zinc and Magnesium Batteries: From Synthetic to Biopolymers. *Polymers* **2021**, *13*, 4284. <https://doi.org/10.3390/polym13244284>

Academic Editors: Ting-Yu Liu and Yu-Wei Cheng

Received: 14 November 2021

Accepted: 28 November 2021

Published: 7 December 2021

Publisher's Note: MDPI stays neutral with regard to jurisdictional claims in published maps and institutional affiliations.



Copyright: © 2021 by the authors. Licensee MDPI, Basel, Switzerland. This article is an open access article distributed under the terms and conditions of the Creative Commons Attribution (CC BY) license (<https://creativecommons.org/licenses/by/4.0/>).

Abstract: The diversification of current forms of energy storage and the reduction of fossil fuel consumption are issues of high importance for reducing environmental pollution. Zinc and magnesium are multivalent ions suitable for the development of environmentally friendly rechargeable batteries. Nanocomposite polymer electrolytes (NCPEs) are currently being researched as part of electrochemical devices because of the advantages of dispersed fillers. This article aims to review and compile the trends of different types of the latest NCPEs. It briefly summarizes the desirable properties the electrolytes should possess to be considered for later uses. The first section is devoted to NCPEs composed of poly(vinylidene Fluoride-co-Hexafluoropropylene). The second section centers its attention on discussing the electrolytes composed of poly(ethylene oxide). The third section reviews the studies of NCPEs based on different synthetic polymers. The fourth section discusses the results of electrolytes based on biopolymers. The addition of nanofillers improves both the mechanical performance and the ionic conductivity; key points to be explored in the production of batteries. These results set an essential path for upcoming studies in the field. These attempts need to be further developed to get practical applications for industry in large-scale polymer-based electrolyte batteries.

Keywords: polymer electrolytes; composites; biopolymers; zinc batteries; magnesium batteries; properties

1. Introduction

The development of new ways of obtaining energy from environmentally friendly materials is directly related to the need for developing devices capable of storing the power generated. Some devices are designed to store energy, such as rechargeable batteries, capacitors, sensors, and dye-sensitized solar cells (DSSC) [1]. Among these devices, batteries are the most used in everyday life around the world. The main disadvantage of the batteries currently in use, for example, lithium-ion batteries (LIBs), is that they can undergo thermal runaway, form protrusions, show low energy density, and low cycling efficiency [2–4]. Moreover, they are highly reactive, expensive, unsafe, and are a pollutant for the environment [5–10].

Some of the devices that could resolve the disadvantages identified for LIBs are redox flow batteries [11–13] and fuel cells [14–16], as they have no thermal runaway problem, and they are safe and less expensive. Among these energy storage options, zinc and magnesium are currently the multivalent ions in the sight of replacing lithium as the most reliable options to develop eco-friendly rechargeable batteries. Magnesium is the 8th most abundant metal in the Earth's crust [17], while zinc is the 24th most abundant [18], with an estimated 2800 million metric tons (Mt) of zinc contained in the Earth's crust [19]. Furthermore, magnesium and zinc can be recycled cheaply; in addition, they do not lose their physical properties [13,14] that contribute significantly to sustainability, aiming

to reduce concentrate demand, energy consumption, and minimize waste disposal and pollutant emissions. On the other hand, it is known that lithium reserves present an amount of only 17 million Mt [20], and recycling lithium, which at present is heavily dependent on cobalt content, requires improvement due to environmental and economic concerns, besides the lower value of the recovered materials [21].

Zinc batteries present key features for battery' performance including high volume capacity [22] and little redox potential [23]. On the other hand, magnesium batteries possess a low electrode potential and a high volumetric capacity, almost double the Li-metal value [24]. Besides, zinc and magnesium have lower reactivity, lower cost, low toxicity, and intrinsic safety [25–29], critical characteristics for developing sustainable energy storage devices.

These batteries have a wide range of application fields in energy storage/release systems ranging from technological and military applications, to vehicles and wearable electronics [30–32]. To develop adequate energy storage devices for the end-users, one of the crucial features is whether the battery is only suitable for base station energy storage, or if it could also be employed for flexible devices. Hence, another point for the development of eco-friendly batteries is the physical state of the electrolyte. Currently, batteries use the electrolyte in a liquid state, which has safety, toxicity, flammability, and leakage drawbacks. In addition, other characteristics of current batteries, such as bulky design, electrode corrosion occurring at the interfaces, and dendrite growth on the metal electrode, reduce the capacity and life cycle of the device [33–35]. They can even lead to preferential nucleation and uneven currents during charging [36] and cause fires [37]. These issues are why current battery development strategies focus on using solid or gel-based electrolytes, improving the electrochemical properties.

Polymer electrolytes (PEs) have the most far-reaching advantages among all types of solid-state and gel-based electrolytes. They stand out for their high flexibility and good performance [38–40]. However, the main problem of these electrolytes is that they present low battery efficiency, insufficient ionic conductivities for practical applications, insufficient electrochemical stabilities, poor mechanical strength, and substantial interfacial resistance [10]. Therefore, recent research has focused on incorporating inorganic phases; these hybrid systems have higher ionic conductivity and mechanical stiffness and are non-flammable [29,41,42].

From this approach, nanocomposite polymer electrolytes (NCPEs) were born. The first report mentioning the addition of inorganic fillers in PEs was reported by Weston et al. in 1982 [43]. These authors showed how the combination of both phases reduced the drawbacks of electrolytes that did not combine inorganic/organic phases. Since then, several papers have been published to assemble PEs and NCPEs for Zn and Mg that could be considered for industrial applications [2,10,44–48].

Biopolymers are in the main scope of this review, focusing on developing electrolytes that can be considered environmentally friendly and biocompatible. However, it is worth mentioning that for a biopolymer to be considered environmentally friendly, the resource and the production method are vital characteristics to be taken into account [49]. On the other hand, biopolymers are characterized by their natural abundance, cost-effectiveness, high solvent compatibility, and film-forming ability. Some reviews focusing on biopolymer electrolytes have been published [50–52]. However, nanofillers are a new approach discussed here to get a precedent for further research and obtain better results for practical applications among this type of polymers.

NCPEs must meet specific requirements to be suitable rechargeable batteries. The polymer that acts as the host should possess an amorphous or low crystalline nature [53]. The cation–polymer interaction must be sufficiently strong to promote dissolution but not so strong as to inhibit ion exchange [54]. The designed electrolyte should be able to take up polar groups with a high molecular weight in its chain apart from sufficient electron-pair donors for coordination with cations [53], to achieve a good performance in

cationic transport number, more significant than with anionic to reduce the concentration gradients for obtaining repeated charge-discharge steps and high-power density [55].

The electrolyte should undergo no net chemical changes of the battery. All Faradaic processes are expected to occur within the electrodes [56] since the electrolyte needs to be an inert battery part. Figure 1 presents the discharge scheme for a typical battery, whose circuit is closed so that electrons can get to the cathode. The performance level requires ionic conductivities values of at least $10^{-3} \text{ S}\cdot\text{cm}^{-1}$. Moreover, it needs to show the lowest glass transition temperature (T_g) [54] possible, key for obtaining the highest conductivities, resulting in increased local segmental motion and, therefore, high diffusivity of the ions.

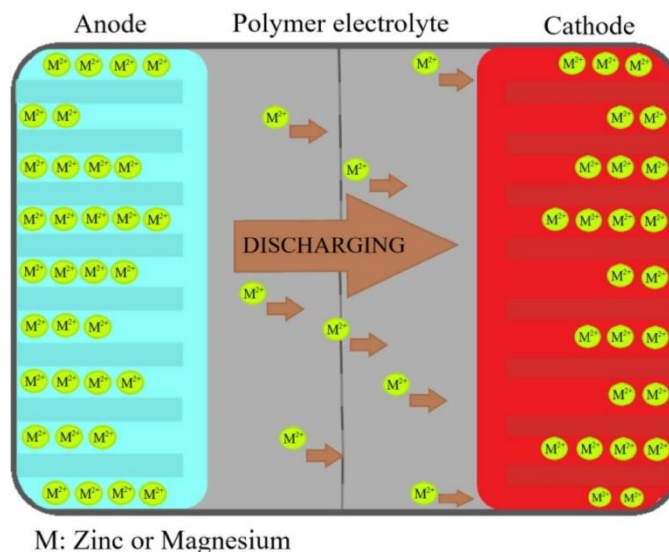


Figure 1. Schematic diagram of Zn-ion and Mg-ion battery discharge. Reproduced with permission from Renew. Sustain. Energy Rev., 65, Singh et al., Perspectives for solid biopolymer electrolytes in dye sensitized solar cell and battery application, 1098–1117, 2016 [50].

For good performance, it is also relevant to fulfill some electrochemical properties [57], such as high decomposition potential, low interfacial resistance, as well as some degree of stiffness, high chemical and thermal stability, to be durable for a long time under the conditions in which the device in which it is to be used operates [53]. Finally, rentability in the production process is indispensable since the main goal of the development is to take it to the industrial scale. As reviewed so far, these are the most important characteristics to consider when studying electrolytes used in zinc and magnesium batteries.

In this review, the recent advances of NCPEs for magnesium and zinc rechargeable batteries are overviewed, with a particular interest in the results regarding their ionic conductivities, electrochemical stabilities, and general performances in battery systems. This field continues thriving; still, new aspects of the nanoparticles' effects on the physical-chemical properties of the polymer electrolytes and their based power sources are ever discovered and need to be discussed to set an outline on future directions and challenges that come with the development of NCPEs for new batteries on worldwide demand.

2. Poly(vinylidene fluoride *co*-hexafluoropropylene)'s-Based Nanocomposite Polymer Electrolytes

Copolymerization is one of the most effective methods to improve the mechanical stability and electrical conductivity of materials [58–60]. Poly(vinylidene Fluoride-*co*-Hexafluoropropylene) polymer matrix (PVDF-*co*-HFP) has been extensively used for different purposes. It has an excellent performance in fuel cells, dye-synthesized solar cells,

membrane distillation, and other electrochromic applications [61–64]. The block copolymer structure includes a crystallizable comonomer ($-\text{CH}_2\text{-CF}_2-$) and an amorphous HFP unit with a high dielectric constant ($\epsilon = 8.4$), thanks to the presence of highly electronegative fluorine and the spontaneous alignment of C–F dipoles in the crystalline phases [65–67].

The copolymer presents a high solubility and lower crystallinity and glass transition temperature [68] than Poly(vinylidene Fluoride) (PVDF), making it a promising matrix for preparing nanocomposites, despite its non-biodegradability. Furthermore, the degree of crystallinity remaining in the system helps retain sufficient mechanical stability and structural rigidity to act as a separator between the battery's electrodes [69]. At the same time, the amorphous phase can serve as the conductive medium.

2.1. Magnesium-Ion Conduction

Within the field of rechargeable batteries, several studies have applied PVDF-co-HFP as a component of the electrolyte. The most recent ones were compiled in a review article, which focuses on lithium-sulfur batteries [70]. However, as reported, the balance between industrial development and environmental protection makes it essential to develop high energy density and non-pollutant rechargeable batteries, with magnesium ion and organic electrode batteries as the directions for post-lithium batteries [71]. For reference, Table 1 lists some properties of the nanocomposites employed along with PDVF-co-HFP as electrolytes for magnesium batteries.

Table 1. A summary of NCPEs composed of PVDF-co-HFP for magnesium batteries.

Nanocomposite	Ionic Salt	Conductivity ($\text{S}\cdot\text{cm}^{-1}$) 10^{-3}	Activation Energy (eV)	Electrochemical Stability Window (V)	State	Reference
No added	$\text{Mg}(\text{Tf})_2$	0.15	-	5	Gel	[72]
	$\text{Mg}(\text{ClO}_4)_2$	0.293	0.33	4	Solid	[73]
	$\text{Mg}(\text{ClO}_4)_2$	3.2	-	4.3	Gel	[74]
SiO_2	$\text{Mg}(\text{ClO}_4)_2$	11	-	3.5	Gel	[75]
	$\text{Mg}(\text{ClO}_4)_2$	10	-	3.5	Gel	[76]
Al_2O_3	$\text{Mg}(\text{Tf})_2$	3.3	-	3.3	Gel	[77]
MgAl_2O_4	$\text{Mg}(\text{Tf})_2$	4.0	-	3.3	Gel	[77]
Al_2O_3 *	$\text{Mg}(\text{NO}_3)_2$	0.101	-	-	Solid	[78]
MgO	$\text{Mg}(\text{ClO}_4)_2$	8	0.235	3.5	Gel	[79]
	$\text{Mg}(\text{ClO}_4)_2$	6	0.032	3.5	Gel	[75]
MgO *	$\text{Mg}(\text{NO}_3)_2$	0.104	0.45	-	Solid	[80]
MgO and SiO_2	$\text{Mg}(\text{ClO}_4)_2$	10 and ~ 9	-	-	Gel	[81]
ZnO	MgCl_2	0.12	0.45	-	Solid	[82]
ZnO *	$\text{Mg}(\text{NO}_3)_2$	0.37	-	-	Solid	[83]
BaTiO_3	$\text{Mg}(\text{Tf})_2$	0.411	-	-	Solid	[84]
TiO_2 *	$\text{Mg}(\text{NO}_3)_2$	0.010	0.30	-	Solid	[85]

* PVDF without copolymerization with HFP.

Maheshwaran et al. [72] studied the role that the salt added to the polymer had and how its amount affected the results. They developed a magnesium ion conducting gel polymer electrolytes (GPE) based on PVdF-co-HFP, magnesium triflate $\text{Mg}(\text{Tf})_2$, in ethylene carbonate (EC), and diethyl carbonate (DEC). The analysis of this polymeric electrolyte by X-ray diffraction (XRD) showed a decrease in the crystallinity with the addition of salt. Moreover, FT-IR confirmed that magnesium triflate could suppress the nonpolar α crystalline phase of PVDF. Consequently, the electrolyte offered a predominant ionic character with a total ion transport number close to unity, making it considered to a certain extent for batteries because it was freestanding and stable. However, its considerably low ionic conductivity made it inappropriate, although it became a precedent for what can be achieved.

Solid polymer electrolytes (SPE) with PVDF-co-HFP as a polymer matrix were also studied. Ponmani et al. [73] blended this matrix with Poly(vinyl acetate) (PVAc) and added magnesium perchlorate $\text{Mg}(\text{ClO}_4)_2$ salt. The SPE film was found to be flexible,

and the maximum ionic conductivity found was $0.293 \times 10^{-3} \text{ S}\cdot\text{cm}^{-1}$, obtained at 363 K. Cyclic voltammetry (CV) studies confirmed the Mg ion reversibility that demonstrated its conduction in the SPE.

One of the first electrolytes that employed PVDF-co-HFP was a magnesium-ion conducting GPE, composed of 15% of PVDF-co-HFP, 73% of $\text{Mg}(\text{ClO}_4)_2$ in EC/propylene carbonate (EC/PC), and 12% silicon dioxide (SiO_2) [74]. The cell in which this electrolyte was tested employed magnesium as anode and vanadium oxide (V_2O_5) as the cathode. The tests demonstrated low initial discharge capacity and poor cycling performances. These disadvantages could be attributed to high interfacial resistance at Mg anode [74]. The main problem identified from this research was the blocking of the charge transfer reaction, highlighting that further research on the interface should be conducted so that the cycling performance could be improved to a practical level.

Magnesium oxide (MgO) showed beneficial features in inducing consistent improvements in liquid electrolyte retention and the overall chemical, physical, and electrochemical properties in the work performed by Pandey et al. [79]. They presented novel research dispersing PVDF-co-HFP with nanosized MgO particles. It was analyzed by XRD patterns, obtaining a semi-crystalline structure with predominant peaks in $2\theta = 14.6, 17, 20, 26.6$, and 38° . These changes in the peaks showed the reduction in crystallinity of the PEs, caused by the entrapment of liquid electrolytes. FT-IR spectroscopic analysis was conducted to look over the ion-polymer interaction and the conformational changes, confirming the reduction of crystallinity. The T_g was observed at -65°C for pure PVDF-co-HFP film, while with the addition of magnesium oxide, the value came down to -90°C .

Electrodes play an important role when performing efficiency analysis. Pandey et al. [75] demonstrated the previous NCPE in a prototype cell of magnesium and multiwalled carbon nanotubes (MWCNT) composite as the negative electrode and the corresponding positive one with vanadium pentoxide (V_2O_5). The rechargeability of the cell was enhanced by substituting magnesium with Mg-MWCNT composite as the negative electrode. The discharge capacity faded away after ten cycles, attributed to the passivation of the negative electrode. Nevertheless, the electrolyte showed to be free-standing and flexible, with enough mechanical strength.

The role of fillers has been shown to be of great importance. These nanocomposites can form space-charge regions and induce a local electric field. This phenomenon was first approached by Kumar [86], who revealed the electric charge and area associated with the particle interact with the structure of the liquid electrolyte, provoking the space-charge region. It can be described as containing free electrons at the surface of the nanocomposite, and cations along with dipoles at the adjacent double-layer balance the surface electronic charge (Figure 2). Magnesium oxide is known to be slightly electronegative in nature. In the systems studied, a reversible reaction between the magnesium oxide and the magnesium (II) ion took place and formed the space-charge region, giving place to the $\text{MgO}:\text{Mg}^{2+}$ species [75].

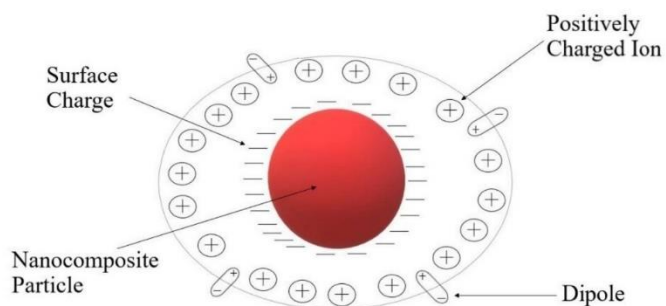


Figure 2. Schematic representation of the space charge and local electric field formation around a nanocomposite particle.

Magnesium oxide nanoparticles were combined with nano-sized silicon dioxide in a novel electrolyte by Pandey et al. [81]. When relating conductivity to filler content (Figure 3), the presence of two conductivity maxima was noticed, explained by the dissociation of ion aggregates/undissociated salt into free ions with the addition of filler particles (the first peak). The second maximum was described using the composite effect and based on a conducting interfacial space-charge double layer between the filler particles and the GPE. This local field was responsible for enhanced Mg^{2+} ion motion and enhanced transport number up to the addition of ~ 10 wt % of MgO. The cationic transport number measurements (t_+) also showed essential results, in which the best improvement was obtained by the presence of MgO particles (~ 0.44). On the other hand, with the addition of SiO_2 dispersion, the t_+ value did not increase substantially. Finally, for this polymer, it was pointed out that the nano-sized MgO supported the cationic motion. In contrast, the nano-sized SiO_2 supports the anion conduction in the filler/gel electrolyte interfacial regions.

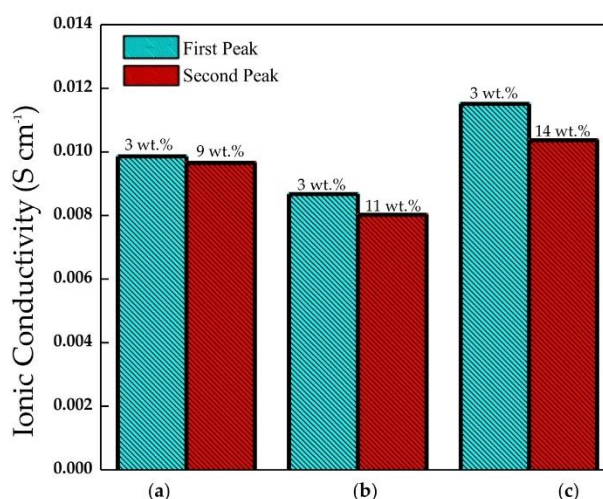


Figure 3. Room temperature conductivity peaks of composite gel polymer electrolyte films vs filler content: (a) nano-sized MgO, (b) micro-sized MgO, and (c) nano-sized SiO_2 . Prepared from data in [81].

Nanosized silicon dioxide was ultimately tested with the addition of molybdenum trioxide (MoO_3) as the positive electrode in a posterior study [76]. This cell showed a discharge capacity of $\sim 175 \text{ mAh} \cdot \text{g}^{-1}$ for an initial ten charge-discharge cycles. In addition, it presented the same conductivity value as the last cell. Finally, good thermal stability with a single-phase behavior was presented at a temperature range from -70 °C to 80 °C. Enhanced conductivity was attributed once again to the space-charge layers formed between the filler and GPE.

The effect of active and passive nanofillers, along with the copolymer, was studied for Mg NCPEs by Sharma et al. [77], incorporating Mg-triflate salt mixed with EC and PC, entrapped in PVDF-co-HFP. Aluminium oxide (Al_2O_3) and Mg aluminate (MgAl_2O_4) were used as passive and active fillers. The reduction of crystallinity was achieved as expected and confirmed by XRD, Field emission scanning electron microscopy (FESEM), and Differential Scanning Calorimetry (DSC) studies. By FESEM (Figure 4), it was observed that undispersed GPE showed larger grain sizes and possessed uniformly distributed pores. The incorporation of nanofillers in the undispersed GPE changes its morphology substantially. It was further proved that as the number of fillers increases its porosity leads to the entrapment of liquid electrolyte in the pores (demonstrated by the fillers not being seen in the NCPE (Figure 4c,f)), which further enhanced the ionic conductivity of the NCPE.

The addition of the passive filler conferred the cell to have a relatively good mechanical stability and thermally stability up to 100 °C. The active filler ensured an improvement in the ion transport number. The obtained electrochemical stability window (ESW) was key, showing their potential as electrolytes in ionic devices.

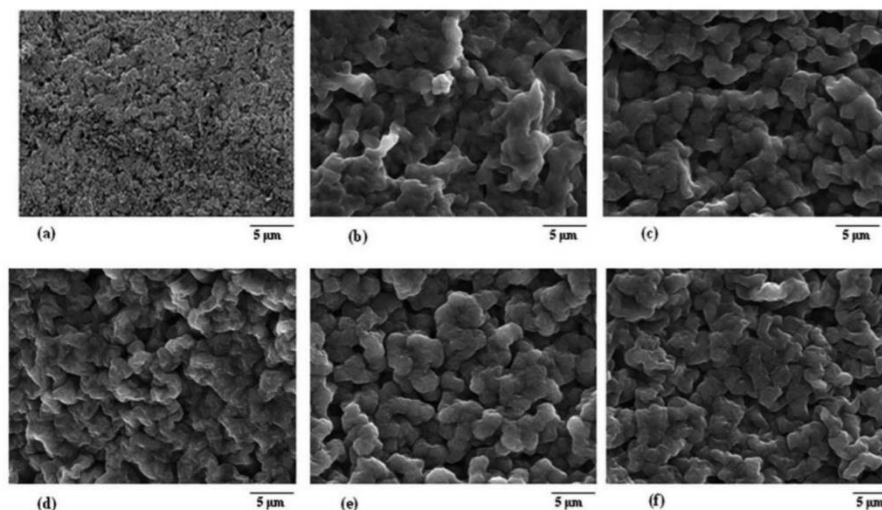


Figure 4. FESEM images of pure (a) PVdF-co-HFP film and nanocomposite GPE films containing (b) 0 wt %, (c) 6 wt % Al_2O_3 , (d) 30 wt % Al_2O_3 , (e) 6 wt % MgAl_2O_4 , and (f) 20 wt % MgAl_2O_4 . Reproduced with permission from Polym. Compos., 40, Sharma et al., Magnesium ion-conducting gel polymer electrolyte nanocomposites: Effect of active and passive nanofillers, 1295–1306, 2019 [77].

The latest report of PVDF-co-HFP electrolyte for magnesium batteries known so far implemented zinc oxide (ZnO) as nanofiller along with Magnesium chloride (MgCl_2) as ionic salt [82]. A transport number of 0.99 was achieved; the current change indicated that conductivity in the NCPE was predominantly ionic. PVDF was incorporated without copolymerizing it with HFP in a magnesium NCPE, along with MgO as a nanofiller [80]. The optimum nanofiller concentration (3wt %) was chosen to be the most suitable one with a conductivity of $1.04 \times 10^{-4} \text{ S}\cdot\text{cm}^{-1}$. On further increase in nanofiller concentrations, the ionic conductivity value decreased. Thermal stability and reduced melting point temperature were confirmed through thermogravimetric analysis (TGA) and XRD. Magnesium oxide nanoparticles enhanced the ionic conductivity and dielectric constant, confirmed by complex impedance spectroscopy [80]. The authors recently presented similar results with the addition of zinc oxide particles [83].

The results presented until now (Table 1) confirm the enhanced high ionic conductivity present in PVDF-co-HFP nanocomposite polymer electrolytes compared to the SPE systems and better thermal and mechanical stability compared to liquid systems. The enhancement in conductivity may be caused by the presence of the nanoparticles, facilitating the new kinetic path for ionic transport and polymer segmental motion. However, another conclusive characteristic is that when a specific percentage of nanofiller is added, a decrease in ionic conductivity is observed. Excessive fillers could provoke this in the NCPE that may trigger the formation of ion pairs and ion aggregation, such as the non-conducting phase presented as an electrically inert component blocking ion transport. So far, they are probably one of the best options to study and meet all the requirements for future use instead of lithium-ion conductive systems.

2.2. Zinc-Ion Conduction

Besides magnesium, zinc presents many advantages associated with zinc chemicals, as batteries of high specific/volumetric energy density can be fabricated. Ionic radii of Zn^{2+} (74 pm) and that of Li^+ (68 pm) are quite comparable, but Zn^{2+} has twice as much charge as Li^+ cation [87]. Furthermore, the natural resources of zinc are plentiful, and its stability makes it able to be handled safely in oxygen and humid atmosphere. The so-mentioned dielectric constant of PVDF-co-HFP is also known to generally assist in more significant ionization of zinc salts and then provide a high concentration of charge carriers. Consequently, Table 2 lists some properties of the nanocomposites employed along with PDVF-co-HFP as electrolyte for zinc batteries.

Table 2. A summary of NCPEs composed of PVDF-co-HFP for zinc batteries.

Nanocomposite	Ionic Salt	Conductivity ($\text{S}\cdot\text{cm}^{-1}$) 10^{-3}	Activation Energy (eV)	Electrochemical Stability Window (V)	State	Reference
No Added	$\text{Zn}(\text{Tf})_2$	1.73	0.025	-	Gel	[88]
	$\text{Zn}(\text{Tf})_2$	2.44×10^{-2}	0.380	3.45	Solid	[89]
	$\text{Zn}(\text{Tf})_2$	0.144	-	4.14	Solid	[90]
TiO_2	$\text{Zn}(\text{Tf})_2$	0.34	-	-	Solid	[91]
ZrO_2	$\text{Zn}(\text{Tf})_2$	0.46	-	2.6	Solid	[92]
ZnO	$\text{Zn}(\text{Tf})_2$	6.7	-	4.5	Gel	[93]
CeO_2SiO_2	$\text{Zn}(\text{Tf})_2$	0.3	-	2.7	Solid	[57]
	$\text{NH}_4\text{CF}_3\text{SO}_3$	1.07	-	-	Solid	[94]

Tafur et al. [88] studied GPEs composed of PVdF-co-HFP with different ionic liquids, with and without zinc triflate salt. From attenuated total reflectance-Fourier transform infrared (ATR-FT-IR) and XRD spectroscopies, it was deduced that incorporating the ionic liquid and salt to the matrix produced more amorphous and polar membranes when comparing it to the original PVDF-co-HFP film. Besides, the electrical properties had shown to be dependent on the ionic liquid employed, aspect confirmed by measurements on ionic conductivity, impedance, and voltammetry. This report also studied the influence of the ionic liquid type on the performance of the GPE for Zn batteries. From ionic conductivity, impedance, and voltammetry measurements, changes in the results were observed when the salt was not added, or the added quantity was too low, indicating that the salt is the important charge carrier independent of the ionic liquid.

In another report, Tafur et al. [95] designed a battery employing manganese dioxide (MnO_2) as the cathode, zinc as the anode, and the GPE was assembled by the use of PVDF-co-HFP including 1-Butyl-3-methylimidazolium trifluoromethanesulfonate, 99% (BMIM Tf), and zinc triflate ($\text{Zn}(\text{Tf})_2$). The electrolyte was then analyzed by X-ray photoelectron spectroscopy and Energy Dispersive X-Ray techniques. The remarkable results from the study showed the charge storage mechanism, which began with the reduction of Mn^{4+} to Mn^{2+} species, at the same time as Zn^{2+} cations, together with triflate ions, intercalate the cathode material during the discharge process. In the recharge process, it was evidenced that Mn^{2+} species returned to the positive electrode, and they were oxidized mainly to Mn^{4+} . Moreover, Mn^{2+} was not reduced to Mn^0 in the anode during the recharge process. Nevertheless, in every completed process, Zn^{2+} cations were not expelled, remaining inside the electrode, probably stabilized by the triflate anions, which were not expelled either. Besides, with the addition of an ionic liquid to the GPE, it was observed that the interaction between the zinc-ion and PVDF chains became weaker, enhancing ion mobility.

A zinc battery was designed with an SPE [89] based on PVDF-co-HFP with zinc triflate, obtaining a low crystallinity elucidated by XRD and scanning electron microscopy (SEM). CV of the SPE curve was flat without the presence of peaks. This fact indicated that the film presented excellent stability. No decomposition occurred in the operating voltage range and ESW of 3.45 V. These results were improved in a recent study performed by Liu et al. [90], where 1-ethyl-3-methylimidazolium trifluoromethanesulfonate (EMITf)

was incorporated along with the PVDF-co-HFP membranes and zinc triflate salt. The ionic liquid has shown to reduce the crystallinity, enrich the nanopores' structure, and enhance the electrical and electrochemical properties of the electrolyte membranes. The ionic conductivity was enhanced by one order of magnitude. The electrolyte membrane was able to sustain a high thermal decomposition temperature of ~ 305 °C, and thus its mechanical performance was sufficient for considering it for practical applications.

Nanocomposites became first used with PVDF-co-HFP by Muda et al. [94], who designed a cell composed of Zn + $\text{ZnSO}_4 \cdot 7\text{H}_2\text{O}$ + polytetrafluoroethylene (PTFE) as the anode, MnO_2 + PTFE as the cathode, and the electrolyte composed by PVDF-co-HFP as host polymer, ammonium trifluoromethane sulfonate ($\text{NH}_4\text{CF}_3\text{SO}_3$) as ionic salt with silicon dioxide as filler. Herein was observed the so mentioned existence of two conductivity maxima at the concentration of 1 and 4 wt % of SiO_2 , in this case, attributed to two percolation thresholds in the NCPE. The voltage was able to achieve a value of ~ 1.50 V to ~ 1.29 V. The assembled cell performed fairly well when discharged at the low current drain or with high load resistance, showing suitability for low current drain applications.

Titanium dioxide was incorporated in an NCPE designed by Johnsi et al. [91]. Differential scanning calorimetric results confirmed that with the addition of TiO_2 , a reduction in the degree of crystallinity and the T_g value was obtained. The glass transition temperature is a fundamental parameter to grasp the structural changes of PEs occurring under various thermal conditions. The effect of filler content on the position of glass temperature could be evaluated from Figure 5. When more TiO_2 was added, these values increased slightly instead, which could be caused by the possible agglomeration of an excess amount of nanofillers. Furthermore, there was also evidence to ascertain that the decrease of the T_g value reflected an increase in flexibility of polymer chains, provoking enabling fast ion conduction within the NCPE system. The low value of conductivity limited the applications that could be obtained for this electrolyte.

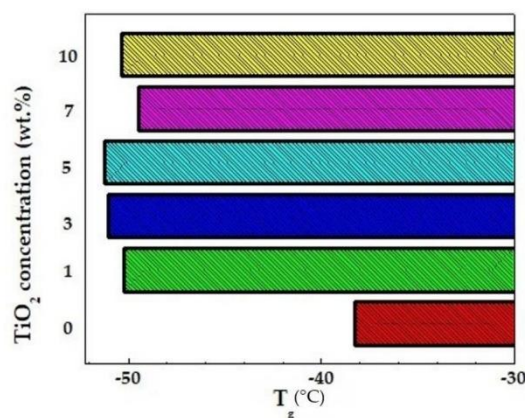


Figure 5. T_g (°C) of the NCPE systems vs the TiO_2 content. Prepared from data in [91].

Active fillers were studied by Hashmi [93] with an electrolyte composed by the addition of 1.0 M solution of zinc triflate in EC/PC immobilized in the host polymer and ZnO nanofiller. The morphological/structural changes for this gel electrolyte were monitored using SEM and XRD techniques. The micrographs obtained (Figure 6) showed that the texture and morphology of the gel polymer system had also been modified, revealing smaller crystallites and pores. For the highest amount (~ 25 wt %) sample, ZnO particles appeared to be disappeared in the SEM picture (Figure 6b), probably due to the polymer fully covering the particles, changing the texture of polymer network. On the other hand, with 10 wt % of filler, white spots could be seen, indicating the presence of nanoparticles in the gel network, forming a separate phase. Dark regions showed

the micron-sized porosity from the micrographs corresponding to the undispersed GPE, where the liquid electrolyte could be retained. Thus, the polymer films established a semi-crystalline nature with enough porosity to maintain the ionic liquid in the electrolyte. For this gel, the increase in ionic conductivity with the dispersion of ZnO did not signify more than an order of magnitude, obtaining that for the undispersed sample, its value was $\sim 6.7 \times 10^{-3} \text{ S}\cdot\text{cm}^{-1}$. Besides, with the increasing of temperature, for the sample of $\sim 10 \text{ wt } \%$ ZnO particles, it offered ionic conductivities of $3.7 \times 10^{-3} \text{ S}\cdot\text{cm}^{-1}$ at 30°C and $1.4 \times 10^{-2} \text{ S}\cdot\text{cm}^{-1}$ at 85°C , which gave a precedent for potential application as an electrolyte in zinc batteries and other electrochemical applications over a wider temperature range. Furthermore, for this NCPE, a local electric field was detected due to the reversible reaction between ZnO and Zn^{2+} , homologous to the one previously presented in Figure 1.

Johnsi et al. [57] continued their work with passive fillers. They constructed a flexible, free-standing, transparent film composed of [75 wt % PVDF-co-HFP:25 wt % ZnTf_2]-x wt % cerium dioxide (CeO_2) where x = 1, 3, 5, 7, and 10, respectively. The film's detailed FT-IR spectral analysis indicated the feasibility of complexation between the host polymer matrix and the salt and nanofiller. The decomposition voltage that reached a range of 2.4 to 2.7 V was a key result for this cell. Johnsi's et al. [92] work continued with implementing zirconium dioxide (ZrO_2), with the same proportion of PVDF-co-HFP and ZnTf_2 , with 7 wt % nanofiller. The obtained value of ionic conductivity represented an increase in an order of magnitude. XRD confirmed an amorphous phase present in the matrix. The cell achieved an ESW of 2.6 V with thermal stability up to 300°C . The resulting cell exhibited many attractive and stable discharge characteristics for room temperature applications.

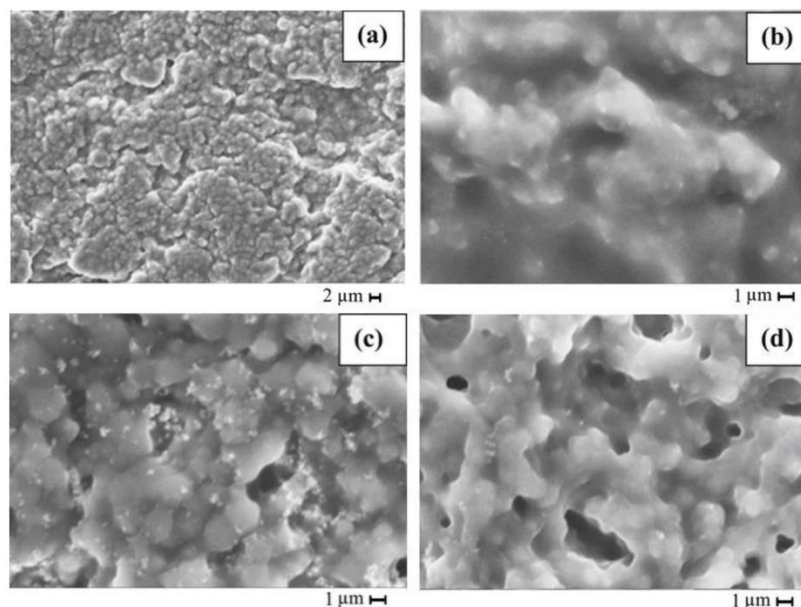


Figure 6. SEM micrographs of EC-PC- $\text{Zn}(\text{Tf})_2$ +PVdF-co-HFP (a) gel polymer electrolyte (magnification, $\times 1000$); (b) gel electrolyte with magnification $\times 5000$; and (c) its nanocomposites dispersed with ZnO particles of 10 wt % (magnification, $\times 5000$); and (d) 25 wt % (magnification, $\times 5000$) Reproduced with permission from J. Solid State Electrochem., 16, Sellam, Enhanced zinc ion transport in gel polymer electrolyte: Effect of nano-sized ZnO dispersion, 3105–3114, 2012 [93].

From the analysis presented in this section, it could be concluded that the addition of active fillers has shown more promising results for the applicability of NCPEs, than the ones with passive fillers. This assumption can be seen in Figure 7. The reports about

PVDF-co-HFP, with the addition of zinc triflate salt and various nanofillers, are presented versus their ionic conductivity obtained. Whereas the first bar, representing the NCPE without nanofillers, has a shallow and almost imperceptible value, the bar corresponding to the ZnO nanofiller has a clear advantage over the other nanofillers considered passive. This assumption is explained by the fact that zinc oxide nanoparticles have been shown to participate in the ionic conduction process. Hence, they deserve special attention for further studies on the field, even with other polymers and ionic salts.

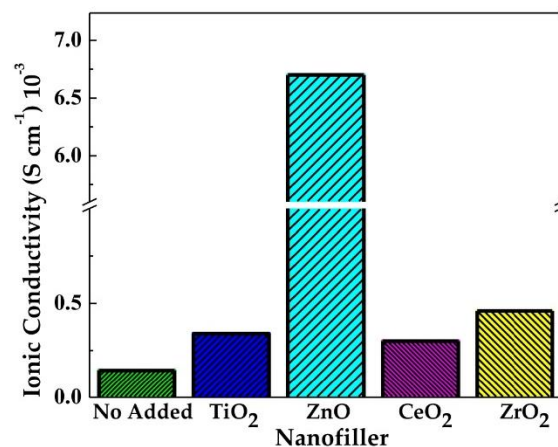


Figure 7. Plot of nanofiller versus ionic conductivity ($\times 10^{-3}$) for nanocomposite polymer electrolyte based on PVDF-co-HFP and zinc triflate salt. Prepared from data in [57,90–93].

3. The Poly(ethylene Oxide)'s Based Nanocomposite Polymer Electrolytes

Poly(ethylene oxide) (PEO) has been the focus of attention for many researchers among various polyethers because it is considered to be the best solvent medium for various ionic salts [96], and it is known to possess relatively high electrochemical stability [97]. It is water-soluble and in a semi-crystalline state at room temperature [98]. It presents a single helical structure, which also supports ionic conduction [99], favoring fast ion transport for the electrochemical processes in the batteries. The main chain of the polymer, known to be polar and flexible, owns vital electron-donating ether-oxygen groups, dissociating the salt, and generating carrier ions. These ions can migrate through the amorphous region of the polymer employing interchain/intrachain segmental motion. However, its high degree of crystallinity makes it necessary to incorporate metal salts that impede crystallization [100]. PEO shows a low ionic conductivity of $3.32 \times 10^{-9} \text{ S cm}^{-1}$ at pure state [101], a fact that could be enhanced by the addition of nanofillers, along with other approaches discussed in this section. A review article was recently published by Feng et al. [102], where the interaction of ceramic fillers on the performance of PEO in lithium batteries is deeply studied. The authors concluded that composite SPEs are one of the most efficient ways to improve the electrolytes' ionic conductivity.

3.1. Magnesium-Ion Conduction

The primary purpose of the subsequent studies has been to elucidate the ion transfer mechanism in the nanocomposite polymer system and enhance the ion conductivity and mechanical strength. The present section discusses how the addition of nanocomposites decreases the degree of crystallinity in these electrolytes. Table 3 refers to the properties of the nanocomposites employed along with PEO as electrolytes for magnesium batteries.

Table 3. A summary of NCPEs composed of PEO for magnesium batteries in solid-state.

Nanocomposite	Ionic Salt	Conductivity (S·cm ^{−1}) 10 ^{−3}	Activation Energy (eV)	Electrochemical Stability Window (V)	Reference
No added	Mg(Tf) ₂	56	0.49	4.6	[103]
	Mg(Tf) ₂	0.277	0.40	-	[101]
	Mg(ClO ₄) ₂	0.277	0.30	-	[104]
	Mg(Tf) ₂	1.67	0.34	-	[101]
MgO	(CH ₃ COO) ₂ Mg × 7H ₂ O	363	0.013	7.6	[105]
	Mg(ClO ₄) ₂	1.04	0.29	-	[104]
TiO ₂	Mg(Tf) ₂	1.53	0.38	-	[101]
	Mg(ClO ₄) ₂	1.14	0.28	-	[104]
SiO ₂	Mg(Tf) ₂	0.586	0.36	-	[101]
	Mg(ClO ₄) ₂	0.87	0.28	-	[104]
B ₂ O ₃	MgCl ₂	0.716	-	-	[106]
Starch nanocrystals (SNCs)	MgBr ₂	0.116	-	-	[107]

The studies involving PEO for magnesium-ion conduction began complexing magnesium triflate and incorporating EMITf ionic liquid, reported by Kumar et al. [103]. The ionic liquid happened to be vital in mediating the Mg²⁺ ion conduction and the gradual enhancement in the Mg²⁺ ion transport number. Raman studies evidenced the interaction of imidazolium cations with ether oxygen of PEO (Figure 8). The peak at 2871 cm^{−1} was found to be affected due to the complexation of PEO with Mg(Tf)₂ salt and the addition of ionic liquid. A peak appeared at 2848 cm^{−1} in curve b indicated the conformational changes of PEO chains after its complexation with Mg-salt. Besides, the PEO peak of 2871 cm^{−1} decreased and almost disappeared for the higher ionic liquid content. An additional peak (shoulder) appears at ~1025 cm^{−1} (Figure 8c–f), presumably because of the free triflate anions from EMITf. Such anions would be free only when EMI⁺ ions have the possibility of interaction with ether oxygen of PEO. Consequently, it has been shown to play an essential role in substantially enhancing the cation transfer value.

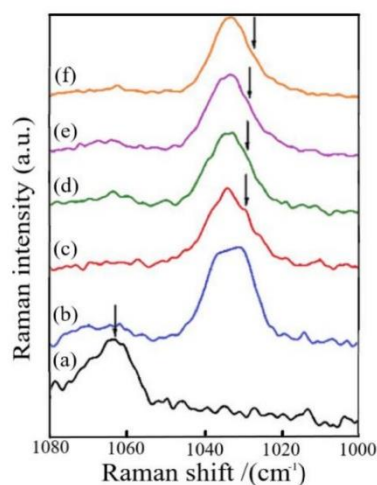


Figure 8. Raman spectra of (a) PEO pure film, (b) PEO25-Mg(Tf)₂ complex, and PEO25-Mg(Tf)₂ + x wt % EMITf system for (c) x = 5, (d) x = 10, (e) x = 20, and (f) x = 30 for spectral region of 1000–1080 cm^{−1}. Reproduced with permission from *Electrochim. Acta*, 56, Kumar et al. Ionic liquid mediated magnesium ion conduction in poly(ethylene oxide) based polymer electrolyte, 3864–3873, 2011 [103].

The approach of adding nanocomposites to PEO began with the report presented by Sundar et al. [106], who created an SPE of PEO with MgCl_2 as electrolytic salt and boron oxide (B_2O_3) as the filler. DSC and FT-IR characterized this cell. The best ionic conductivity was achieved with 2 wt % B_2O_3 . The cell was assembled by adopting Mg as anode and MnO_2 as cathode, sandwiching the SPE between the electrodes. It got an open circuit voltage (OCV) of 1.9 V. The low ionic conductivity obtained made this cell unsuitable for practical applications. It indicated that this type of matrix could be considered for its cell performance, using fillers in the nanoscale.

In the work presented by Shao et al. [108] comprised a novel electrolyte based on PEO, magnesium borohydride ($\text{Mg}(\text{BH}_4)_2$), and MgO nanoparticles. A key feature presented by this work was a high coulombic efficiency of 98% for Mg plating/stripping and high cycling stability. The experiments and modeling performed established a correlation between improved solvation of the salt and solvent chain length, chelation, and oxygen denticity. A further development in experimentation with this polymer revealed that it could be used in NCPE for other multivalent chemistry to delineate the ionic association and solvation interactions within these electrolytes.

Another approach for a casting technique by dry/solution free hot press is presented in the following studies as an alternate way of synthesis since no organic solvent as the medium for mixing ingredients is needed, which is the most significant difference from solvent casting [102]. The main steps for solvent-casting and hot-pressing are shown in Figure 9a,b. Thermocompression avoids contact with air during the process, which results in more stable productions. On the other hand, the solvent-casting method can disperse the ceramic fillers more uniformly, resulting in more ductile films. Besides, the residual liquid in this procedure can act as a plasticizer for the further performance of the SPE. These features need to be taken into consideration depending on the application the electrolytes will have.

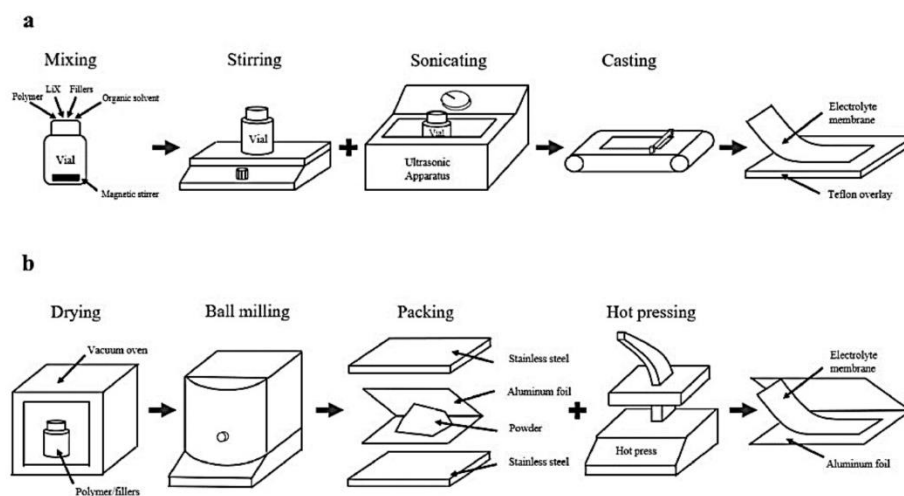


Figure 9. Schematic procedures for preparing solid polymer electrolytes by (a) solvent casting technique and (b) thermo-compression. Reproduced with permission from Nano Converg., 8, Feng et al. PEO based polymer-ceramic hybrid solid electrolytes: a review, 2, 2021 [102].

Thermocompression was implemented in the work done by Agrawal et al. [104]. The assembled electrolyte, composed of phases, has an SPE film of PEO and $\text{Mg}(\text{ClO}_4)_2$ salt, the first phase host matrix with a conductivity of $\sim 2.77 \times 10^{-6} \text{ S}\cdot\text{cm}^{-1}$. The second phase had MgO nano/micro-sized particles as active fillers and $\text{TiO}_2/\text{SiO}_2$ nano-sized particles as

passive fillers. The dispersion increased the room temperature conductivity of the SPE host by ~ 3 – 5 -fold. The values of cation transport, however, remained in the range 0.21–0.30.

Casting by hot-press technique was performed as the synthesis process in the research developed by Agrawal et al. [101], with a primary phase host composed of PEO and magnesium triflate and micro/nano-sized materials TiO_2 (passive filler) and MgO (active filler). The employment of all of these substances together achieved an enhancement in the room temperature conductivity of the SPE host. Characterization was performed with XRD, FT-IR, DSC analysis. The total ionic transference number data (~ 0.98 – 0.99) showed the predominantly ionic character of the materials employed. Analyzing the concentration vs. log of conductivity (Figure 10) obtained two maximum peaks that suggested the presence of two conductivity mechanisms in the system, previously discussed in this report with reference [81]. The first peak could be related to dissociating undissociated salt and ion aggregates (if existed) into free ions. The second s-peak was then attributed to forming a high conducting interfacial space-charge double layer around insulating filler nanoparticles that could correspond to a filler particle percolation threshold. It is also concluded that nanofillers were more effective in increasing the cation transport number than micro fillers, increasing the cation transport number t_+ .

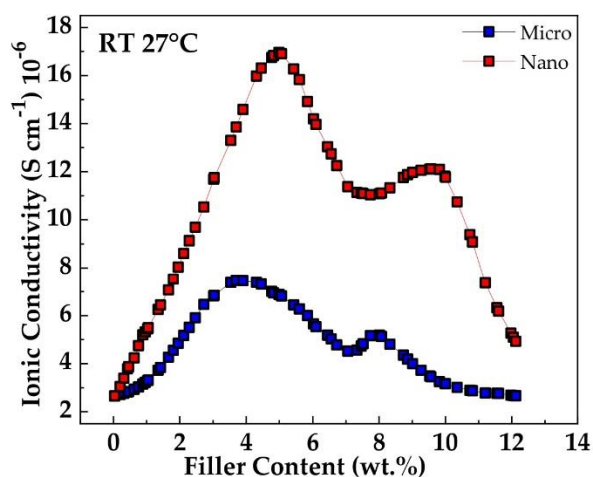


Figure 10. Active filler concentration-dependent conductivity variation for NCPE films: [80PEO: 20Mg(Tf)₂] + xMgO micro/nano. Reproduced with permission from Mater. Chem. Phys., 139, Agrawal et al., Investigations on ion transport properties of hot-press cast magnesium ion conducting Nano-Composite Polymer Electrolyte (NCPE) films: Effect of filler particle dispersal on room temperature conductivity, 410–415, 2013 [101].

One of the latest reports on electrolytes based on PEO for Mg batteries was reported by Zaky et al. [105], with the incorporation of Mg salts treated with gamma irradiation to improve the PEO-Mg salt particle sizes. The electrical conductivity evaluated was more than three orders of magnitude than pure PEO, with a maximum value of $3.63 \times 10^{-3} \text{ S}\cdot\text{cm}^{-1}$. The optimum ionic conductivity of MgO in the irradiated sample was obtained with 20 mL, while 30 mL was the best for un-irradiated. The addition of MgO also improved the electrochemical potential window to about -3.2 to 4.4 V .

3.2. Zinc-Ion Conduction

In terms of zinc batteries, some works have been developed with the use of PEO. They are summarized in Table 4. For this metal, the first attempts were also designed without the addition of nanofillers. Therefore, an SPE with the addition of zinc chloride (ZnCl_2) was developed by Carrilho et al. [109] in a cell composed of zinc and niobium pentoxide

(Nb₂O₅) as electrodes. Their studies were performed at a temperature of 55 °C, obtaining a conductivity of $2.7 \times 10^{-4} \text{ S}\cdot\text{cm}^{-1}$ and a cationic transference number value of 0.44 ± 0.05 .

Table 4. A summary of NCPEs composed of PEO for zinc batteries in solid-state.

Nanocomposite	Ionic Salt	Conductivity (S·cm ⁻¹) 10 ⁻³	Activation Energy (eV)	Electrochemical Stability Window (V)	Reference
No added	ZnCl ₂	2.7 *	-	2.60	[109]
Al ₂ O ₃	Zn(Tf) ₂	2.1	0.44	3.6	[110]
	Zn(Tf) ₂	~0.101	0.19	-	[111]
TiO ₂	ZnCl ₂	~100	0.087	-	[112,113]
SiO ₂	NH ₄ HSO ₄	0.61	-	-	[114]
ZnO	Zn(Tf) ₂	0.184	0.23	-	[115]
Zn Fe ₂ O ₄	NH ₄ SCN	~10 ⁻³	-	-	[116]

* Results obtained at 55 °C.

The cell testing showed a decrease in the cell voltage without attaining any constant value. This result suggested the discharge product was the result of a topochemical insertion. The capacity retention of the cell was observed to be very poor. After the second cycle, the cell was not able to retain its charge. Galvanostatic/potentiostat cycles were performed at a lower time (in discharges) and fixed potentials (in charges) to improve the latter result. After this, shallower discharges were obtained, resulting in a longer cycle life, with a less marked decrease in cell capacity at a constant voltage. Lifetime evaluation for the studied cell was 4.9 years if maintained at 55 °C, under non-operating conditions.

Agrawal et al. [114] designed two cells that employed PEO and NH₄HSO₄ and SiO₂ for the electrolyte that performed in two types of cells: MnO₂ + C and PbO₂ + V₂O₅ + C as cathodes, respectively. The researchers achieved an enhancement in the room temperature conductivity of polymer electrolyte approximately by an order of magnitude. Furthermore, it obtained a substantial increase in the mechanical strength of the films. The OCV was found to be in the range of 1.5–1.8 V for both batteries. The cell potential was stable through the discharges, but it discharged more quickly during higher current drain or low load resistance.

Gamma (γ) irradiation was presented as a novel technique to inhibit the crystalline phase in an electrolyte composed of PEO and ZnCl₂ as salt, with the addition of nanosized TiO₂ grains, by Turković et al. [112,113]. The polymer was subjected to γ-radiation from a Co-60 source. This approach was attempted since high-energy radiation could induce interchain linking of the polymer, inhibiting the crystalline phase in the polymer matrix. Small-angle X-ray scattering (SAXS) was recorded simultaneously with DSC, and wide-angle X-ray diffraction (WAXD) analyses were performed. Thanks to these techniques, it was obtained that the nanostructure of the γ-irradiated electrolyte changed during the crystalline-amorphous phase transition to a highly conductive superionic phase. Reduction in the T_g was observed, and ionic conductivity was enhanced, two desired changes in these processes. The conductivity of the nanocomposite prepared with irradiated powder ensured an improvement of two orders of magnitude compared to its homologous without irradiation.

An NCPE film was prepared using an SPE composed of PEO and zinc trifluoromethanesulfonate (Zn(Tf)₂) and then incorporating Al₂O₃ nano-filler particles by Karan et al. [111] using a completely dry hot-press cast technique. The complexation of the salt and the dispersal of filler in the host substantially increased the amorphous region, which supported the increase in ionic conductivity and cationic transport number. Nevertheless, the obtained values need to be improved for possible applications in high-energy batteries.

As another approach for employing nanocrystalline Al₂O₃, PEO was blended with polypropylene glycol (PPG) and Zn(Tf)₂ as dopant salt by Nancy et al. [110]. This matrix resulted in an enhanced ionic conductivity of one magnitude, compared to the previous work where this nanofiller was employed with alone PEO. This feature caused segmental

flexibility and an increase in the amorphous phase. The SEM, XRD, and DSC measurements showed that conductivity was controlled by segmental motions of the polymer chain and ion hopping mechanism at Lewis acid-base sites and at elevated temperatures exhibited Arrhenius behavior which was satisfactorily explained by free volume theory.

Zinc ferrite nanoparticles were presented as a relatively new approach for NCPEs by Agrawal et al. [116]. This nanofiller has been widely used in technological applications because of its high magnetic permeability in the radio frequency region and low core loss. In their research, they posited the changing of the bonding behavior of the system when compared to the original PEO. Herein, the decrease in crystallinity was confirmed by the DSC study of the system. The presumed hopping mechanism between coordinated sites, local structural relaxation, and segmental motion of the polymer was stated because of the increase of ionic conductivity with temperature. The rise in $\sim 3\text{--}4$ order of magnitude of ionic conductivity concerning the pure polymeric host confirmed its promising results for electrolyte applications.

The hot-press technique was attempted with ZnO active fillers by Karan et al. [115], who composed a two-layer electrolyte. The first layer obtained the highest conductivity of $1.09 \times 10^{-6} \text{ S}\cdot\text{cm}^{-1}$. A 5 wt % of ZnO revealed an optimum conduction composition with a conductivity of $\sim 1.84 \times 10^{-5} \text{ S}\cdot\text{cm}^{-1}$, meaning that the filler's dispersal causes an enhancement of one order. The overall enhancement of four orders of magnitude from the pure PEO was obtained. The battery in which the films were assembled performed well under a low current drain state.

Ultimately, the outlook of incorporating branched aramid nanofibers (BANFs) to PEO was investigated by Wang et al. [117]. This combination enhanced the effective suppression of dendrites and fast cation transport due to the high stiffness of the BANF network combined with the high ionic conductivity of soft PEO, resulting in high tensile strength. The resulting battery showed the ability to withstand elastic deformation during bending and plastic deformation and remain functional (Figure 11). There have been different types of batteries that have shown to be capable of elastic deformations [118–120]; the ability to withstand plastic deformations while retaining the charge storage functions was a novel feature presented in this work. These features set it apart from other promising storage devices, improving the safety of the battery and its resistance to impact.

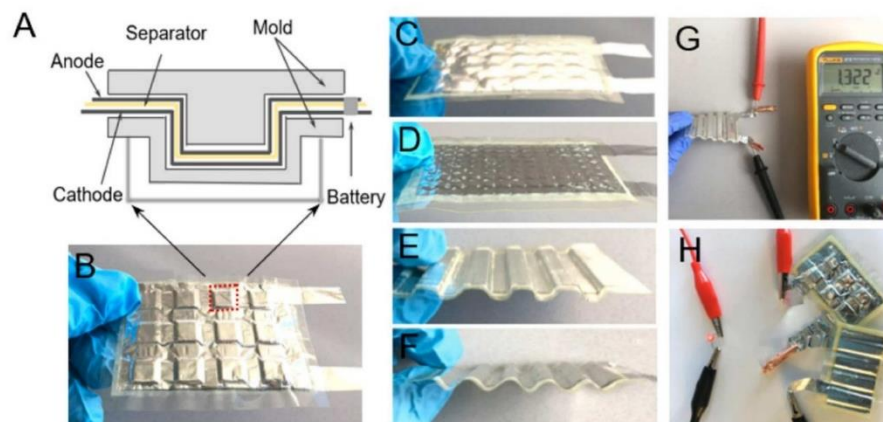


Figure 11. (A) Schematic of the mold used for plastic deformation studies. (B–F) Different plastically deformed shapes of Zn battery with solid-state biomimetic electrolyte. (G) The open-circuit voltage of Zn/PZB-931/ γ -MnO₂ battery with square wave shape plastic deformation. (H) LED light powered by the two serial structural batteries. Reproduced with permission from ACS Nano, 13, Wang et al., Biomimetic Solid-State Zn²⁺ Electrolyte for Corrugated Structural Batteries, 1107–1115, 2019 [117].

The review in this section of the paper has shown that active fillers are supposed to be the first choice when choosing ceramic additives for PEO electrolytes. Moreover, the most optimized concentrations for these nanofillers are between 10–20 wt % to obtain the highest conductivity of each medium. Besides, the mechanical strength is shown to get better with the doping of ceramic particles. Moreover, the interfacial stability is assumed to be improved due to the water-scavenging effect of the nanofillers, previously reported in similar systems designed with PEO [121] in lithium batteries. Hence, the overviewed hybrid systems are in sight of being the most effective approach for improving the performance of solid-state electrolytes.

4. Nanocomposite Polymer Electrolytes Based on Other Synthetic Polymers

As discussed, the development of electrochemical devices that make use of polymer electrolytes has gotten considerable interest. It is currently developing PEs with sufficiently high room temperature conductivity. The choice of the polymer is then known to depend principally on the presence of polar groups with sufficient electron donor power to form coordination with cations and a low hindrance to bond rotation [122], besides biodegradability and recyclability. Some synthetic polymers have been successfully used as a host material to prepare PEs for specific applications (Table 5). Few studies in the field have developed electrolytes with these polymers. However, the results presented left a precedent that deserves to be discussed for later studies that imply their use (Table 6).

Table 5. Chemical structures of some synthetic polymers employed in nanocomposite polymer electrolytes NCPEs.

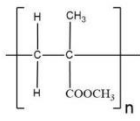
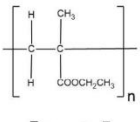
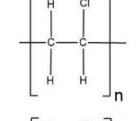
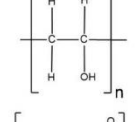
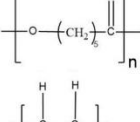
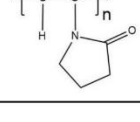
Name	Structure	Glass Transition Temperature (T_g) ($^{\circ}\text{C}$) [123]
Poly(methyl methacrylate) (PMMA)		105
Poly(ethyl methacrylate) (PEMA)		65
Poly(vinyl chloride) (PVC)		83
Poly(vinyl alcohol) (PVA)		80
Poly(ϵ -caprolactone) (PCL)		−66
Poly(vinylpyrrolidone) (PVP)		182

Table 6. NCPEs for magnesium and zinc batteries using other synthetic polymers.

Polymer	Nanocomposite	Ionic Salt	Conductivity (S·cm ⁻¹) 10 ⁻³	Activation Energy (eV)	Electrochemical Stability Window (V)	State	Reference
Magnesium							
PMMA + PVdF	MgO	Mg(Tf) ₂	1.29 × 10 ⁻²	-	-	Solid	[124]
PEMA	MgO	Mg(Tf) ₂	0.12	0.46	3.4	Solid	[125]
PVP	Al ₂ O ₃	MgCl ₂ · 6H ₂ O	1.22 × 10 ⁻²	-	-	Solid	[126]
Zinc							
PMMA/PVDF-co-HFP	SiO ₂	NH ₄ SCN	43	0.196	3.2	Gel	[127]
	SiO ₂	Zn(Tf) ₂	6.71	-	5.07	Gel	[128]
	Al ₂ O ₃ + TiO ₂	Zn(Tf) ₂	4.27	-	~4	Gel	[129]
PVC/PEMA	ZrO ₂	Zn(Tf) ₂	3.63	-	3.87	Gel	[130]
	SnO ₂	Zn(Tf) ₂	4.92	-	4.37	Gel	[131]
	ODAMMT	Zn(Tf) ₂	0.95	0.46	4.5	Gel	[132]
PCL	Al ₂ O ₃	Zn(Tf) ₂	0.25	-	-	Gel	[133]
	SiO ₂	-	5.73 × 10 ²	-	-	Gel	[134]
PVA	ZnO	NH ₄ NO ₃	4.71	0.92	-	Solid	[135]

Poly(methyl methacrylate) (PMMA) has been the focus of a few studies due to its beneficial effects on the stabilization of the electrode-electrolyte interface [136]. PMMA is non-biodegradable, and 100% recyclable [137]. Nevertheless, its recycling process is not environmentally viable due to the produced harmful products, limiting its use [138]. PMMA based GPEs happen to present very high transparency in the visible region. Furthermore, they present the ability to be diluted in various organic solvents [139]. However, they show poor dimensional stability. Although they appear solid-like, they exhibit flow properties. Poor mechanical properties offset a good conductivity achieved of such plasticized film at a high concentration of the plasticizer [140]. To overcome the drawbacks presented by PMMA film, it has been blended with other polymers to improve the segmental motion in polymer hybrid systems and hence a more flexible and elastic material.

Sarojini et al. [124] developed a blended polymer matrix of PMMA and PVdF for magnesium cells. It also included ethylene carbonate as a plasticizer, Mg(Tf)₂ as ionic salt and MgO as nanofiller. The best ionic conductivity increased the value by five orders of magnitude (~10⁻⁶ S·cm⁻¹). This result was obtained thanks to the addition of the nanofiller, causing high conduction pathways. Nevertheless, the result was deficient to be considered for any application.

A blended polymer matrix composed of PMMA and PVdF-co-HFP was developed by Mishra et al. [127] for the design of an NCPE system for Zn cells. XRD and SEM studies confirmed the desirable amorphous and porous structure for the electrolyte. The best ionic conductivity, 4.3 × 10⁻³ S·cm⁻¹, was obtained with 2 wt % of SiO₂. The conductivity variation for these films obeyed the behavior of having two maxima, previously reported in other works [81,101]. A proton battery was assembled with the electrolyte, employing Zn/ZnSO₄·7H₂O as anode and PbO₂/V₂O₅ as the cathode. The OCV for the battery was found at 1.55V. Besides, it showed rechargeability up to three cycles, and afterward, its discharge capacity faded away substantially.

Poly(ethyl methacrylate) (PEMA) is a very similar material to PMMA but with a lower T_g and has been shown to possess higher mechanical strength than PMMA [141]. Besides, PEMA shows excellent chemical and high surface resistance. In addition, it offers high optical transparency [142], a property that could be desired for devices where the electrolyte is located in a visible region of the device. PEMA was employed for an NCPE in work [125], along with magnesium triflate and 1-ethyl-3-methylimidazolium bis(trifluoromethylsulfonyl) imide (EMITFSI), dispersed with MgO for Mg cell electrolytes. SEM analysis confirmed the obtention of the amorphous nature of the films. In addition, TGA curves revealed that the more significant amount of MgO in NCPE slowed down the mass loss rate of decomposition products. However, the electrochemical potential window for the highest conducting sample assumed that magnesium ion was not predominantly the factor to the ionic conductivity enhancement of NCPE.

A blended polymer matrix was developed with PEMA and poly(vinyl chloride) (PVC), plasticized with zinc triflate, and EMIMTFSI ionic liquid was added for a novel NCPE by Candhadai et al. [128]. After that, it was doped with fumed SiO_2 as a nanofiller. This film exhibited the highest ionic conductivity value of $6.71 \times 10^{-4} \text{ S}\cdot\text{cm}^{-1}$ for a 3 wt % SiO_2 . The increment of the amorphous phase was confirmed by XRD analysis. It resulted in slight progress in the zinc ion transport number and a wide ESW of $\sim 5.07 \text{ V}$. This value ensured feasible zinc stripping/plating in the redox process involved. TG and DSC ascertained the improved thermal stability up to 180°C and the reduction in T_g . The exact blend, PVC and PEMA, was filled with nano-sized fillers Al_2O_3 , TiO_2 in the report by Prasanna et al. [129] for a zinc rechargeable battery. A high transport number value of 0.67 was obtained. From the studies analyzing glass transition temperature, the addition of fillers attenuated the values obtained, effect understood in terms of the obstruction of the polymer chains by the formation of cross-linking centers due to the interaction between the Lewis acid groups of the ceramic particles and the polar groups of the polymer chains.

Based on the previous work, Prasanna et al. [130] continued the research by changing the nanofiller employed, being zirconia (ZrO_2) the object of the study. The zinc ion transference number of 0.66 was almost the same obtained before with Al_2O_3 and TiO_2 . DSC and TG analysis confirmed the improved thermal behavior of ZrO_2 added GPE compared to that of filler-free gel electrolytes. The interaction and complexation of the polymer components were probed by ATR-FT-IR analysis (Figure 12). The amplified coordination of Zn^{2+} cations and ceramic phase with C=O group was evidenced by the existence of a peak at 1721 cm^{-1} ascribed to the C=O group of PEMA in Figure 12b–e, upon the addition of 1 wt % nanofiller. The oxygen atoms of C=O group in PEMA generally acts as an electron donor resulting in the formation of a coordinate bond with zinc ions, and the addition of fillers enhances the intensity of this band, through hydrogen bonding between carbonyl oxygen (C=O) and the hydroxyl surface group (Zr-OH) of ZrO_2 thus forming $-\text{Zr-O} \dots \text{H} \dots \text{O}=\text{C}-$ species. Ultimately, it was observed better thermal stability up to 180°C , and ESW to 3.87 V .

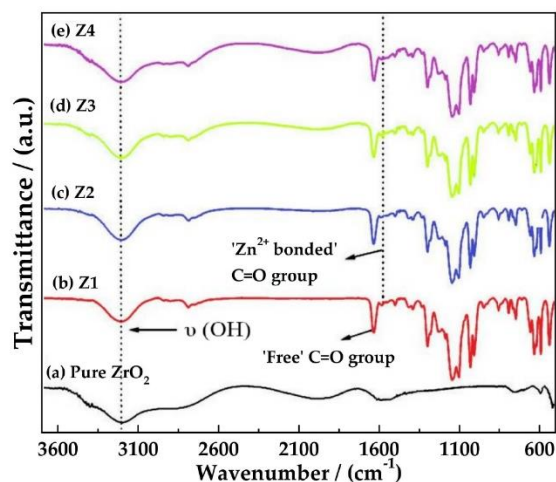


Figure 12. Room temperature ATR-FT-IR spectra of (a) pure ZrO_2 (b–e) NCPEs with varying concentrations of ZrO_2 in the wavenumber ranging from 4000 to 400 cm^{-1} at room temperature. Reproduced with permission from Polym. Compos., 40, Sai Prassana et al., PVC/PEMA-based blended nanocomposite gel polymer electrolytes plasticized with room temperature ionic liquid and dispersed with nano- ZrO_2 for zinc ion batteries, 3402–3411, 2019 [130].

These authors, in another work, incorporated the use of nano-sized tin oxide (SnO_2) [131]. XRD and SEM studies were performed, confirming the existence of porous morphologies.

Furthermore, the dispersion of SnO_2 improved the thermal behavior of the composite system to 185°C , which was ascertained by TG analysis. The ESW was found to be 4.37 V. Together with a feasible zinc plating/stripping process of the gel composite sample, these features implied good potential applicability of such films as electrolytes.

Poly(vinylpyrrolidone) (PVP) is a biocompatible polymer. It is a virtually non-biodegradable polymeric lactam with an internal amide bond. The tertiary amide carbonyl groups of PVP present a Lewis base character such that PVP can form a variety of complexes with a wide range of inorganic salts [143]. It is also hygroscopic and easily soluble in water and organic solvents such as alcohol. It presents a high T_g of 170°C , because of the rigid pyrrolidone group. However, water can be employed as a plasticizer lowering this value to below 40°C [144]. Besides, it is inert, shows good environmental stability, easy processing, excellent transparency, and a strong tendency for complex formation with smaller molecules [145]. This polymer is studied because of its thermal stability and cross-linked composites having high mechanical strength. It also has good mechanical and electrical characteristics.

Basha et al. [126] developed an SPE composed of PVP and $\text{MgCl}_2 \cdot 6\text{H}_2\text{O}$, with the addition of Al_2O_3 particles. Structural analysis showed orthorhombic lattice as evidence of a semi-crystalline nature present in the films. Optical analysis was used to identify the optical band gap of the material in the transmitting radiation. Graphs were plotted between absorption coefficient α , $(\alpha h\nu)^2$ and $(\alpha h\nu)^{1/2}$ as a function of $h\nu$ (Figure 13a–c) to calculate bandgap energy values. The optical properties revealed that for the composition of 15%, the bandgap energy was the lowest among all weight ratios. Hence, it was obtained that the films with the lowest activation energy had the highest conductivity. UV–Vis spectroscopy was performed in the 300–700 nm (Figure 13d). This tool showed to be helpful for the identification of intra molecular vibrations of inorganic complexes in solution. Two spectral peaks are observed at 350 nm, which is due to the π – π^* transition. Besides, a small peak was at 425 nm, correlated with the benzene and quinone rings in the polymer chain.

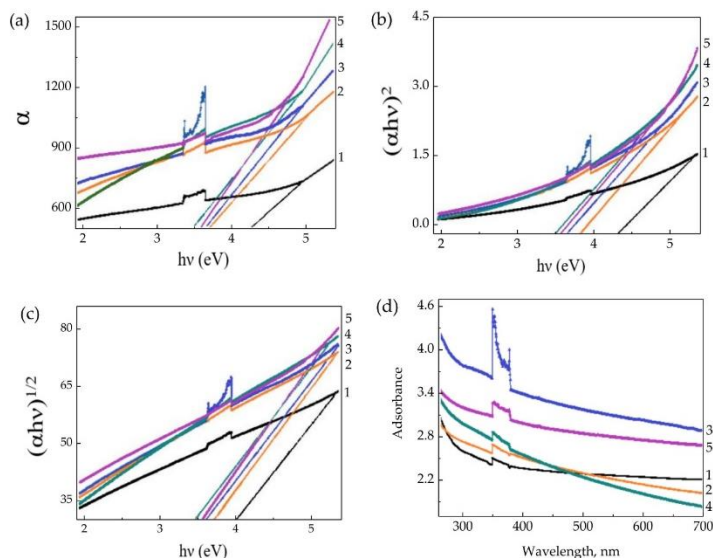


Figure 13. (a) $h\nu$ vs α plots, (b) $h\nu$ vs $(\alpha h\nu)^2$ ($\times 10^7$) plots and (c) $h\nu$ vs $(\alpha h\nu)^{1/2}$ plots and (d) UV–Vis spectra of polymer electrolyte films for different wt % ratios of pure PVP and polymer electrolytes: (1) pure PVP, (2) (95:5), (3) (90:10), (4) (85:15), (5) (80:20), Reproduced with permission from Polym. Sci.—Ser. A., 59, Shahenoor Basha et al., Optical and dielectric properties of PVP based composite polymer electrolyte films. 554–565, 2017 [126].

Poly(vinyl alcohol) is a semi-crystalline synthetic biodegradable polymer from petroleum sources that presents various hydrophilic functional hydroxyl groups, which can favor water absorption. As a result, it shows a very high dielectric strength ($>1000 \text{ kV mm}^{-1}$), good charge storage capacity, good mechanical properties, high tensile strength, abrasion resistance, and dopant-dependent electrical and optical properties [146]. In addition, PVA has several advantages, such as high hydrophilicity, high gel strength, nontoxicity, and low cost [147]. Fan et al. [134] designed a zinc-air battery (ZAB) assembled with a semi-solid/solid-state electrolyte constructed with PVA and the optimum addition of SiO_2 . The ZAB presented excellent cycling stability over 48 h, stable discharge performance, and relatively high-power output. Flexibility was an outstanding feature obtained with no degradation through bending conditions. In the results, this cell was able to power a handheld electric fan, a light-emitting diode screen, or even a mobile phone (Figure 14), showing its promising potential for high-performance ZABs along with high safety, cost-effectiveness, excellent flexibility, electrolyte retention capability, as well as good thermal and mechanical properties.

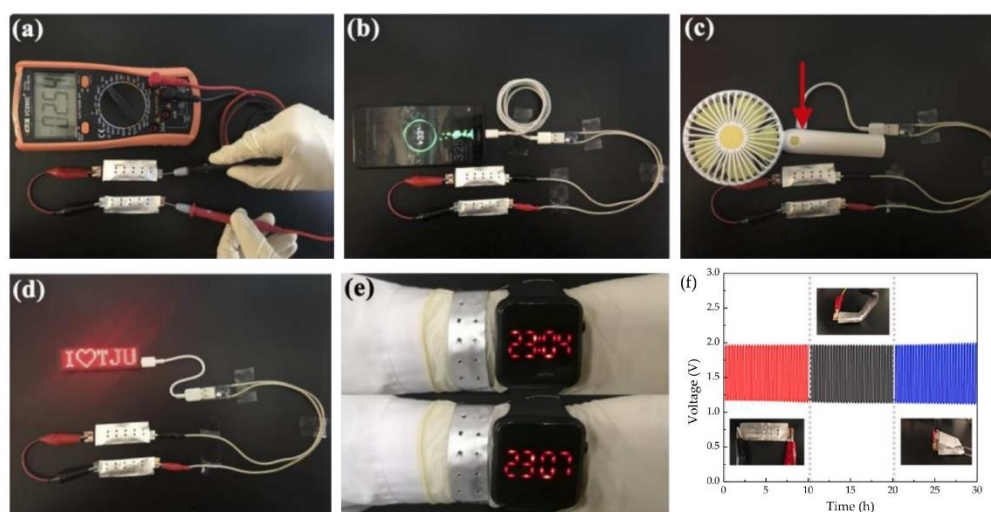


Figure 14. (a) Open circuit potential demonstration with two ZABs in series. A demonstration of (b) a mobile phone, (c) a handheld electric fan, and (d) an LED screen powered by two ZAB sets. (e) Photographs of an LED watch powered by a fabricated bracelet-type ZAB. (f) GCD curves of the ZAB under different bending conditions with corresponding photographs. Reproduced with permission from Nano Energy, 56, Fan et al., Porous nanocomposite gel polymer electrolyte with high ionic conductivity and superior electrolyte retention capability for long-cycle-life flexible zinc–air batteries, 454–462, 2019 [134].

The PVA electrolytes filled with nano ZnO transport parameters were conducted by Abdullah et al. [135] using the Rice–Roth model for proton-conducting batteries, explaining that the moderate addition of nanofiller enhances ionic conductivity by increasing mobility and number density of mobile proton ions. Another ZAB was designed to implement MWCNTs into the electrodes by Wang et al. [148], to improve the performance of the cell. It was found that MWCNTs were effective conductive additives in the anode as they bridged the zinc particles. The electrolyte was composed of poly(acrylic acid) (PAA) and PVA. A limitation for this NCPE was water evaporation because of the volatility character of the films.

Poly(ϵ -caprolactone) (PCL) is a biodegradable polymer that is nontoxic and widely used in biomedical applications because of its considerable degradation time in an aqueous medium and contact with microorganisms [149]. It is a synthetic thermoplastic polymer derived from crude oil and synthesized through the polymerization of ϵ -caprolactone monomer by a stannous octanoate catalyzed ring-opening mechanism [150]. It presents good mechanical properties [151]. Furthermore, it is a candidate polymer host for ionic

conduction because it contains a Lewis base (ester oxygen) that can coordinate cations due to carbonyl functional groups in its backbone structure.

PCL was doped with zinc triflate and octadecylamine modified montmorillonite (ODAMMT) nano clay by Sownthari et al. [132]. The maximum electrical conductivity was $9.5 \times 10^{-5} \text{ S}\cdot\text{cm}^{-1}$ for 15 wt % loadings of nano clay into the polymer-salt complex. XRD and DSC analysis confirmed the decrease in crystallinity. The electrolyte degradation happened in 90 days, making this electrolyte a promising candidate for battery applications.

An optimized NCPE composed of PCL, zinc triflate and the incorporation of Al_2O_3 was prepared by Sownthari et al. [133]. The complexation of polymer, salt, and filler was confirmed from FT-IR studies. The various relaxation processes associated with the conductivity mechanism were also analyzed during the investigation. From this, it was revealed that the chain length of polymer PCL was so long that the bond rotation was favorable only at low frequency, so the filler increased the amorphicity within the polymer network, and thus the rotation becomes feasible, making a shift toward higher frequency side which meant a shorter relaxation time. The increase of conductivity was mainly due to an apparent rise in the number density of charge carriers which was confirmed from FT-IR and dielectric studies. The increasing trend of dielectric constant matched well with the conductivity variation as a function of filler concentration.

5. Nanocomposite Polymer Electrolytes Based on Biopolymers

Most synthetic polymers are detrimental to the environment because of their non-biodegradability [152]. Consequently, the application of biodegradable polymers in energy storage devices is currently paramount in designing the next generation of batteries to reduce environmental impact. For a biobased polymer to be considered ecological, its origin and production technique are also of importance. Cellulose, starch, chitosan, agar, and carrageenan are some of the most common polymers used as hosts for batteries [51] (Table 7).

Table 7. Chemical structures of some biopolymers employed in nanocomposite polymer electrolytes NCPEs.

Name	Structure	Glass Transition Temperature (T_g) ($^{\circ}\text{C}$) [123]
Agar		98
Carrageenan		41
Cellulose		220
Chitosan		200
Starch		227
	Amylopectin Amylose	

Among the wide range of applications available for batteries, there is a need to design biocompatible batteries for implants that need a power source to perform their functions in the biomedical field. They go from sensing or stimulation to influencing critical biological processes like wound healing, tissue regeneration, or brain activity. Unfortunately, little work has been done so far to develop bioresorbable electronics or self-deployable power sources [153–155]. However, the present review pretends to show the promising results obtained so far with electrolytes that, with some modifications, could be employed in the biomedical field. Table 8 summarizes the features presented by these NCPEs.

Table 8. Polymer electrolytes based on biopolymers for electrochemical applications.

Polymer	Nanocomposite	Ionic Salt	Conductivity (S·cm ⁻¹) 10 ⁻³	Activation Energy (eV)	Electrochemical Stability Window (V)	State	Reference
Cellulose (NFC)	No added	-	0.1	-	-	Hydrogel	[156]
Cellulose acetate	SiO ₂	NH ₄ BF ₄	7.9 × 10 ⁻³	-	-	Gel	[157]
	TiO ₂	NH ₄ BF ₄	1.4 × 10 ⁻²	0.12	-	Gel	[158]
	TiO ₂	LiClO ₄	3.06 × 10 ⁻⁴	-	-	Solid	[159,160]
Hexanoyl Chitosan	TiO ₂	LiClO ₄	3.1 × 10 ⁻⁴	0.08	-	Solid	[161]
	SiO ₂	LiClO ₄	1.96 × 10 ⁻⁴	0.12	-	Solid	[161]
	Al ₂ O ₃	NH ₄ SCN	5.86 × 10 ⁻⁴	-	-	Solid	[162]
Chitosan	SiO ₂	Li(Tf) ₂	4.38 × 10 ⁻⁵	0.26	-	Solid	[163]
	ZrO ₂	LiClO ₄	3.6 × 10 ⁻⁴	-	-	Solid	[164]
Potato Starch	No added	Mg(C ₂ H ₃ O ₂) ₂	1.12 × 10 ⁻⁵	-	-	Solid	[165]
Rice Starch	TiO ₂	LiI	3.6 × 10 ⁻⁴	0.22	-	Solid	[166]
Corn Starch	SiO ₂	LiClO ₄	1.23 × 10 ⁻⁴	0.25	3.0	Solid	[167,168]
Corn Starch/Chitosan	No added	NH ₄ Cl	5.11 × 10 ⁻⁴	-	-	Solid	[169]
Sago (starch)	No added	KOH	4.45 × 10 ⁻¹	-	-	Gel	[170]
κ-carrageenan	No added	-	3.32 × 10 ⁻²	-	-	Solid	[171]
	No added	MgCl ₂	4.76 × 10 ⁻³	-	1.94	Solid	[172]
	No added	NH ₄ SCN	1.03 × 10 ⁻³	0.25	-	Solid	[173]
Agar	No added	Mg(Tf) ₂	1.0 × 10 ⁻³	-	-	Solid	[174]
	TiO ₂	LiI	5.12 × 10 ⁻⁴	-	-	Solid	[175]

5.1. Cellulose

Cellulose is a biopolymer known to be the most abundant polymer in nature. It presents a molecular weight ranging from 300,000 to 500,000 Da. Its molecule offers three hydroxyls groups that can be modified to make the molecule water-soluble [176]. Many cellulose derivatives can be obtained from this modification, classified between cellulose ethers and cellulose esters. Cellulose has been applied in batteries for electrodes or separators as GPEs [176] and as binders/surface modifiers for graphite anodes for batteries. Moreover, synthetic polymers often need high-temperature processing stages to prepare GPEs, while with nanofiber cellulose (NFC) hydrogels, they can be cured at temperatures close to ambient temperature [177].

Cellulose was never intensively used as a polymer electrolyte in advanced batteries until Johari et al. [157] reported an NCPE based on cellulose acetate dispersed with SiO₂ for a battery with the configuration Zn/composite cellulose electrolytes/MnO₂. The results showed the expected increase in ionic conductivity and an OCV of 1.6V. The constancy of the assembled cell was tested for 24 hours. However, no further electrochemical studies were performed. In a posterior work [158], the same authors reported an NCPE based on cellulose acetate dispersed with nanosized TiO₂ particles for a battery with the same composition as the previous one. The OCV characteristic of the cell at room temperature showed that the initial voltage of the cell is 1.55 V, dropping to 1.40 V within the first two hours of assembly. The cell voltage was observed to have stabilized at this voltage, and the OCV remained constant at 1.40 V for a period of 24 h. The fabricated cell was reasonably stable in the open cell condition.

An NFC hydrogel was synthesized by Poosapati et al. [156] by adding gelatine, polyacrylic acid (PAA), and potassium hydroxide (KOH) as additives. The hydrogel with the most appropriate amounts of additives got an ionic conductivity of 0.1 S·cm⁻¹, representing an increase of five orders of magnitude from the pristine hydrogel. This report concluded

that the small amounts of additive present helped enhance the mechanical stability and ionic conductivity by changing the degree of crystallinity and ionic concentration in the hydrogel layers.

Another approach for cellulose applications has been made by employing it as a soaked separator electrolyte. Zhang et al. [178] studied a functionalized with quaternary ammonium (QA) laminate-structured nanocellulose/GO membrane, developed for a hydroxide-conducting electrolyte for zinc-air batteries. Herein, cellulose was utilized to interconnect the framework to integrate GO into a flexible membrane with higher water content. Achieving a laminated cross-linked structure eliminated the risk of pushing water out of the membrane when handling or bending, besides good adhesion to the electrodes. The membrane's enlarged d-spacing enhanced the mobility of hydroxide ions by vehicle mechanism, besides its lower activation energy. Water molecules also could have caused mobility by the Grotthuss mechanism. At 70 °C, the ionic conductivity of 0.0588 S·cm⁻¹ and an OCV of 1.4 V was achieved.

5.2. Chitosan

Chitosan is environmentally friendly and an excellent membrane-forming polymer material. It is known for being non-toxic, biodegradable, and biocompatible, making it a good solution for many electrochemical applications that can be modified to get electrolytes. Chitosan is produced from the deacetylation reaction of chitin. Chitin is a natural polysaccharide generally found in the exoskeleton of arthropods and various fungi [179]. Chitosan is widely applied in lots of fields, as in biotechnology, biomedicine [180]. Its molecule presents several polar groups, such as hydroxyl and amino groups, forming complexes with inorganic salts. However, pristine chitosan shows a very low ionic conductivity (10⁻⁹ S·cm⁻¹) [181], the fact that it is tried to be enhanced by the addition of salts and fillers. Very little work has been done for chitosan NCPE applied in zinc or magnesium batteries. However, some authors have endeavored to implement nanofillers for lithium electrolyte applications [160,182–188], so the most noteworthy ones are now discussed.

Hexanoyl chitosan was employed as a polymer matrix with TiO₂ as filler and lithium perchlorate (LiClO₄) as doping salt to design NCPEs by Muhammad et al. [159]. The electrolyte system was characterized by impedance spectroscopy. It was shown that the increment in conductivity was caused by the increase in the mobility of free ions and the increase in the free ion concentration. The XRD results obtained for this electrolyte in a posterior work of the authors [189] confirmed the decrease in crystallinity, leading to the expected increase in conductivity that was modeled by the Rice and Roth model.

A system of the same composition based on hexanoyl chitosan + LiClO₄ + TiO₂ was reported by Winie et al. [190], who reported the complexation of the polymer and the salt as a result of the shift of N(COR₂), O=C-NHR, and OCOR bands of hexanoyl chitosan to lower wavenumbers, and supported the use of chitosan as a polymer host in terms of the presence of lone pair electrons at the nitrogen and oxygen atoms where inorganic salts can be solvated. Results showed that both dielectric constant and dielectric loss decreased with increased frequency and increased with increased temperature.

Aziz et al. [162] reported novel chitosan-ammonium thiocyanate (NH₄SCN) complexes doped with nanosized Al₂O₃ filler. FT-IR and XRD confirmed the complexation between the cation of the salt and the donor atom in chitosan polymer. The high filler content increased the T_g value since it increased the crystallinity of the sample, as depicted by XRD. Alumina was employed in chitosan and lithium triflate (Li(Tf)₂) [191], where the AC conductivity studies showed the promising features already told for this kind of biopolymer system.

In a work by Navaratnam et al. [163] chitosan was used as the host polymer in a designed system consisting on LiCF₃SO₃ as the dopant salt, EC and PC as the plasticizers, and different concentrations of SiO₂ as the inorganic filler. The obtained ionic conductivity for this system was very low to consider for practical applications. However, in a following article by Rosli et al. [161], it was presented a study comparing the type of filler and their effect on the electrical properties in the polymer electrolyte, resulting in a

higher conductivity enhancement brought about by TiO_2 compared to SiO_2 for the system hexanoyl chitosan- LiClO_4 polymer electrolyte. This finding can be understood by the more acidic nature of TiO_2 , which promoted a greater degree of salt dissociation. Zirconia was employed as a nanofiller for the previous electrolyte composition of LiClO_4 as salt and chitosan by Sudaryanto et al. [164], and the films were characterized by XRD and EIS. The obtained results were quite comparable to the previously discussed work since the ionic conductivity was slightly higher. Besides, the obtained ion transference number of 0.55 was considered quite enough to apply it in an ion battery.

For magnesium batteries, a GPE based on chitosan, magnesium triflate, and EMITf was developed by Wang et al. [192]. The results showed that the Mg-ion mechanism was the complexation and decomplexation of Mg^{2+} with amine band (NH_2) from chitosan. The relaxation time of the electrolyte membrane was as low as 1.25×10^{-6} s, indicating that the mobility of ions was relatively high. The electrochemical properties of this GPE, presented in Table 7, were considered a precedent for future practical applications, and some latest reports were reported until the present date for chitosan polymer electrolytes for EDLC devices [193–195]. Still, they are out of the scope of this review. To the best of our knowledge, no studies are reporting NCPEs made of chitosan for magnesium batteries.

5.3. Starch

Starch is one of the most popular renewables and biodegradable polymers found as granules in plants. It is composed of a mixture of linear amylose ($\alpha(1,4)$ linked anhydroglucose) and branched amylopectin ($\alpha(1,6)$ linked anhydroglucose) polysaccharide chains. At the same time, it can undergo derivatization reactions. It is introduced some functional groups into the starch molecule, resulting in the alteration of its gelatinization, pasting, and retrogradation behavior [196]. Starch is known to be abundant in nature due to its wide variety of sources, consisting of several kinds of food plants from which it comes. Hence, besides its application in the food industry, it is applied industrially as binders and adhesives, absorbents and encapsulants, as coatings and sizes on paper, textiles, and carpets [197]. In addition, efforts have been made to use starch to create thermoplastic materials [198,199].

In terms of application for magnesium batteries, potato starch was doped with magnesium acetate ($\text{Mg}(\text{C}_2\text{H}_3\text{O}_2)_2$) [165], and the effect of glycerol and 1-butyl-3-methylimidazolium chloride (BmImCl) was studied in terms of conductivity and dielectric properties. It was concluded that too much plasticizer causes the salt to recrystallize, causing the cations to hardly coordinate at the polar atoms, decreasing the ionic conductivity. The effect of salt concentration in the biopolymer electrolyte matrix is demonstrated through dissociated ions model (Figure 15). Rice starch was employed for an NCPE composed of lithium iodide (LiI), 1-methyl-3-propylimidazolium iodide (MPII) as an ionic liquid, and TiO_2 nanopowder by Khanmirzaei et al. [166]. The resulting electrolyte was employed to build a DSSC, showing an efficiency of 0.17 at $1000 \text{ W} \cdot \text{m}^{-2}$ light intensity.

From the variety of sources available for starch, a biodegradable corn starch–lithium perchlorate (LiClO_4)-based SPE with the addition of nano-sized fumed silica [167] was prepared by solution casting technique. FT-IR results confirmed some complexation between corn starch, LiClO_4 , and silica. Excessive SiO_2 content decreased the ionic conductivity through agglomeration of particles and cross-linking in the polymer, showed by DSC, TGA, and SEM studies. The same investigation group reported the NCPE applied in electric double-layer capacitors (EDLCs) [168]. The device was characterized by CV, galvanostatic charge-discharge, and AC impedance spectroscopy. The discharge characteristics were almost linear, which confirmed the capacitive behavior of the EDLC cell. The fabricated EDLC cells performed good cyclability up to 500 cycles with more than 90% coulombic efficiency.

A solid electrolyte designed by blending chitosan with corn starch for application in an electrochemical double-layer capacitor (EDLC) and proton batteries was reported [169]. From transference number measurements (TNM), the electrolytes' transference number of ion (t_{ion}) showed that ion is the dominant conducting species. The transference number

of cation (t_+) for the highest conducting electrolyte was found to be 0.56. Linear sweep voltammetry (LSV) result confirmed the suitability of the highest conducting electrolyte to be used to fabricate EDLC and proton batteries. The open-circuit potential (OCP) of the primary proton batteries for 48 h was lasted at (1.54 ± 0.02) V, while that of secondary proton batteries lasted at (1.58 ± 0.01) V.

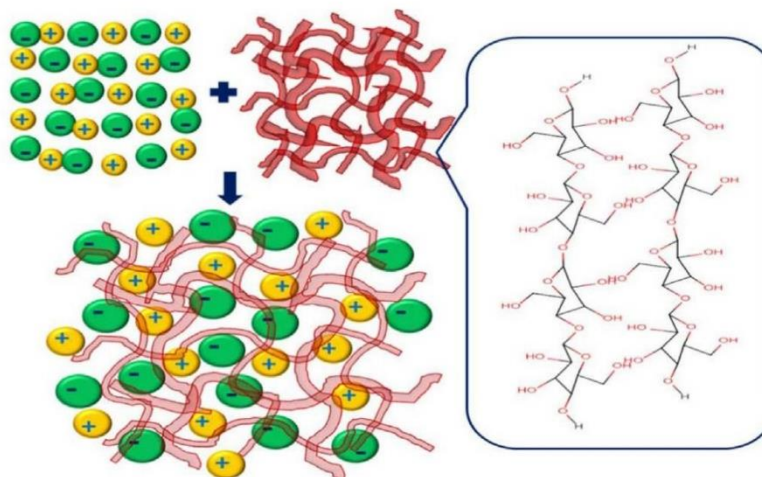


Figure 15. Schematic diagram showing ion dissociation in biopolymer salt matrix. Reproduced with permission from *Renew. Sustain. Energy Rev.*, 65, Singh et al., Perspectives for solid biopolymer electrolytes in dye sensitized solar cell and battery application, 1098–1117, 2016 [50].

Masri et al. [170] used sago powder (starch from various tropical palms) to design a sago-KOH GPE. Then, it was employed in an experimental Zn-air battery using a porous Zn electrode as the anode. The battery showed outstanding discharge capacity and practical capacity obtained of $505 \text{ mAh} \cdot \text{g}^{-1}$. In parallel, Zahid et al. [200] designed a GPE for zinc-air batteries based on cassava (*Manihot esculenta*), one of the most essential starch sources in tropical and subtropical areas. The highest ionic conductivity obtained was $4.34 \times 10^{-3} \text{ S} \cdot \text{cm}^{-1}$.

5.4. Carrageenan

Carrageenan is a linear sulfated polysaccharide polymer extracted from a marine red seaweed called Rhodophyceae and *Kappaphycus alvarezii*. It is consisted of repeating units of (1,3)-D-glucopyranose and (1,4)-3,6-anhydro- α -D-glucopyranose [201]. Besides, based on the number of sulfate groups, it is classified into three types: Kappa (κ)-carrageenan (one sulfate per disaccharide), iota (ι)-carrageenan (two sulfates per disaccharide), and lambda (λ)-carrageenan (three sulfates per disaccharide). Carrageenan is hydrophilic due to the presence of hydroxyl groups and the mentioned sulfate groups in it. In terms of electrochemical properties, this polymer is known for being in rich hydroxyl groups and oxygen atoms which are essential for interaction and coordination with cations [202]. Carrageenan has been used in various applications, including food, pharmaceutical, and cosmetic industries as viscosity builders, gelling agents, and stabilizers [203], even proving to have anti-tumor and anti-angiogenic activity [204], besides being applied in drug delivery systems and other biomedical applications [205]. In this field, Sabbagh et al. [206] have investigated the nanocomposite positive effects on structural, functional, morphological, and thermal properties of carrageenan hydrogels, obtaining promising results for drug-delivery systems. Moreover, it is known that carrageenan could be used as a prominent electrolyte in electrochemical devices with suitable modifications.

A rechargeable quasi-solid-state zinc ion battery using κ -carrageenan bio-polymer electrolyte was reported by Huang et al. [171]. The mechanical robustness of the electrolyte was

reinforced by using a rice paper scaffold, which reduced the chances of short circuits as well. The κ -carrageenan electrolyte was found to be highly conductive. Furthermore, electrolyte production did not need water and oxygen-free environment or other protection measures, which is ideal for scaling up production. The zinc ion battery assembled with this biopolymer electrolyte also showed excellent cycling stability; 80% of its initial capacity still remained even the cyclic number extended to 450 cycles at $6.0 \text{ A} \cdot \text{g}^{-1}$ (Figure 16a). The morphology of cathode and anode materials remained after 450 cycles, almost unchanged compared to the morphology of the pristine MnO_2 and Zn (Figure 16b,c). Experimental results showed that the batteries maintained the discharge profile and AC impedance spectra after the test (Figure 16d). Besides, after 300 bending cycles, 95% capacity was retained (Figure 16e). This work brought new research opportunities in developing low-cost, flexible solid-state zinc ion batteries using green natural polymer, besides being capable of powering a timer under bending condition (Figure 16f), and also powered a timer when the entire device was immersed in water, demonstrating its good waterproofness (Figure 16g).

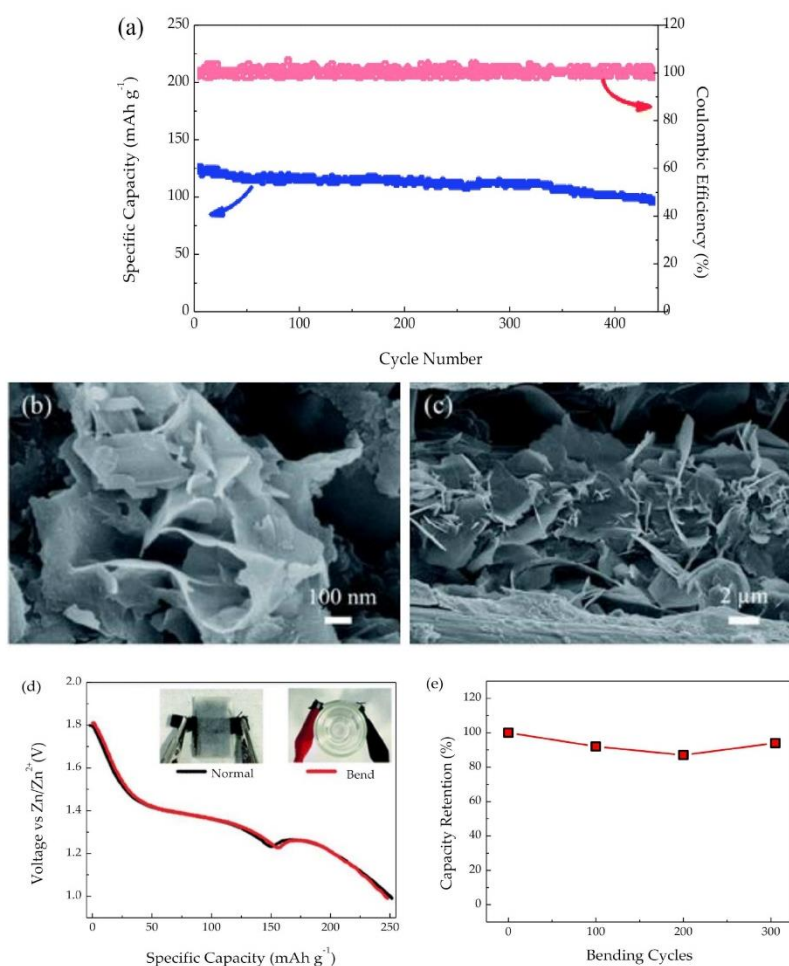


Figure 16. Cont.

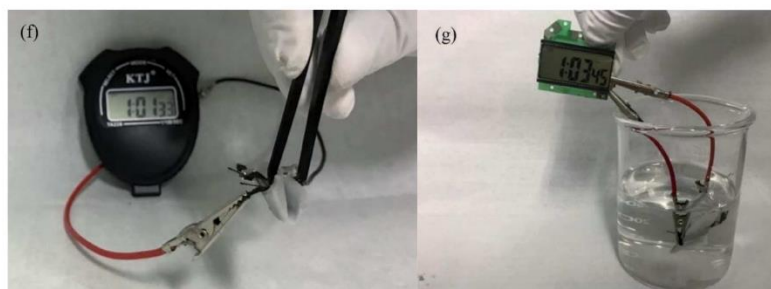


Figure 16. (a) Cycling stability of the solid-state ZIBs with KCR electrolyte cycled at $6.0 \text{ A} \cdot \text{g}^{-1}$ and corresponding coulombic efficiency. SEM images of (b) the MnO_2 cathode and (c) the electroplated Zn anode after 450 charge/discharge cycles. (d) Discharge curves under normal and bending conditions. (e) The bending test of solid-state ZIBs with KCR electrolyte for 300 cycles. (f) A solid-state ZIB with KCR electrolyte powers a timer under 180 degrees of bending conditions. (g) A solid-state ZIB with KCR electrolyte powers a timer when the battery is fully immersed in the water. Reproduced with permission from RSC Adv., 9, Flexible quasi-solid-state zinc ion batteries enabled by highly conductive carrageenan bio-polymer electrolyte, 16313–16319, 2019 [171].

For magnesium ion conduction, an SPE consisted of κ -carrageenan with MgCl_2 salt was designed by Sangeetha et al. [172], employing it in a primary magnesium battery. The resulting OCV for the battery was 2.17 V. In another report, κ -carrageenan containing tri-iodide/iodide redox couple was modified for dye-sensitized solar cell applications with nanofillers such as TiO_2 , iron (III) oxide Fe_2O_3 , and halloysite by Chan et al. [207]. For this system, the addition of various fillers to the PE system increased the dissociation of iodide ions and improved the ionic conductivity of the cells. DSSC characterization revealed a low efficiency due to relatively high charge transfer resistances at the TiO_2 /dye/electrolyte interface.

5.5. Agar

Agar is defined as a strong gelling hydrocolloid from marine algae. It is constituted by repetitive units of D-galactose and 3,6-anhydro-L-galactose, with few variations and low content of sulfate esters [208]. Agar is widely known because of its gelling power, based exclusively on the hydrogen bonds formed among its linear galactan chains, providing excellent reversibility. Its unique properties make it suitable for many applications, especially in preparing microbiological culture media [209]. It is widely used in the food industry, in cosmetics, and in microbiology [210]. In terms of electrochemical properties, agar forms a slightly viscous solution on dissolving in hot water and then turns into a thermo-reversible gel when cooled down. Agar attracts attention because of its best film-forming capability, used in synthesizing agar hydrogel used as an electrode binder in fuel cells [211].

A novel PE based on agar and doped with NH_4SCN was prepared for zinc cells by Selvalakshmi et al. [173]. The obtained results ensured that it is a good candidate for a low-cost biopolymer electrolyte membrane for fuel cell applications and solid-state devices. Similarly, Alves et al. [174] prepared a PE-based on agar doped with magnesium triflate for magnesium ion conduction, but the obtained results were not suitable for practical applications.

In terms of the implementation of nanofillers, some studies of agar applied in electrolytes for dye-sensitized solar cells have been presented. A polysaccharide GPE composed of agar in 1-methyl-2-pyrrolidinone (NMP) as a polymer matrix, LiI /iodine (I_2) as a redox couple, and TiO_2 nanoparticles as fillers were reported by Yang et al. [212]. Results showed that optimizing the electrolyte composition, such as agar and TiO_2 concentration, is necessary to improve the energy conversion efficiency of the DSSCs. Likewise, similar results were obtained for the same electrolyte system by Wang et al. [175], where the effects of LiI concentration were analyzed.

All the presented results so far show that NCPEs based on biopolymers solve the issues presented by all the kinds of PEs (increasing the low ionic conductivities and improving the mechanical properties). Furthermore, nanofillers have been shown to help prevent the dissolution of the salts provoked by the polar groups presented in the polysaccharide structure of most of the studied biopolymers, enhancing the ionic conductivity. Moreover, in contrast to the synthetic polymers mentioned in the previous sections, the presence of a wide variety of functional groups in biopolymers make them capable of showing various kinds of bonds and intermolecular forces. This feature is of vast importance in terms of enhancing the mechanical stability of the matrix. Nevertheless, to confirm the benefits of these kinds of forces, more attention to mechanical testing is recommended to determine the best application for these matrixes after paying attention to the alternates of material processing available so far.

6. Conclusions

According to the literature available so far, the key aspects related to nanocomposite polymer electrolytes for batteries composed of zinc or magnesium have been presented and discussed along with the review to know their suitability for application in rechargeable cells.

The copolymer matrix composed of PVDF-co-HFP has been shown to hold on to the ionic liquid and retain it in the membranes. Moreover, according to the results by the number of publications so far, the improved results in conductivity obtained for this matrix along with the addition of nanofillers, provoke a space-charge region, understood by the existence of free electrons at the surface of the nanocomposite, facilitating the new kinetic path for ionic transport and polymer segmental motion. This mechanism ensures the electrolyte to be capable of ion transference. Improved high ionic conductivity and better thermal and mechanical stability compared to liquid electrolyte systems have been confirmed. Moreover, when a specific percentage of nanofiller is added, a decrease in ionic conductivity is observed. Excessive fillers could provoke this in the NCPE that may trigger the formation of ion pairs and ion aggregation, such as the non-conducting phase presented as an electrically inert component blocking ion transport.

By adding nanoparticles, it has been possible to reduce the degree of crystallinity of the polymers, an aspect proven in the investigations on PEO electrolytes. This feature is a crucial issue because the membrane's amorphous degree is responsible for conduction along with the electrolyte. Furthermore, conductivity is improved because the nanoparticles can act as a solid plasticizer, ensuring electrochemical properties and mechanical strength. Besides, it is discussed the NCPEs assembled with other synthetic polymers. Despite some minor variations, the results presented replicate the argument of improving the electrolyte properties by adding nanofillers, setting a solid precedent regarding the applicability of these polymers, where not much research has been found with the discussed approach.

Biopolymer electrolytes based on natural molecules have shown comparable ion conduction and electrochemical properties with traditional synthetic polymer electrolytes as the ones discussed in previous sections. Besides, when discussing stability, the natural polymer-based electrolytes are comparable, if not better, than the synthetic ones. The processes for enhancing their properties are reachable by the same methods. The conduction mechanism in both electrolytes is the same and is explained in terms of the exchange of ions between complexed sites. Moreover, their abundance, low cost, and easier processing ability make biopolymer electrolytes expected to bring a better future of green technologies than non-biodegradable, toxic, and harmful materials used in commercial batteries today.

When choosing which state is better for the electrolyte, between making it a solid or a gel, it is paramount to consider the device's application. Gel polymer electrolytes have been shown to be capable of being employed in conditions where flexibility is well appreciated. However, GPEs currently need mobile liquids to perform the conduction process, and the current ones present concerns in terms of stability, safety, and general sustainability. Hence, the search for more benign and environmentally-friendly mobile liquids is a current issue to increase the expectation on developing batteries based on sustainable components.

In general, for all the polymer electrolytes, the addition of nanoparticles (ZnO, MgO, TiO₂, Al₂O₃, SnO₂) has been proved to enhance the electrical conductivity by, in the least of the cases, one order of magnitude. Moreover, conductivity is improved, but cationic species' electrochemical properties, mechanical strength, and transport properties are. Ultimately, the awareness of the addition of nanofillers improving the mechanical stability and ionic conductivity is a crucial point to be explored in the production of batteries. However, the state-of-the-art is still lacking in terms of the development of NCPes based on biopolymers. The few investigations overviewed so far set a precedent for the demand for further research with this specific approach. These attempts need to be further developed to get practical applications for the industry in large scale of polymer-based electrolyte batteries, as well as other electrochemical devices, such as bioresorbable electronic devices that include biobatteries, offering an innovative solution to the problems currently faced by biomedical applications, generating positive impacts to the wellness of human beings and the environment.

The research in this field needs to continue developing. Still, zinc and magnesium are absolutely the future of batteries that present electrolytes in solid-state. These metals are likely to replace lithium, thanks to their high energy potential, inherent safety, cost-effectiveness, and environmental-friendliness, along with the employment of the biodegradable biopolymers discussed in this article for the electrolyte. These features set the path for developing novel environment-friendly battery systems in the present world that urges for more sustainable options.

Author Contributions: Conceptualization, formal analysis, data curation, investigation, writing—original draft preparation, M.F.B.-C.; writing—review and editing, S.H.-B., V.M.C. and R.M.M.; Conceptualization, methodology, supervision, project administration, funding acquisition, writing—review and editing, J.P.T. All authors have read and agreed to the published version of the manuscript.

Funding: This research was funded by Corporación Ecuatoriana para el Desarrollo de la Investigación y Academia, CEDIA, through its CEPRA program, grant number CEPRA 2021–012 Hacia la economía circular: desarrollo de eco-empaques a partir de desechos agroindustriales and The APC was funded by Corporación Ecuatoriana para el Desarrollo de la Investigación y Academia, CEDIA.

Institutional Review Board Statement: Not applicable.

Informed Consent Statement: Not applicable.

Data Availability Statement: Not applicable.

Conflicts of Interest: The authors declare no conflict of interest. The funders had no role in the design of the study; in the collection, analyses, or interpretation of data; in the writing of the manuscript, or in the decision to publish the results.

References

1. Lorca, S.; Santos, F.; Fernández Romero, A.J. A review of the use of GPEs in zinc-based batteries. A step closer to wearable electronic gadgets and smart textiles. *Polymers* **2020**, *12*, 1–79. [\[CrossRef\]](#) [\[PubMed\]](#)
2. Jaschin, P.W.; Gao, Y.; Li, Y.; Bo, S.H. A materials perspective on magnesium-ion-based solid-state electrolytes. *J. Mater. Chem. A* **2020**, *8*, 2875–2897. [\[CrossRef\]](#)
3. Qiu, L.; Xiang, W.; Tian, W.; Xu, C.L.; Li, Y.C.; Wu, Z.G.; Chen, T.R.; Jia, K.; Wang, D.; He, F.R.; et al. Polyanion and cation co-doping stabilized Ni-rich Ni–Co–Al material as cathode with enhanced electrochemical performance for Li-ion battery. *Nano Energy* **2019**, *63*, 103818. [\[CrossRef\]](#)
4. Xu, Y.D.; Xiang, W.; Wu, Z.G.; Xu, C.L.; Li, Y.C.; Guo, X.D.; Lv, G.P.; Peng, X.; Zhong, B.H. Improving cycling performance and rate capability of Ni-rich LiNi_{0.8}Co_{0.1}Mn_{0.1}O₂ cathode materials by Li₄Ti₅O₁₂ coating. *Electrochim. Acta* **2018**, *268*, 358–365. [\[CrossRef\]](#)
5. Etacheri, V.; Marom, R.; Elazari, R.; Salitra, G.; Aurbach, D. Challenges in the development of advanced Li-ion batteries: A review. *Energy Environ. Sci.* **2011**, *4*, 3243–3262. [\[CrossRef\]](#)
6. Wang, Y.; Yi, J.; Xia, Y. Recent progress in aqueous lithium-ion batteries. *Adv. Energy Mater.* **2012**, *2*, 830–840. [\[CrossRef\]](#)
7. Yi, J.; Wang, C.; Xia, Y. Comparison of thermal stability between micro- and nano-sized materials for lithium-ion batteries. *Electrochim. Commun.* **2013**, *33*, 115–118. [\[CrossRef\]](#)
8. Yi, J.; Hou, M.Y.; Bao, H.L.; Wang, C.X.; Wang, J.Q.; Xia, Y.Y. In-situ generation of Li₂FeSiO₄/C nanocomposite as cathode material for lithium ion battery. *Electrochim. Acta* **2014**, *133*, 564–569. [\[CrossRef\]](#)

9. Kim, H.; Hong, J.; Park, K.Y.; Kim, H.; Kim, S.W.; Kang, K. Aqueous rechargeable Li and Na ion batteries. *Chem. Rev.* **2014**, *114*, 11788–11827. [\[CrossRef\]](#)
10. Wu, K.; Huang, J.; Yi, J.; Liu, X.; Liu, Y.; Wang, Y.; Zhang, J.; Xia, Y. Recent Advances in Polymer Electrolytes for Zinc Ion Batteries: Mechanisms, Properties, and Perspectives. *Adv. Energy Mater.* **2020**, *10*, 1–32. [\[CrossRef\]](#)
11. Xiong, P.; Zhang, L.; Chen, Y.; Peng, S.; Yu, G. A Chemistry and Microstructure Perspective on Ion-Conducting Membranes for Redox Flow Batteries. *Angew. Chemie Int. Ed.* **2021**, *60*, 24770–24798. [\[CrossRef\]](#) [\[PubMed\]](#)
12. Arévalo-Cid, P.; Dias, P.; Mendes, A.; Azevedo, J. Redox flow batteries: A new frontier on energy storage. *Sustain. Energy Fuels* **2021**. [\[CrossRef\]](#)
13. Zhang, H.; Sun, C. Cost-effective iron-based aqueous redox flow batteries for large-scale energy storage application: A review. *J. Power Sources* **2021**, *493*. [\[CrossRef\]](#)
14. Pankratova, G.; Bollella, P.; Pankratov, D.; Gorton, L. Supercapacitive biofuel cells. *Curr. Opin. Biotechnol.* **2022**, *73*, 179–187. [\[CrossRef\]](#)
15. Wang, Y.; Ruiz Diaz, D.F.; Chen, K.S.; Wang, Z.; Adroher, X.C. Materials, technological status, and fundamentals of PEM fuel cells—A review. *Mater. Today* **2020**, *32*, 178–203. [\[CrossRef\]](#)
16. Wang, Y.; Seo, B.; Wang, B.; Zamel, N.; Jiao, K.; Adroher, X.C. Fundamentals, materials, and machine learning of polymer electrolyte membrane fuel cell technology. *Energy AI* **2020**, *1*, 100014. [\[CrossRef\]](#)
17. Pollock, T.M. Weight loss with magnesium alloys. *Science* **2010**, *328*, 986–987. [\[CrossRef\]](#) [\[PubMed\]](#)
18. Wu, X.F.; Neumann, H. Zinc-catalyzed organic synthesis: C–C, C–N, C–O bond formation reactions. *Adv. Synth. Catal.* **2012**, *354*, 3141–3160. [\[CrossRef\]](#)
19. Anyadike, N. *Lead and Zinc*; Woodhead Publishing Ltd.: Sawston, UK, 2015; pp. 2010–2011.
20. USGS. Lithium statistics and information. *U.S. Geol. Surv.* **2020**, *53*, 98–99.
21. Chen, M.; Ma, X.; Chen, B.; Arsenault, R.; Karlson, P.; Simon, N.; Wang, Y. Recycling End-of-Life Electric Vehicle Lithium-Ion Batteries. *Joule* **2019**, *3*, 2622–2646. [\[CrossRef\]](#)
22. Pan, H.; Shao, Y.; Yan, P.; Cheng, Y.; Han, K.S.; Nie, Z.; Wang, C.; Yang, J.; Li, X.; Bhattacharya, P.; et al. Reversible aqueous zinc/manganese oxide energy storage from conversion reactions. *Nat. Energy* **2016**, *1*, 16039. [\[CrossRef\]](#)
23. Kundu, D.; Adams, B.D.; Duffort, V.; Vajargah, S.H.; Nazar, L.F. A high-capacity and long-life aqueous rechargeable zinc battery using a metal oxide intercalation cathode. *Nat. Energy* **2016**, *1*, 16119. [\[CrossRef\]](#)
24. Saha, P.; Datta, M.K.; Velikokhatnyi, O.I.; Manivannan, A.; Alman, D.; Kumta, P.N. Rechargeable magnesium battery: Current status and key challenges for the future. *Prog. Mater. Sci.* **2014**, *66*, 1–86. [\[CrossRef\]](#)
25. Wang, F.; Borodin, O.; Gao, T.; Fan, X.; Sun, W.; Han, F.; Faraone, A.; Dura, J.A.; Xu, K.; Wang, C. Highly reversible zinc metal anode for aqueous batteries. *Nat. Mater.* **2018**, *17*, 543–549. [\[CrossRef\]](#)
26. Deivanayagam, R.; Ingram, B.J.; Shahbazian-Yassar, R. Progress in development of electrolytes for magnesium batteries. *Energy Storage Mater.* **2019**, *21*, 136–153. [\[CrossRef\]](#)
27. Liu, F.; Chen, Z.; Fang, G.; Wang, Z.; Cai, Y.; Tang, B.; Zhou, J.; Liang, S. V₂O₅ Nanospheres with Mixed Vanadium Valences as High Electrochemically Active Aqueous Zinc-Ion Battery Cathode. *Nano-Micro Lett.* **2019**, *11*, 1–11. [\[CrossRef\]](#)
28. Fang, G.; Zhu, C.; Chen, M.; Zhou, J.; Tang, B.; Cao, X.; Zheng, X.; Pan, A.; Liang, S. Suppressing Manganese Dissolution in Potassium Manganate with Rich Oxygen Defects Engaged High-Energy-Density and Durable Aqueous Zinc-Ion Battery. *Adv. Funct. Mater.* **2019**, *29*. [\[CrossRef\]](#)
29. Boaretto, N.; Meabe, L.; Martinez-Ibañez, M.; Armand, M.; Zhang, H. Review—Polymer Electrolytes for Rechargeable Batteries: From Nanocomposite to Nanohybrid. *J. Electrochem. Soc.* **2020**, *167*, 070524. [\[CrossRef\]](#)
30. Zhao, J.; Zha, J.; Zeng, Z.; Tan, C. Recent advances in wearable self-powered energy systems based on flexible energy storage devices integrated with flexible solar cells. *J. Mater. Chem. A* **2021**, *9*, 18887–18905. [\[CrossRef\]](#)
31. Volontsevich, D.; Strimovsky, S.; Veretennikov, I.; Sivykh, D.; Karpov, V. The Choice of the Electric Energy Storage Device Type for the Hybrid Power Drive of Military Wheeled Vehicles. In *International Conference Innovation in Engineering*; Springer: Cham, Switzerland, 2022; pp. 201–212.
32. Luo, Y.; Wu, Y.; Li, B.; Qu, J.; Feng, S.P.; Chu, P.K. Optimization and cutting-edge design of fuel-cell hybrid electric vehicles. *Int. J. Energy Res.* **2021**, *45*, 18392–18423. [\[CrossRef\]](#)
33. He, W.; Zuo, S.; Xu, X.; Zeng, L.; Liu, L.; Zhao, W.; Liu, J. Challenges and strategies of zinc anode for aqueous zinc-ion batteries. *Mater. Chem. Front.* **2021**, *5*, 2201–2217. [\[CrossRef\]](#)
34. Ye, T.; Li, L.; Zhang, Y. Recent Progress in Solid Electrolytes for Energy Storage Devices. *Adv. Funct. Mater.* **2020**, *30*, 1–20. [\[CrossRef\]](#)
35. Zhao, C.; Liu, L.; Qi, X.; Lu, Y.; Wu, F.; Zhao, J.; Yu, Y.; Hu, Y.S.; Chen, L. Solid-State Sodium Batteries. *Adv. Energy Mater.* **2018**, *8*, 1703012. [\[CrossRef\]](#)
36. Wood, K.N.; Kazyak, E.; Chadwick, A.F.; Chen, K.-H.; Zhang, J.-G.; Thornton, K.; Dasgupta, N.P. Dendrites and Pits: Untangling the Complex Behavior of Li Metal Anodes through Operando Video Microscopy. *ECS Meet. Abstr.* **2017**, MA2017-01, 518. [\[CrossRef\]](#) [\[PubMed\]](#)
37. Wu, F.; Yuan, Y.X.; Cheng, X.B.; Bai, Y.; Li, Y.; Wu, C.; Zhang, Q. Perspectives for restraining harsh lithium dendrite growth: Towards robust lithium metal anodes. *Energy Storage Mater.* **2018**, *15*, 148–170. [\[CrossRef\]](#)

38. Zhang, H.; Li, C.; Piszcz, M.; Coya, E.; Rojo, T.; Rodriguez-Martinez, L.M.; Armand, M.; Zhou, Z. Single lithium-ion conducting solid polymer electrolytes: Advances and perspectives. *Chem. Soc. Rev.* **2017**, *46*, 797–815. [\[CrossRef\]](#)
39. Hallinan, D.T.; Villaluenga, I.; Balsara, N.P. Polymer and composite electrolytes. *MRS Bull.* **2018**, *43*, 775–781. [\[CrossRef\]](#)
40. Mindemark, J.; Lacey, M.J.; Bowden, T.; Brandell, D. Beyond PEO—Alternative host materials for Li⁺-conducting solid polymer electrolytes. *Prog. Polym. Sci.* **2018**, *81*, 114–143. [\[CrossRef\]](#)
41. Wan, J.; Xie, J.; Mackanic, D.G.; Burke, W.; Bao, Z.; Cui, Y. Status, promises, and challenges of nanocomposite solid-state electrolytes for safe and high performance lithium batteries. *Mater. Today Nano* **2018**, *4*, 1–16. [\[CrossRef\]](#)
42. Yu, J.; Lyu, Y.Q.; Liu, J.; Effat, M.B.; Kwok, S.C.T.; Wu, J.; Ciucci, F. Enabling non-flammable Li-metal batteries via electrolyte functionalization and interface engineering. *J. Mater. Chem. A* **2019**, *7*, 17995–18002. [\[CrossRef\]](#)
43. Weston, J.E.; Steele, B.C.H. Effects of inert fillers on the mechanical and electrochemical properties of lithium salt-poly(ethylene oxide) polymer electrolytes. *Solid State Ionics* **1982**, *7*, 75–79. [\[CrossRef\]](#)
44. Zhao, Q.; Stalin, S.; Zhao, C.Z.; Archer, L.A. Designing solid-state electrolytes for safe, energy-dense batteries. *Nat. Rev. Mater.* **2020**, *5*, 229–252. [\[CrossRef\]](#)
45. Arya, A.; Sharma, A.L. Electrolyte for energy storage/conversion (Li⁺, Na⁺, Mg²⁺) devices based on PVC and their associated polymer: A comprehensive review. *J. Solid State Electrochem.* **2019**, *23*, 997–1059. [\[CrossRef\]](#)
46. Park, B.; Schaefer, J.L. Review—Polymer Electrolytes for Magnesium Batteries: Forging Away from Analogs of Lithium Polymer Electrolytes and Towards the Rechargeable Magnesium Metal Polymer Battery. *J. Electrochem. Soc.* **2020**, *167*, 070545. [\[CrossRef\]](#)
47. Huy, V.P.H.; So, S.; Hur, J. Inorganic fillers in composite gel polymer electrolytes for high-performance lithium and non-lithium polymer batteries. *Nanomaterials* **2021**, *11*, 1–40. [\[CrossRef\]](#)
48. Lu, K.; Jiang, T.; Hu, H.; Wu, M. Hydrogel Electrolytes for Quasi-Solid Zinc-Based Batteries. *Front. Chem.* **2020**, *8*, 1–12. [\[CrossRef\]](#) [\[PubMed\]](#)
49. Nakajima, H.; Dijkstra, P.; Loos, K. The recent developments in biobased polymers toward general and engineering applications: Polymers that are upgraded from biodegradable polymers, analogous to petroleum-derived polymers, and newly developed. *Polymers* **2017**, *9*, 523. [\[CrossRef\]](#) [\[PubMed\]](#)
50. Singh, R.; Polu, A.R.; Bhattacharya, B.; Rhee, H.W.; Varlikli, C.; Singh, P.K. Perspectives for solid biopolymer electrolytes in dye sensitized solar cell and battery application. *Renew. Sustain. Energy Rev.* **2016**, *65*, 1098–1117. [\[CrossRef\]](#)
51. Rayung, M.; Aung, M.M.; Azhar, S.C.; Abdullah, L.C.; Su'ait, M.S.; Ahmad, A.; Jamil, S.N.A.M. Bio-based polymer electrolytes for electrochemical devices: Insight into the ionic conductivity performance. *Materials* **2020**, *13*, 838. [\[CrossRef\]](#)
52. Lizundia, E.; Kundu, D. Advances in Natural Biopolymer-Based Electrolytes and Separators for Battery Applications. *Adv. Funct. Mater.* **2021**, *31*, 2005646. [\[CrossRef\]](#)
53. Austin Suthanthiraraj, S.; Johnsi, M. Nanocomposite polymer electrolytes. *Ionics* **2017**, *23*, 2531–2542. [\[CrossRef\]](#)
54. Armand, M.B.; Bruce, P.G.; Forsyth, M.; Scrosati, B.; Wieczorek, W. Polymer Electrolytes. In *Energy Materials*; Bruce, D.W., O'Hare, D., Walton, R.I., Eds.; Wiley: West Sussex, UK, 2011; pp. 1–31. ISBN 9780470997529.
55. Abdullah, M.; Lenggoro, W.; Okuyama, K. Polymer Electrolyte Nanocomposites. In *Encyclopedia of Nanoscience and Nanotechnology*; Nalwa, H.S., Ed.; American Scientific Publishers: Stevenson Ranch, CA, USA, 2004; pp. 731–762. ISBN 1-58883-064-0.
56. Li, Q.; Chen, J.; Fan, L.; Kong, X.; Lu, Y. Progress in electrolytes for rechargeable Li-based batteries and beyond. *Green Energy Environ.* **2016**, *1*, 18–42. [\[CrossRef\]](#)
57. Johnsi, M.; Austin Suthanthiraraj, S. Electrochemical and structural properties of a polymer electrolyte system based on the effect of CeO₂ nanofiller with PVDF-co-HFP for energy storage devices. *Ionics* **2016**, *22*, 1075–1083. [\[CrossRef\]](#)
58. Abbrent, S.; Plestil, J.; Hlavata, D.; Lindgren, J.; Tegenfeldt, J.; Wendsjö, Å. Crystallinity and morphology of PVdF-HFP-based gel electrolytes. *Polymer* **2001**, *42*, 1407–1416. [\[CrossRef\]](#)
59. Brigandi, P.J.; Cogen, J.M.; Pearson, R.A. Electrically conductive multiphase polymer blend carbon-based composites. *Polym. Eng. Sci.* **2014**, *54*, 1–16. [\[CrossRef\]](#)
60. Kaur, G.; Adhikari, R.; Cass, P.; Bown, M.; Gunatillake, P. Electrically conductive polymers and composites for biomedical applications. *RSC Adv.* **2015**, *5*, 37553–37567. [\[CrossRef\]](#)
61. Puguang, J.M.C.; Chung, W.J.; Kim, H. Ion-conductive and transparent PVdF-HFP/silane-functionalized ZrO₂ nanocomposite electrolyte for electrochromic applications. *Electrochim. Acta* **2016**, *196*, 236–244. [\[CrossRef\]](#)
62. Lalia, B.S.; Guillen, E.; Arafat, H.A.; Hashaikh, R. Nanocrystalline cellulose reinforced PVDF-HFP membranes for membrane distillation application. *Desalination* **2014**, *332*, 134–141. [\[CrossRef\]](#)
63. Prabakaran, K.; Mohanty, S.; Nayak, S.K. PEO/PVdF-HFP electrolytes for natural dye sensitized solar cell applications: Effect of modified nano-TiO₂ on electrochemical and photovoltaic performance. *J. Mater. Sci. Mater. Electron.* **2015**, *26*, 3887–3897. [\[CrossRef\]](#)
64. Shin, J.; Nho, Y.C.; seon Hwang, I.; Fei, G.; Kim, A.R.; Nahm, K.S. Irradiated PVdF-HFP-tin oxide composite membranes for the applications of direct methanol fuel cells. *J. Memb. Sci.* **2010**, *350*, 92–100. [\[CrossRef\]](#)
65. Xie, L.; Huang, X.; Yang, K.; Li, S.; Jiang, P. “Grafting to” route to PVDF-HFP-GMA/BaTiO₃ nanocomposites with high dielectric constant and high thermal conductivity for energy storage and thermal management applications. *J. Mater. Chem. A* **2014**, *2*, 5244–5251. [\[CrossRef\]](#)
66. Zhu, L.; Wang, Q. Novel ferroelectric polymers for high energy density and low loss dielectrics. *Macromolecules* **2012**, *45*, 2937–2954. [\[CrossRef\]](#)

67. Xiong, M.; Tang, H.; Wang, Y.; Lin, Y.; Sun, M.; Yin, Z.; Pan, M. Expanded polytetrafluoroethylene reinforced polyvinylidene fluoride-hexafluoropropylene separator with high thermal stability for lithium-ion batteries. *J. Power Sources* **2013**, *241*, 203–211. [\[CrossRef\]](#)
68. Ataollahi, N.; Ahmad, A.; Hamzah, H.; Rahman, M.Y.A.; Mohamed, N.S. Preparation and Characterization of PVDF-HFP/MG49 Based Polymer Blend Electrolyte. *Int. J. Electrochem. Sci* **2012**, *7*, 6693–6703.
69. Ma, T.; Cui, Z.; Wu, Y.; Qin, S.; Wang, H.; Yan, F.; Han, N.; Li, J. Preparation of PVDF based blend microporous membranes for lithium ion batteries by thermally induced phase separation: I. Effect of PMMA on the membrane formation process and the properties. *J. Memb. Sci.* **2013**, *444*, 213–222. [\[CrossRef\]](#)
70. Yang, Q.; Deng, N.; Chen, J.; Cheng, B.; Kang, W. The recent research progress and prospect of gel polymer electrolytes in lithium-sulfur batteries. *Chem. Eng. J.* **2020**, 127427. [\[CrossRef\]](#)
71. Zhou, H. New energy storage devices for post lithium-ion batteries. *Energy Environ. Sci.* **2013**, *6*, 2256. [\[CrossRef\]](#)
72. Maheshwaran, C.; Mishra, K.; Kanchan, D.K.; Kumar, D. Mg^{2+} conducting polymer gel electrolytes: Physical and electrochemical investigations. *Ionics* **2020**, *26*, 2969–2980. [\[CrossRef\]](#)
73. Ponmani, S.; Prabhu, M.R. Development and study of solid polymer electrolytes based on PVdF-HFP/PVAc: Mg (ClO_4)₂ for Mg ion batteries. *J. Mater. Sci. Mater. Electron.* **2018**, *29*, 15086–15096. [\[CrossRef\]](#)
74. Oh, J.S.; Ko, J.M.; Kim, D.W. Preparation and characterization of gel polymer electrolytes for solid state magnesium batteries. *Electrochim. Acta* **2004**, *50*, 903–906. [\[CrossRef\]](#)
75. Pandey, G.P.; Agrawal, R.C.; Hashmi, S.A. Performance studies on composite gel polymer electrolytes for rechargeable magnesium battery application. *J. Phys. Chem. Solids* **2011**, *72*, 1408–1413. [\[CrossRef\]](#)
76. Pandey, G.P.; Agrawal, R.C.; Hashmi, S.A. Magnesium ion-conducting gel polymer electrolytes dispersed with fumed silica for rechargeable magnesium battery application. *J. Solid State Electrochem.* **2011**, *15*, 2253–2264. [\[CrossRef\]](#)
77. Sharma, J.; Hashmi, S. Magnesium ion-conducting gel polymer electrolyte nanocomposites: Effect of active and passive nanofillers. *Polym. Compos.* **2019**, *40*, 1295–1306. [\[CrossRef\]](#)
78. Patel, S.; Kumar, R. Effect of Al_2O_3 on electrical properties of polymer electrolyte for electrochemical device application. *Mater. Today Proc.* **2021**, *46*, 2175–2178. [\[CrossRef\]](#)
79. Pandey, G.P.; Agrawal, R.C.; Hashmi, S.A. Magnesium ion-conducting gel polymer electrolytes dispersed with nanosized magnesium oxide. *J. Power Sources* **2009**, *190*, 563–572. [\[CrossRef\]](#)
80. Patel, S.; Kumar, R. Synthesis and characterization of magnesium ion conductivity in PVDF based nanocomposite polymer electrolytes disperse with MgO. *J. Alloys Compd.* **2019**, *789*, 6–14. [\[CrossRef\]](#)
81. Pandey, G.P.; Agrawal, R.C.; Hashmi, S.A. Electrical and electrochemical properties of magnesium ion conducting composite gel polymer electrolytes. *J. Phys. D. Appl. Phys.* **2010**, *43*, 255501. [\[CrossRef\]](#)
82. Nidhi Sandhya, P.; Kumar, R. PVDF-HFP based nanocomposite polymer electrolytes for energy storage devices dispersed with various nano-fillers. *AIP Conf. Proc.* **2020**, *2220*, 080044. [\[CrossRef\]](#)
83. Patel, S.; Kumar, R. Effect of nanoparticles on electrical properties of PVDF-based Mg^{2+} ion conducting polymer electrolytes. *Bull. Mater. Sci.* **2021**, *44*, 1–9. [\[CrossRef\]](#)
84. Jayanthi, S.; Kalapriya, K. Structural, transport, morphological, and thermal studies of nano barium titanate-incorporated magnesium ion conducting solid polymer electrolytes. *Polym. Polym. Compos.* **2021**. [\[CrossRef\]](#)
85. Patel, S.; Kumar, R. Effect of dispersion of ceramic filler on thermal, structural and transport properties of polymer electrolyte for electrochemical applications. *AIP Conf. Proc.* **2021**, *2352*, 020004. [\[CrossRef\]](#)
86. Kumar, B. From colloidal to composite electrolytes: Properties, peculiarities, and possibilities. *J. Power Sources* **2004**, *135*, 215–231. [\[CrossRef\]](#)
87. Polu, A.R.; Kumar, R.; Joshi, G.M. Effect of zinc salt on transport, structural, and thermal properties of PEG-based polymer electrolytes for battery application. *Ionics* **2014**, *20*, 675–679. [\[CrossRef\]](#)
88. Tafur, J.P.; Fernández Romero, A.J. Electrical and spectroscopic characterization of PVdF-HFP and TFSI-ionic liquids-based gel polymer electrolyte membranes. Influence of $Zn(Tf)_2$ salt. *J. Memb. Sci.* **2014**, *469*, 499–506. [\[CrossRef\]](#)
89. Liu, J.; Khanam, Z.; Muchakayala, R.; Song, S. Fabrication and characterization of Zn-ion-conducting solid polymer electrolyte films based on PVdF-HFP/ $Zn(Tf)_2$ complex system. *J. Mater. Sci. Mater. Electron.* **2020**, *31*, 6160–6173. [\[CrossRef\]](#)
90. Liu, J.; Ahmed, S.; Khanam, Z.; Wang, T.; Song, S. Ionic liquid-incorporated zn-ion conducting polymer electrolyte membranes. *Polymers* **2020**, *12*, 1755. [\[CrossRef\]](#)
91. Johnsi, M.; Suthanthiraraj, S.A. Preparation, zinc ion transport properties, and battery application based on poly(vinylidene fluoride-co-hexa fluoro propylene) polymer electrolyte system containing titanium dioxide nanofiller. *High Perform. Polym.* **2015**, *27*, 877–885. [\[CrossRef\]](#)
92. Johnsi, M.; Suthanthiraraj, S.A. Compositional effect of ZrO_2 nanofillers on a PVDF-co-HFP based polymer electrolyte system for solid state zinc batteries. *Chin. J. Polym. Sci.* **2016**, *34*, 332–343. [\[CrossRef\]](#)
93. Hashmi, S.A. Enhanced zinc ion transport in gel polymer electrolyte: Effect of nano-sized ZnO dispersion. *J. Solid State Electrochem.* **2012**, *16*, 3105–3114. [\[CrossRef\]](#)
94. Muda, N.; Ibrahim, S.; Kamarulzaman, N.; Mohamed, N.S. PVDF-HFP- $NH_4CF_3SO_3$ - SiO_2 nanocomposite polymer electrolytes for protonic electrochemical cell. *Key Eng. Mater.* **2011**, *471–472*, 373–378. [\[CrossRef\]](#)
95. Tafur, J.P.; Abad, J.; Román, E.; Fernández Romero, A.J. Charge storage mechanism of MnO_2 cathodes in Zn/ MnO_2 batteries using ionic liquid-based gel polymer electrolytes. *Electrochem. Commun.* **2015**, *60*, 190–194. [\[CrossRef\]](#)

96. Jaipal Reddy, M.; Chu, P.P. Ion pair formation and its effect in PEO:Mg solid polymer electrolyte system. *J. Power Sources* **2002**, *109*, 340–346. [\[CrossRef\]](#)
97. Agrawal, R.C.; Pandey, G.P. Solid polymer electrolytes: Materials designing and all-solid-state battery applications: An overview. *J. Phys. D. Appl. Phys.* **2008**, *41*, 223001. [\[CrossRef\]](#)
98. Prodduturi, S.; Manek, R.V.; Kolling, W.M.; Stodghill, S.P.; Repka, M.A. Solid-State Stability and Characterization of Hot-Melt Extruded Poly(ethylene oxide) Films. *J. Pharm. Sci.* **2005**, *94*, 2232–2245. [\[CrossRef\]](#)
99. Chawla, P.; Trivedi, S.; Pandey, K.; Tripathi, M. Dielectric Studies of [PEO: CH₃COOLi]: Graphite System Synthesized by Hot Press and Solution Cast Technique. *Proc. Natl. Acad. Sci. India Sect. A Phys. Sci.* **2018**, *88*, 187–193. [\[CrossRef\]](#)
100. Lascaud, S.; Perrier, M.; Vallee, A.; Besner, S.; Prud'homme, J.; Armand, M. Phase Diagrams and Conductivity Behavior of Poly(ethylene oxide)-Molten Salt Rubbery Electrolytes. *Macromolecules* **1994**, *27*, 7469–7477. [\[CrossRef\]](#)
101. Agrawal, R.C.; Sahu, D.K.; Mahipal, Y.K.; Ashrafi, R. Investigations on ion transport properties of hot-press cast magnesium ion conducting Nano-Composite Polymer Electrolyte (NCPE) films: Effect of filler particle dispersal on room temperature conductivity. *Mater. Chem. Phys.* **2013**, *139*, 410–415. [\[CrossRef\]](#)
102. Feng, J.; Wang, L.; Chen, Y.; Wang, P.; Zhang, H.; He, X. PEO based polymer-ceramic hybrid solid electrolytes: A review. *Nano Converg.* **2021**, *8*, 1–12. [\[CrossRef\]](#) [\[PubMed\]](#)
103. Kumar, Y.; Hashmi, S.A.; Pandey, G.P. Ionic liquid mediated magnesium ion conduction in poly(ethylene oxide) based polymer electrolyte. *Electrochim. Acta* **2011**, *56*, 3864–3873. [\[CrossRef\]](#)
104. Agrawal, R.C.; Sahu, D.K.; Mahipal, Y.K.; Ashrafi, R. Ion transport property of hot-press cast Mg²⁺-ion conducting nano-composite polymer electrolyte membranes: Study of effect of active/passive filler particle dispersal on conductivity. *Indian J. Pure Appl. Phys.* **2013**, *51*, 320–323.
105. Zaky, M.M.; Eyssa, H.M.; Sadek, R.F. Improvement of the magnesium battery electrolyte properties through gamma irradiation of nano polymer electrolytes doped with magnesium oxide nanoparticles. *J. Vinyl Addit. Technol.* **2019**, *25*, 243–254. [\[CrossRef\]](#)
106. Sundar, M.; Selladurai, S. Effect of fillers on magnesium-poly(ethylene oxide) solid polymer electrolyte. *Ionics* **2006**, *12*, 281–286. [\[CrossRef\]](#)
107. Koduru, H.K.; Marinov, Y.G.; Kaleemulla, S.; Rafailov, P.M.; Hadjichristov, G.B.; Scaramuzza, N. Fabrication and characterization of magnesium—ion-conducting flexible polymer electrolyte membranes based on a nanocomposite of poly(ethylene oxide) and potato starch nanocrystals. *J. Solid State Electrochem.* **2021**, *25*, 2409–2428. [\[CrossRef\]](#)
108. Shao, Y.; Rajput, N.N.; Hu, J.; Hu, M.; Liu, T.; Wei, Z.; Gu, M.; Deng, X.; Xu, S.; Han, K.S.; et al. Nanocomposite polymer electrolyte for rechargeable magnesium batteries. *Nano Energy* **2015**, *12*, 750–759. [\[CrossRef\]](#)
109. Carrilho-Plancha, M.J.; Rangel, C.M.; Correia De Sequeira, C.A. Electrochemical characterisation of a Zn/(PEO)₄ZnCl₂/Nb₂O₅ solid-state cell. *J. Solid State Electrochem.* **2012**, *16*, 665–671. [\[CrossRef\]](#)
110. Nancy, A.C.; Suthanthiraraj, S.A. Effect of Al₂O₃ nanofiller on the electrical, thermal and structural properties of PEO:PPG based nanocomposite polymer electrolyte. *Ionics* **2017**, *23*, 1439–1449. [\[CrossRef\]](#)
111. Karan, S.; Agrawal, R.C. Ion Transport and Materials Characterization Studies on Hot-Press Cast Zn²⁺ Conducting Nano-Composite Polymer Electrolyte (NCPE) Films: [90 PEO: 10Zn (CF₃SO₃)₂] + xAl₂O₃. *J. Ravishankar Univ.* **2019**, *32*, 76–83. [\[CrossRef\]](#)
112. Turković, A.; Pavlović, M.; Dubček, P.; Lučić-Lavčević, M.; Etlinger, B.; Bernstorff, S. SAXS/DSC Study of Polymer Electrolyte for Zn Rechargeable Nanostructured Galvanic Cells. *J. Electrochem. Soc.* **2007**, *154*, A554. [\[CrossRef\]](#)
113. Turković, A.; Dubček, P.; Pavlović, M.; Bernstorff, S. SAXS/DSC/WAXD Study of γ -irradiated Polymer Electrolyte for Zn Rechargeable Nanostructured Galvanic Cells. *ECS Trans.* **2009**, *16*, 437–443. [\[CrossRef\]](#)
114. Agrawal, R.C.; Hashmi, S.A.; Pandey, G.P. Electrochemical cell performance studies on all-solid-state battery using nano-composite polymer electrolyte membrane. *Ionics (Kiel)* **2007**, *13*, 295–298. [\[CrossRef\]](#)
115. Karan, S.; Sahu, M.; Sahu, T.B.; Mahipal, Y.K.; Sahu, D.K.; Agrawal, R.C. Investigations on materials and ion transport properties of Zn²⁺ conducting nano-composite polymer electrolytes (NCPEs): [(90 PEO: 10Zn(CF₃SO₃)₂) + xZnO]. *Mater. Today Commun.* **2017**, *13*, 269–274. [\[CrossRef\]](#)
116. Agrawal, S.L.; Singh, M.; Dwivedi, M.M.; Pandey, K. Investigation on ion conduction behaviour in Zn-ferrite based polymer nanocomposite electrolyte. *Fibers Polym.* **2011**, *12*, 864–874. [\[CrossRef\]](#)
117. Wang, M.; Emre, A.; Tung, S.; Gerber, A.; Wang, D.; Huang, Y.; Cecen, V.; Kotov, N.A. Biomimetic Solid-State Zn²⁺ Electrolyte for Corrugated Structural Batteries. *ACS Nano* **2019**, *13*, 1107–1115. [\[CrossRef\]](#)
118. Liu, J.; Guan, C.; Zhou, C.; Fan, Z.; Ke, Q.; Zhang, G.; Liu, C.; Wang, J. A Flexible Quasi-Solid-State Nickel–Zinc Battery with High Energy and Power Densities Based on 3D Electrode Design. *Adv. Mater.* **2016**, *28*, 8732–8739. [\[CrossRef\]](#) [\[PubMed\]](#)
119. Li, H.; Han, C.; Huang, Y.; Huang, Y.; Zhu, M.; Pei, Z.; Xue, Q.; Wang, Z.; Liu, Z.; Tang, Z.; et al. An extremely safe and wearable solid-state zinc ion battery based on a hierarchical structured polymer electrolyte. *Energy Environ. Sci.* **2018**, *11*, 941–951. [\[CrossRef\]](#)
120. Fu, J.; Zhang, J.; Song, X.; Zarrin, H.; Tian, X.; Qiao, J.; Rasen, L.; Li, K.; Chen, Z. A flexible solid-state electrolyte for wide-scale integration of rechargeable zinc–air batteries. *Energy Environ. Sci.* **2016**, *9*, 663–670. [\[CrossRef\]](#)
121. Li, Q.; Sun, H.Y.; Takeda, Y.; Imanishi, N.; Yang, J.; Yamamoto, O. Interface properties between a lithium metal electrode and a poly(ethylene oxide) based composite polymer electrolyte. *J. Power Sources* **2001**, *92*, 201–205. [\[CrossRef\]](#)

122. Rao, C.V.S.; Ravi, M.; Raja, V.; Bhargav, P.B.; Sharma, A.K.; Rao, V.V.R.N. Preparation and characterization of PVP-based polymer electrolytes for solid-state battery applications. *Iran. Polym. J.* **2012**, *21*, 531–536. [\[CrossRef\]](#)
123. CROW Polymer Database. Available online: <http://polymerdatabase.com/index.html> (accessed on 11 April 2021).
124. Sarojini, S.; Anjalai, C. AC Impedance Studies on Magnesium Ion Conducting Polymer Electrolyte System with Ethylene Carbonate as Plasticizer and MgO as Nanofiller. *Chem. Sci. Trans.* **2016**, *5*, 56–60. [\[CrossRef\]](#)
125. Zain, N.F.; Zainal, N.; Mohamed, N.S. The effects of MgO nanofiller to the physicochemical and ionic liquid retention properties of PEMA-MgTf2-EMITFSI nanocomposite polymer electrolytes. *Polym. Compos.* **2018**, *39*, 1500–1506. [\[CrossRef\]](#)
126. Shahrenoor Basha, S.K.; Sunita Sundari, G.; Vijay Kumar, K.; Rao, M.C. Optical and dielectric properties of PVP based composite polymer electrolyte films. *Polym. Sci. Ser. A* **2017**, *59*, 554–565. [\[CrossRef\]](#)
127. Mishra, K.; Hashmi, S.A.; Rai, D.K. Nanocomposite blend gel polymer electrolyte for proton battery application. *J. Solid State Electrochem.* **2013**, *17*, 785–793. [\[CrossRef\]](#)
128. Candhadai Murali, S.P.; Samuel, A.S. Zinc ion conducting blended polymer electrolytes based on room temperature ionic liquid and ceramic filler. *J. Appl. Polym. Sci.* **2019**, *136*, 1–14. [\[CrossRef\]](#)
129. Sai Prasanna, C.M.; Austin Suthanthiraraj, S. Investigations of Zinc Ion Dissociation in Gel Polymer Electrolytes Based on Poly(vinyl chloride) and Poly(ethyl methacrylate) Blend on the Addition of Two Different Ceramic Nanofillers. *J. Inorg. Organomet. Polym. Mater.* **2019**, *29*, 483–501. [\[CrossRef\]](#)
130. Sai Prasanna, C.M.; Austin Suthanthiraraj, S. PVC/PEMA-based blended nanocomposite gel polymer electrolytes plasticized with room temperature ionic liquid and dispersed with nano-ZrO₂ for zinc ion batteries. *Polym. Compos.* **2019**, *40*, 3402–3411. [\[CrossRef\]](#)
131. Sai Prasanna, C.M.; Austin Suthanthiraraj, S. Improved zinc ion transportation in gel polymer electrolyte upon the addition of nano-sized SnO₂. *Polym. Polym. Compos.* **2020**, *28*, 54–65. [\[CrossRef\]](#)
132. Sowthari, K.; Suthanthiraraj, S.A. Preparation and properties of biodegradable polymer-layered silicate nanocomposite electrolytes for zinc based batteries. *Electrochim. Acta* **2015**, *174*, 885–892. [\[CrossRef\]](#)
133. Sowthari, K.; Suthanthiraraj, S.A. Structural and AC impedance studies on nanocomposite polymer electrolytes based on poly(ϵ -caprolactone). *J. Appl. Polym. Sci.* **2014**, *131*. [\[CrossRef\]](#)
134. Fan, X.; Liu, J.; Song, Z.; Han, X.; Deng, Y.; Zhong, C.; Hu, W. Porous nanocomposite gel polymer electrolyte with high ionic conductivity and superior electrolyte retention capability for long-cycle-life flexible zinc–air batteries. *Nano Energy* **2019**, *56*, 454–462. [\[CrossRef\]](#)
135. Abdullah, O.G.; Salman, Y.A.K.; Tahir, D.A.; Jamal, G.M.; Ahmed, H.T.; Mohamad, A.H.; Azawy, A.K.; Abdullah, C.; Salman, O.G.; Tahir, Y.A.K.; et al. Effect of ZnO nanoparticle content on the structural and ionic transport parameters of polyvinyl alcohol based proton-conducting polymer electrolyte membranes. *Membranes* **2021**, *11*, 163. [\[CrossRef\]](#) [\[PubMed\]](#)
136. Chen, H.W.; Lin, T.P.; Chang, F.C. Ionic conductivity enhancement of the plasticized PMMA/LiClO₄ polymer nanocomposite electrolyte containing clay. *Polymer (Guildf)* **2002**, *43*, 5281–5288. [\[CrossRef\]](#)
137. Jäger, M.; Wilke, A. Comprehensive biocompatibility testing of a new PMMA-HA bone cement versus conventional PMMA cement in vitro. *J. Biomater. Sci. Polym. Ed.* **2003**, *14*, 1283–1298. [\[CrossRef\]](#)
138. Kikuchi, Y.; Hirao, M.; Ookubo, T.; Sasaki, A. Design of recycling system for poly(methyl methacrylate) (PMMA). Part 1: Recycling scenario analysis. *Int. J. Life Cycle Assess.* **2014**, *19*, 120–129. [\[CrossRef\]](#)
139. Su'Ait, M.S.; Ahmad, A.; Hamzah, H.; Rahman, M.Y.A. Preparation and characterization of PMMA-MG49-LiClO₄ solid polymeric electrolyte. *J. Phys. D. Appl. Phys.* **2009**, *42*. [\[CrossRef\]](#)
140. Ahmad, S.; Ahmad, S.; Agnihotry, S.A. Nanocomposite electrolytes with fumed silica in poly(methyl methacrylate): Thermal, rheological and conductivity studies. *J. Power Sources* **2005**, *140*, 151–156. [\[CrossRef\]](#)
141. Han, H.S.; Kang, H.R.; Kim, S.W.; Kim, H.T. Phase-separated polymer electrolyte based on poly(vinyl chloride)/poly(ethyl methacrylate) blend. *J. Power Sources* **2002**, *112*, 461–468. [\[CrossRef\]](#)
142. Reiter, J.; Krejza, O.; Sedlářiková, M. Electrochromic devices employing methacrylate-based polymer electrolytes. *Sol. Energy Mater. Sol. Cells* **2009**, *93*, 249–255. [\[CrossRef\]](#)
143. Turner, D.T.; Schwartz, A. The glass transition temperature of poly(N-vinyl pyrrolidone) by differential scanning calorimetry. *Polymer* **1985**, *26*, 757–762. [\[CrossRef\]](#)
144. Ramaswamy, M.; Malayandi, T.; Subramanian, S.; Srinivasalu, J.; Rangaswamy, M. Magnesium ion conducting polyvinyl alcohol–polyvinyl pyrrolidone-based blend polymer electrolyte. *Ionics* **2017**, *23*, 1771–1781. [\[CrossRef\]](#)
145. Majhi, P.R.; Mouluk, S.P.; Burke, S.E.; Rodgers, M.; Palepu, R. Physicochemical investigations on the interaction of surfactants and salts with polyvinylpyrrolidone in aqueous medium. *J. Colloid Interface Sci.* **2001**, *235*, 227–234. [\[CrossRef\]](#) [\[PubMed\]](#)
146. Rajendran, S.; Sivakumar, M.; Subadevi, R. Investigations on the effect of various plasticizers in PVA-PMMA solid polymer blend electrolytes. *Mater. Lett.* **2004**, *58*, 641–649. [\[CrossRef\]](#)
147. Dubal, D.P.; Chodankar, N.R.; Kim, D.H.; Gomez-Romero, P. Towards flexible solid-state supercapacitors for smart and wearable electronics. *Chem. Soc. Rev.* **2018**, *47*, 2065–2129. [\[CrossRef\]](#) [\[PubMed\]](#)
148. Wang, Z.; Meng, X.; Wu, Z.; Mitra, S. Development of flexible zinc–air battery with nanocomposite electrodes and a novel separator. *J. Energy Chem.* **2017**, *26*, 129–138. [\[CrossRef\]](#)
149. Aziz, S.B. Li⁺ ion conduction mechanism in poly(ϵ -caprolactone)-based polymer electrolyte. *Iran. Polym. J.* **2013**, *22*, 877–883. [\[CrossRef\]](#)

150. Flieger, M.; Kantorová, M.; Prell, A.; Řezanka, T.; Votruba, J. Biodegradable plastics from renewable sources. *Folia Microbiol.* **2003**, *48*, 27–44. [\[CrossRef\]](#)
151. Ray, S.S.; Bousmina, M. Biodegradable polymers and their layered silicate nanocomposites: In greening the 21st century materials world. *Prog. Mater. Sci.* **2005**, *50*, 962–1079. [\[CrossRef\]](#)
152. Salleh, N.S.; Aziz, S.B.; Aspanut, Z.; Kadir, M.F.Z. Electrical impedance and conduction mechanism analysis of biopolymer electrolytes based on methyl cellulose doped with ammonium iodide. *Ionics* **2016**, *22*, 2157–2167. [\[CrossRef\]](#)
153. Huang, X.; Wang, D.; Yuan, Z.; Xie, W.; Wu, Y.; Li, R.; Zhao, Y.; Luo, D.; Cen, L.; Chen, B.; et al. A Fully Biodegradable Battery for Self-Powered Transient Implants. *Small* **2018**, *14*, 1800994. [\[CrossRef\]](#) [\[PubMed\]](#)
154. Majdecka, D.; Drami ska, S.; Stolarczyk, K.; Kizling, M.; Kryszewski, P.; Golimowski, J.; Bilewicz, R. Sandwich Biobattery with Enzymatic Cathode and Zinc Anode for Powering Sensors. *ECS Trans.* **2014**, *61*, 1–7. [\[CrossRef\]](#)
155. Huang, X. Materials and applications of bioresorbable electronics. *J. Semicond.* **2018**, *39*, 011003. [\[CrossRef\]](#)
156. Poosapati, A.; Jang, E.; Madan, D.; Jang, N.; Hu, L.; Lan, Y. Cellulose hydrogel as a flexible gel electrolyte layer. *MRS Commun.* **2019**, *9*, 122–128. [\[CrossRef\]](#)
157. Johari, N.A.; Kudin, T.I.T.; Ali, A.M.M.; Winie, T.; Yahya, M.Z.A. Studies on cellulose acetate-based gel polymer electrolytes for proton batteries. *Mater. Res. Innov.* **2009**, *13*, 232–234. [\[CrossRef\]](#)
158. Johari, N.A.; Kudin, T.I.T.; Ali, A.M.M.; Yahya, M.Z.A. Effects of TiO₂ on conductivity performance of cellulose acetate based polymer gel electrolytes for proton batteries. *Mater. Res. Innov.* **2011**, *15*, s229–s231. [\[CrossRef\]](#)
159. Muhammad, F.H.; Subban, R.H.Y.; Winie, T. Electrical studies on hexanoyl chitosan-based nanocomposite polymer electrolytes. *AIP Conf. Proc.* **2009**, *1136*, 61–65. [\[CrossRef\]](#)
160. Muhammad, F.H.; Subban, R.H.Y.; Winie, T. Structural and electrical characterization of hexanoyl chitosan- LiClO₄-TiO₂-DMC polymer electrolytes. *Key Eng. Mater.* **2014**, *594–595*, 608–612. [\[CrossRef\]](#)
161. Rosli, N.H.A.; Muhammad, F.H.; Chan, C.H.; Winie, T. Effect of filler type on the electrical properties of hexanoyl chitosan- based polymer electrolytes. *Adv. Mater. Res.* **2014**, *832*, 224–227. [\[CrossRef\]](#)
162. Aziz, N.A.; Majid, S.R.; Yahya, R.; Arof, A.K. Conductivity, structure, and thermal properties of chitosan-based polymer electrolytes with nanofillers. *Polym. Adv. Technol.* **2011**, *22*, 1345–1348. [\[CrossRef\]](#)
163. Navaratnam, S.; Ramesh, K.; Basirun, W.J. Investigation of ion conducting behaviour of composite chitosan based polymer electrolytes. *Mater. Res. Innov.* **2011**, *15*, s184–s186. [\[CrossRef\]](#)
164. Sudaryanto; Yulianti, E.; Patimatuzzohrah. Structure and properties of solid polymer electrolyte based on chitosan and ZrO₂ nanoparticle for lithium ion battery. *AIP Conf. Proc.* **2016**, *1710*, 020003. [\[CrossRef\]](#)
165. Shukur, M.F.; Ithnin, R.; Kadir, M.F.Z. Ionic conductivity and dielectric properties of potato starch-magnesium acetate biopolymer electrolytes: The effect of glycerol and 1-butyl-3-methylimidazolium chloride. *Ionics* **2016**, *22*, 1113–1123. [\[CrossRef\]](#)
166. Khanmirzaei, M.H.; Ramesh, S. Nanocomposite polymer electrolyte based on rice starch/ionic liquid/TiO₂ nanoparticles for solar cell application. *Meas. J. Int. Meas. Confed.* **2014**, *58*, 68–72. [\[CrossRef\]](#)
167. Teoh, K.H.; Ramesh, S.; Arof, A.K. Investigation on the effect of nanosilica towards corn starch-lithium perchlorate-based polymer electrolytes. *J. Solid State Electrochem.* **2012**, *16*, 3165–3170. [\[CrossRef\]](#)
168. Teoh, K.H.; Lim, C.S.; Liew, C.W.; Ramesh, S.; Ramesh, S. Electric double-layer capacitors with corn starch-based biopolymer electrolytes incorporating silica as filler. *Ionics* **2015**, *21*, 2061–2068. [\[CrossRef\]](#)
169. Shukur, M.F.; Kadir, M.F.Z. Hydrogen ion conducting starch-chitosan blend based electrolyte for application in electrochemical devices. *Electrochim. Acta* **2015**, *158*, 152–165. [\[CrossRef\]](#)
170. Masri, M.N.; Nazeri, M.F.M.; Mohamad, A.A. Sago Gel Polymer Electrolyte for Zinc-Air Battery. *Adv. Sci. Technol.* **2010**, *72*, 305–308. [\[CrossRef\]](#)
171. Huang, Y.; Liu, J.; Zhang, J.; Jin, S.; Jiang, Y.; Zhang, S.; Li, Z.; Zhi, C.; Du, G.; Zhou, H. Flexible quasi-solid-state zinc ion batteries enabled by highly conductive carrageenan bio-polymer electrolyte. *RSC Adv.* **2019**, *9*, 16313–16319. [\[CrossRef\]](#)
172. Sangeetha, P.; Selvakumari, T.M.; Selvasekarapandian, S.; Srikumar, S.R.; Manjuladevi, R.; Mahalakshmi, M. Preparation and characterization of biopolymer K-carrageenan with MgCl₂ and its application to electrochemical devices. *Ionics* **2020**, *26*, 233–244. [\[CrossRef\]](#)
173. Selvalakshmi, S.; Vijaya, N.; Selvasekarapandian, S.; Premalatha, M. Biopolymer agar-agar doped with NH₄SCN as solid polymer electrolyte for electrochemical cell application. *J. Appl. Polym. Sci.* **2017**, *134*. [\[CrossRef\]](#)
174. Alves, R.D.; Rodrigues, L.C.; Andrade, J.R.; Pawlicka, A.; Pereira, L.; Martins, R.; Fortunato, E.; Silva, M.M. Study and characterization of a novel polymer electrolyte based on agar doped with magnesium triflate. *Mol. Cryst. Liq. Cryst.* **2013**, *570*, 1–11. [\[CrossRef\]](#)
175. Wang, W.; Guo, X.; Yang, Y. Lithium iodide effect on the electrochemical behavior of agarose based polymer electrolyte for dye-sensitized solar cell. *Electrochim. Acta* **2011**, *56*, 7347–7351. [\[CrossRef\]](#)
176. Sudhakar, Y.N.; Selvakumar, M.D.; Krishna, B. *Biopolymer Electrolytes Fundamentals and Applications in Energy Storage*, 1st ed.; Elsevier: Amsterdam, The Netherlands; Oxford, UK, 2018; ISBN 9780128136119.
177. Wang, W.; Zhang, X.; Teng, A.; Liu, A. Mechanical reinforcement of gelatin hydrogel with nanofiber cellulose as a function of percolation concentration. *Int. J. Biol. Macromol.* **2017**, *103*, 226–233. [\[CrossRef\]](#)
178. Zhang, J.; Fu, J.; Song, X.; Jiang, G.; Zarrin, H.; Xu, P.; Li, K.; Yu, A.; Chen, Z. Laminated Cross-Linked Nanocellulose/Graphene Oxide Electrolyte for Flexible Rechargeable Zinc–Air Batteries. *Adv. Energy Mater.* **2016**, *6*, 1600476. [\[CrossRef\]](#)

179. Yahya, M.Z.A.; Arof, A.K. Effect of oleic acid plasticizer on chitosan-lithium acetate solid polymer electrolytes. *Eur. Polym. J.* **2003**, *39*, 897–902. [\[CrossRef\]](#)
180. Yang, R.; Li, H.; Huang, M.; Yang, H.; Li, A. A review on chitosan-based flocculants and their applications in water treatment. *Water Res.* **2016**, *95*, 59–89. [\[CrossRef\]](#)
181. Mohamed, N.S.; Subban, R.H.Y.; Arof, A.K. Polymer batteries fabricated from lithium complexed acetylated chitosan. *J. Power Sources* **1995**, *56*, 153–156. [\[CrossRef\]](#)
182. Winie, T.; Jamal, A.; Hanif, N.S.M.; Shahril, N.S.M. Hexanoyl chitosan-polystyrene blend based composite polymer electrolyte with surface treated TiO₂ fillers. *Key Eng. Mater.* **2014**, *594–595*, 656–660. [\[CrossRef\]](#)
183. Winie, T.; Hanif, N.S.M.; Chan, C.H.; Arof, A.K. Effect of the surface treatment of the TiO₂ fillers on the properties of hexanoyl chitosan/polystyrene blend-based composite polymer electrolytes. *Ionics* **2014**, *20*, 347–352. [\[CrossRef\]](#)
184. Winie, T.; Mohd Shahril, N.S. Conductivity enhancement by controlled percolation of inorganic salt in multiphase hexanoyl chitosan/polystyrene polymer blends. *Front. Mater. Sci.* **2015**, *9*, 132–140. [\[CrossRef\]](#)
185. Aziz, S.B.; Rasheed, M.A.; Abidin, Z.H.Z. Optical and Electrical Characteristics of Silver Ion Conducting Nanocomposite Solid Polymer Electrolytes Based on Chitosan. *J. Electron. Mater.* **2017**, *46*, 6119–6130. [\[CrossRef\]](#)
186. Aziz, S.B. Role of dielectric constant on ion transport: Reformulated Arrhenius equation. *Adv. Mater. Sci. Eng.* **2016**, *2016*, 2527013. [\[CrossRef\]](#)
187. Aziz, S.B.; Abidin, Z.H.Z. Ion-transport study in nanocomposite solid polymer electrolytes based on chitosan: Electrical and dielectric analysis. *J. Appl. Polym. Sci.* **2015**, *132*, 41774. [\[CrossRef\]](#)
188. Muhammad, F.H.; Azmar, A.; Winie, T. Transport properties of hexanoyl chitosan-LiClO₄-TiO₂ composite polymer electrolyte. *AIP Conf. Proc.* **2015**, *1674*, 020029. [\[CrossRef\]](#)
189. Rosli, N.H.A.; Muhammad, F.H.; Subban, R.H.Y.; Winie, T. Structural and electrical studies of hexanoyl chitosan based electrolyte system. *Mater. Res. Innov.* **2011**, *15*, s94–s96. [\[CrossRef\]](#)
190. Winie, T.; Han, C.C.; Subban, R.H.Y. Ac conductivity and dielectric properties of hexanoyl chitosan-LiClO₄-TiO₂ composite polymer electrolytes. *Adv. Mater. Res.* **2011**, *335–336*, 873–880. [\[CrossRef\]](#)
191. Winie, T.; Hanif, N.S.M.; Rosli, N.H.A.; Subban, R.H.Y. Ac Conductivity Study of Hexanoyl Chitosan-LiCF₃SO₃-EC-Al₂O₃ Nanocomposite Polymer Electrolytes. *Adv. Mater. Res.* **2013**, *667*, 93–98. [\[CrossRef\]](#)
192. Wang, J.; Song, S.; Gao, S.; Muchakayala, R.; Liu, R.; Ma, Q. Mg-ion conducting gel polymer electrolyte membranes containing biodegradable chitosan: Preparation, structural, electrical and electrochemical properties. *Polym. Test.* **2017**, *62*, 278–286. [\[CrossRef\]](#)
193. Dannoun, E.M.A.; Aziz, S.B.; Brza, M.A.; Nofal, M.M.; Asnawi, A.S.F.M.; Yusof, Y.M.; Al-Zangana, S.; Hamsan, M.H.; Kadir, M.F.Z.; Woo, H.J. The study of plasticized solid polymer blend electrolytes based on natural polymers and their application for energy storage EDLC devices. *Polymers* **2020**, *12*, 1–19. [\[CrossRef\]](#) [\[PubMed\]](#)
194. Aziz, S.B.; Dannoun, E.M.A.; Hamsan, M.H.; Abdulwahid, R.T.; Mishra, K.; Nofal, M.M.; Kadir, M.F.Z.; Appetecchi, B.; Kim, D. Improving EDLC Device Performance Constructed from Plasticized Magnesium Ion Conducting Chitosan Based Polymer Electrolytes via Metal Complex Dispersion. *Membranes* **2021**, *11*, 289. [\[CrossRef\]](#) [\[PubMed\]](#)
195. Hamsan, M.H.; Aziz, S.B.; Nofal, M.M.; Brza, M.A.; Abdulwahid, R.T.; Hadi, J.M.; Karim, W.O.; Kadir, M.F.Z. Characteristics of EDLC device fabricated from plasticized chitosan:MgCl₂ based polymer electrolyte. *J. Mater. Res. Technol.* **2020**, *9*, 10635–10646. [\[CrossRef\]](#)
196. Pawlicka, A.; Sabadini, A.C.; Raphael, E.; Dragunski, D.C. Ionic conductivity thermogravimetry measurements of starch-based polymeric electrolytes. *Mol. Cryst. Liq. Cryst.* **2008**, *485*, 804–816. [\[CrossRef\]](#)
197. Khair, A.S.A.; Arof, A.K. Conductivity studies of starch-based polymer electrolytes. *Ionics* **2010**, *16*, 123–129. [\[CrossRef\]](#)
198. Sen, A.; Bhattacharya, M. Residual stresses and density gradient in injection molded starch/synthetic polymer blends. *Polymer* **2000**, *41*, 9177–9190. [\[CrossRef\]](#)
199. Wang, J.; Liang, Y.; Zhang, Z.; Ye, C.; Chen, Y.; Wei, P.; Wang, Y.; Xia, Y. Thermoplastic starch plasticized by polymeric ionic liquid. *Eur. Polym. J.* **2021**, *148*, 110367. [\[CrossRef\]](#)
200. Zahid, A.R.M.; Masri, M.N.; Hussin, M.H.; Bakar, M.B.A. The preliminary study on cassava (*Manihot esculenta*) as gel polymer electrolyte for zinc-air battery. *AIP Conf. Proc.* **2018**, *2030*, 020278. [\[CrossRef\]](#)
201. Mobarak, N.N.; Jumaah, F.N.; Ghani, M.A.; Abdullah, M.P.; Ahmad, A. Carboxymethyl Carrageenan Based Biopolymer Electrolytes. *Electrochim. Acta* **2015**, *175*, 224–231. [\[CrossRef\]](#)
202. Moniha, V.; Alagar, M.; Selvasekarapandian, S.; Sundaresan, B.; Boopathi, G. Conductive bio-polymer electrolyte iota-carrageenan with ammonium nitrate for application in electrochemical devices. *J. Non. Cryst. Solids* **2018**, *481*, 424–434. [\[CrossRef\]](#)
203. De Ruiter, G.A.; Rudolph, B. Carrageenan biotechnology. *Trends Food Sci. Technol.* **1997**, *8*, 389–395. [\[CrossRef\]](#)
204. Yao, Z.; Wu, H.; Zhang, S.; Du, Y. Enzymatic preparation of κ-carrageenan oligosaccharides and their anti-angiogenic activity. *Carbohydr. Polym.* **2014**, *101*, 359–367. [\[CrossRef\]](#) [\[PubMed\]](#)
205. Pacheco-Quito, E.M.; Ruiz-Caro, R.; Veiga, M.D. Carrageenan: Drug Delivery Systems and Other Biomedical Applications. *Mar. Drugs* **2020**, *18*, 583. [\[CrossRef\]](#)
206. Sabbagh, F.; Kiarostami, K.; Khatir, N.M.; Rezaei, S.; Muhamad, I.I.; Hosseini, F. Effect of zinc content on structural, functional, morphological, and thermal properties of kappa-carrageenan/NaCMC nanocomposites. *Polym. Test.* **2021**, *93*, 106922. [\[CrossRef\]](#)

-
207. Chan, S.; Paolo, J.; Bantang, O.; Bantang, J.P.; Camacho, D. Influence of Nanomaterial Fillers in Biopolymer Electrolyte System for Squaraine-based Dye-Sensitized Solar Cells. *Int. J. Electrochem. Sci* **2015**, *10*, 7696–7706.
208. Armisen, R.; Galatas, F. Agar. In *Handbook of Hydrocolloids: Second Edition*; Elsevier Inc.: Amsterdam, The Netherlands, 2009; pp. 82–107, ISBN 9781845695873.
209. Kato, S.; Yamagishi, A.; Daimon, S.; Kawasaki, K.; Tamaki, H.; Kitagawa, W.; Abe, A.; Tanaka, M.; Sone, T.; Asano, K.; et al. Isolation of previously uncultured slowgrowing bacteria by using a simple modification in the preparation of agar media. *Appl. Environ. Microbiol.* **2018**, *84*, e00807-18. [[CrossRef](#)] [[PubMed](#)]
210. Selvalakshmi, S.; Mathavan, T.; Selvasekarapandian, S.; Premalatha, M. Effect of ethylene carbonate plasticizer on agar-agar: NH₄Br-based solid polymer electrolytes. *Ionics* **2018**, *24*, 2209–2217. [[CrossRef](#)]
211. An, L.; Zhao, T.S.; Zeng, L. Agar chemical hydrogel electrode binder for fuel-electrolyte-fed fuel cells. *Appl. Energy* **2013**, *109*, 67–71. [[CrossRef](#)]
212. Yang, Y.; Hu, H.; Zhou, C.H.; Xu, S.; Sebo, B.; Zhao, X.Z. Novel agarose polymer electrolyte for quasi-solid state dye-sensitized solar cell. *J. Power Sources* **2011**, *196*, 2410–2415. [[CrossRef](#)]

2.2. Article published in the Journal *Batteries* “Chitosan-Carboxymethylcellulose Hydrogels as Electrolytes for Zinc–Air Batteries: An Approach to the Transition towards Renewable Energy Storage Devices.”

In this paper, it is reported the synthesis and characterization of hydrogels based on CMC, CS, and different amounts of CA, as well as a sample with the absence of the latter in order to contrast the effects of the chemical crosslinker on the properties to be evaluated. In order to dope the hydrogels with the conductive aqueous medium, 12 M KOH solutions were used to evaluate the capacity of the membranes to retain the liquid and incorporate it into the polymeric matrix, in order to carry out the conduction process in the desired battery application.

In the first part, an analysis of the chemical reactions' effects in the synthesis and the trigger of new functional groups expected in the matrix is presented. Subsequently, the modification of the chemical structures of the system is analyzed through the ATR-FTIR and XRD structural characterizations. The esterification reaction expected by the insertion of CA is confirmed. The addition of KOH molecules to the system provokes conformational changes, and a lower degree of crystallinity, relevant for the ionic conduction process. Higher thermal stability is also evidenced by the TGA and DSC studies.

Regarding the electrochemical studies, Arrhenius behavior was confirmed in the range of 0 °C to 60 °C for the CA-containing membranes, obtaining the activation energy for each hydrogel. A maximum value of $0.19 \text{ S}\cdot\text{cm}^{-1}$ was found at 30 °C through the PEIS studies. The swelling behavior was analyzed, resulting in an inversely proportional trend between the swelled KOH and the ionic conductivity values. This apparent contradictory behavior was related to the capability of the hydrogel to retain the swelled KOH when it is pressed between the electrodes and its further integrity. A high ionic transfer was confirmed by the cyclic voltammetry studies, with intensity peaks of $360 \text{ mA}\cdot\text{cm}^{-2}$. The intensity peak value depends on the number of electrons transferred between the redox species and the electrode, which depends on the ion's movement. Besides, a quasi-reversible behavior was evidenced.

Finally, the hydrogels were tested in a zinc–air battery prototype, with high performance in terms of power densities, bulk resistances, and discharge times. The maximum specific capacity was $1026 \text{ mA}\cdot\text{h g}^{-1}$ for the battery assembled with the hydrogel electrolyte containing the highest amount of CA. Overall, the importance of the chemical crosslinker employed was corroborated by the enhancement of the relevant properties required by the electrochemical application.



batteries



Article

Chitosan-Carboxymethylcellulose Hydrogels as Electrolytes for Zinc–Air Batteries: An Approach to the Transition towards Renewable Energy Storage Devices

María Fernanda Bósquez-Cáceres, Lola De Lima, Vivian Morera Córdova, Anabel D. Delgado, José Béjar, Noé Arjona, Lorena Álvarez-Contreras and Juan P. Tafur

Special Issue

Zn-Ion and Zn–Air Batteries: Materials, Mechanisms and Applications

Edited by




Dr. Jingwen Zhao, Dr. Fei Wang and Dr. Ziyang Guo



<https://doi.org/10.3390/batteries8120265>

Article

Chitosan-Carboxymethylcellulose Hydrogels as Electrolytes for Zinc–Air Batteries: An Approach to the Transition towards Renewable Energy Storage Devices

María Fernanda Bósquez-Cáceres ¹, Lola De Lima ¹, Vivian Morera Córdova ¹, Anabel D. Delgado ², José Béjar ², Noé Arjona ³, Lorena Álvarez-Contreras ^{2,*} and Juan P. Tafur ^{1,*}

- ¹ Grupo de Investigación Aplicada en Materiales y Procesos (GIAMP), School of Chemical Sciences & Engineering, Yachay Tech University, Urcuquí 100115, Ecuador
² Centro de Investigación en Materiales Avanzados S.C. (CIMAV), Miguel de Cervantes No. 120, Complejo Industrial Chihuahua, Chihuahua 31136, Mexico
³ Centro de Investigación y Desarrollo Tecnológico en Electroquímica S.C., Pedro Escobedo, Querétaro 76703, Mexico
* Correspondence: lorena.alvarez@cimav.edu.mx (L.Á.-C.); jtafur@yachaytech.edu.ec (J.P.T.)



Citation: Bósquez-Cáceres, M.F.; Lima, L.D.; Morera Córdova, V.; Delgado, A.D.; Béjar, J.; Arjona, N.; Álvarez-Contreras, L.; Tafur, J.P. Chitosan-Carboxymethylcellulose Hydrogels as Electrolytes for Zinc–Air Batteries: An Approach to the Transition towards Renewable Energy Storage Devices. *Batteries* **2022**, *8*, 265. <https://doi.org/10.3390/batteries8120265>

Academic Editors: Jingwen Zhao, Fei Wang and Ziyang Guo

Received: 20 October 2022

Accepted: 25 November 2022

Published: 30 November 2022

Publisher's Note: MDPI stays neutral with regard to jurisdictional claims in published maps and institutional affiliations.



Copyright: © 2022 by the authors. Licensee MDPI, Basel, Switzerland. This article is an open access article distributed under the terms and conditions of the Creative Commons Attribution (CC BY) license (<https://creativecommons.org/licenses/by/4.0/>).

Abstract: Biopolymers are promising materials as electrolytes with high flexibility, good performance, cost effectiveness, high compatibility with solvents, and film-forming ability. Chitosan (CS) and carboxymethylcellulose (CMC) can form an intermolecular complex, giving rise to hydrogels capable of absorbing ionic solutions. Citric acid (CA) is an effective biological chemical crosslinker that assists the formation of amide and ester bonds between CMC and CS, resulting in a structure with high ionic conductivity and good structural integrity. In this study, a chemical crosslinking strategy is used to synthesize electrolyte hydrogels for zinc–air batteries. The effects of crosslinking are studied on the structural and electrochemical performance of the membranes. The results show an improvement in the ionic conductivity with respect to the homologous electrolyte hydrogel systems reported, with a maximum of $0.19 \text{ S} \cdot \text{cm}^{-1}$ at 30°C . In addition, the cyclic voltammetry studies showed a current intensity increase at higher CA content, reaching values of $360 \text{ mA} \cdot \text{cm}^{-2}$. Structural characterization suggests a higher thermal stability and a decrease in the degree of crystallinity caused by the polymers' crosslinking. Finally, these membranes were tested in Zn–air batteries, obtaining power densities of $85 \text{ mW} \cdot \text{cm}^{-2}$. The proposed hydrogels show to be appropriate for energy zinc–air battery applications and present an alternative to support the sustainable energy transition.

Keywords: zinc–air batteries; electrolytes; hydrogels; biopolymers; crosslinking; casting technique

1. Introduction

To mitigate environmental problems, a transition to clean energy sources is essential, such as wind and solar, which have the limitation of being intermittent. An attractive alternative is the development of sustainable rechargeable batteries for renewable energy storage, such as metal–air batteries. In aqueous metal–air batteries, zinc as an anode presents strategic characteristics for battery performance, such as a high volumetric capacity, low redox potential (-0.76 V vs. standard hydrogen electrode), and lower reactivity. It is a chemical element of high abundance, and its use lowers the battery manufacturing cost and toxicity, and it has good safety [1–8]. These characteristics make it an appropriate element to develop ecofriendly batteries. In addition, zinc–air batteries (ZABs) are of great research interest, since they are characterized by the electrochemical coupling of a negative metal electrode to an air-breathing positive electrode, with high theoretical energy densities, even 10 times higher than their lithium ion counterparts [9–11].

A key feature in the design of new batteries is the physical state of the electrolyte. Most commercial batteries use liquid electrolytes. These batteries present safety, toxicity,

flammability, and leakage problems [12–14]. On the other hand, the growth of dendrites on the metal electrode and the corrosion that occurs at the interfaces reduce the capacity and life cycle of the battery and can even generate unequal currents during charging and preferential nucleation, causing fires [15–20]. This is why great attention is currently devoted to the development of solid or gel electrolytes.

Polymer electrolytes (PEs) have very attractive characteristics. They are flexible and have good performance [21–24]. Mo et al. [25] proposed a polymer electrolyte for flexible Zn batteries. The proposal of these authors demonstrated that PEs are an effective solution to avoid dendrite penetration, hydrogen evolution reaction, and corrosion. However, the main problems of these materials are their low battery efficiencies from poor ionic conductivities, low electrochemical stabilities, insufficient mechanical strength, and huge interfacial resistance [26,27].

Chitosan (CS) is an alternative for electrochemical applications, because it is an ecofriendly and biopolymeric material that is nontoxic, biodegradable, and a good hydrogel former [28]. Its molecular structure presents lone electron pairs at the oxygen atom from hydroxyl and a nitrogen atom from amino groups, making it an appropriate polymer host for ionic conduction. Due to the fact of these characteristics, hydrogels, membranes/films, fiber, and sponges formed of chitosan biomaterial have been reported for numerous biotechnology, medicine engineering, environmental, and industrial applications [29,30]. CS has been used to form blends with carboxymethylcellulose (CMC), a biopolymer that forms intermacromolecular complexes through strong electrostatic and hydrogen bonding interactions with CS [31,32]. Bakar et al. [33] reported that the highest ionic conductivity achieved by solid CMC-CS PEs doped with dodecyl trimethyl ammonium bromide was 1.82×10^{-6} S/cm. This result was improved by Rani et al. [34] to 1.03×10^{-5} S cm⁻¹ by adding ammonium nitrate to the polymer blend.

Biopolymer hydrogels solve many of the drawbacks of other types of electrolytes. They have better ductility and flexibility, adapt to various working environments because of their self-healing ability, exhibit shape memory, and have the ability to stretch their crosslinked network of polymer chains with fluid-filled interstitial spaces [35,36]. CMC-CS hydrogels can be synthesized by chemical crosslinking. There is scientific evidence for the use of glutaraldehyde [32], arginine [37], sodium alginate [38], fumaric acid, and tartaric acid [39] as crosslinking agents. In particular, citric acid (CA) is an effective chemical crosslinker that leads to the formation of amide and ester bonds between CMC and CS, generating a structure with porous networks and good mechanical stability [40].

KOH is an ionic salt used as an ion source to improve the ionic conductivity of the system [41,42]. Iles et al. [43] achieved a maximum ionic conductivity of 0.019 S cm⁻¹ with a polymer gel electrolyte composed of polyvinyl alcohol (PVA) and a terpolymer composed of butyl acrylate, vinyl acetate, and vinyl neodecanoate (VAVTD) and a KOH solution. In this work, hydrogels were synthesized from CS and CMC with the addition of CA to form the host matrix doped with a concentrated 12 M KOH solution. The structural, thermal, and electrochemical properties of the synthesized membranes were analyzed as a function of the crosslinker addition and ratios. The results indicate that it is a good material to be applied as hydrogel electrolytes in Zn–air batteries.

2. Materials and Methods

Chitosan food grade (90.6% deacetylated [44]) (purity 100%, BioFitnest), carboxymethyl cellulose sodium salt (sodium glycolate max. 0.4%, high viscosity grade), and citric acid anhydrous (purity 99.5%) were acquired from Loba Chemie. Acetic acid glacial anhydrous for the analysis (purity 100%) and KOH pellets anhydrous (purity $\geq 99.95\%$) were acquired from Sigma Aldrich. The reagents were used directly for electrolyte membrane preparation. Distilled water was used as a solvent in the polymer blending.

The Zn discs (99.999%) and Pt plates (99.97%) used in these cells were purchased from Goodfellow. Hydrogel electrolytes were sandwiches between Zn and Pt electrodes

(Zn/Hydrogel/Pt cell) or two Zn discs (Zn/hydrogel/Zn cell) (Beit Shemesh, Israel) and Al_2O_3 polishing suspension (1 and 0.05 micron), Buehler (Lake Bluff, IL, USA).

2.1. Preparation of the CMC-CS and CMC-CS-CA Hydrogels

The hydrogels were synthesized using the solution polymerization/crosslinking methods reported by Calderon et al., with some modifications [44]. The hydrogel components were prepared separately; 2 g of CS was dissolved in 100 mL of 1% (v/v) acetic acid solution, 2 g of CMC in 100 mL of distilled water, and 4 g of CA in 100 mL of distilled water. The polymer solutions were stirred overnight until homogeneous solutions were obtained. Subsequently, the hydrogels were synthesized in a 3:1 CMC/CS volume ratio, varying the amounts of CA added (Table 1). A membrane without CA was prepared to contrast the results of the crosslinker effect. The different mixtures were prepared using an immersion mixer for 3 min. Then, the mixtures were sonicated at 40 kHz at 60 °C for 60 min. The hydrogels were dried in an oven at 80 °C for 60 min. The excess liquid was removed to proceed to drying under a fume hood for over a week. The resulting membranes were stored in a desiccator for further characterization in a dry form. In parallel, another set of hydrogels was immersed in a 12 M KOH solution for 48 h before being subjected to the different characterization techniques. To label the latter as hydrogels, “sw” was added to the hydrogel codes (Table 1).

Table 1. Codes to name the hydrogel polymer electrolytes used in this work.

Electrolyte	Hydrogel Code
CMC90/CS30	CMC-CS
CMC90/CS30/CA30	CA30
CMC90/CS30/CA40	CA40
CMC90/CS30/CA50	CA50
CMC90/CS30 “sw”	CMC-CS sw
CMC90/CS30/CA30 “sw”	CA30 sw
CMC90/CS30/CA40 “sw”	CA40 sw
CMC90/CS30/CA50 “sw”	CA50 sw

2.2. Swelling Behavior of the Hydrogels

The hydrogels were weighed before the hydration in 12 M KOH and after 48 h of being immersed. For calculation, the swelling ratio (SR) shown in Equation (1) was used.

$$\text{SR} = \frac{W_T - W_0}{W_0} \times 100\% \quad (1)$$

where W is weight or volume, and the subindexes _T and ₀ represent the swollen hydrogel and the initial hydrogel, respectively.

2.3. Structural, Thermal, and Electrochemical Characterization

2.3.1. ATR-FTIR Methods

To analyze the specific functional groups of the CMC and CS polymers and the developed composite hydrogels, FT-infrared spectroscopy (FTIR) was conducted in the solid state by attenuated total reflectance (ATR) using a spectrophotometer (Cary 630, Agilent Technologies Inc., Santa Clara, CA, USA) equipped with a 1-bounce diamond ATR accessory. The spectra were registered in the range of 4000–400 cm^{-1} , with a resolution of 4 cm^{-1} , and 64 scans were performed.

2.3.2. XRD Characterization

X-ray diffraction (XRD) patterns were recorded using a computer-controlled Rigaku Mini-flex-600 with a D/tex Ultra 2 detector 26 (Rigaku, Tokyo, Japan). The measurement conditions were 40 kV and 15 mA for the X-ray generator in a sealed tube with a Ni-filtered Cu K α radiation source ($\lambda = 0.15418 \text{ nm}$). For data collection, the membranes were placed

in a sample holder, and the angular region selected was $2\theta = 5^\circ\text{--}80^\circ$ with a step width of 0.01° . Match! Software (Crystal Impact, Bonn, Germany) was used to quantify the degree of crystallinity of each membrane [45].

2.3.3. SEM and BET Characterization

In order to study the hydrogels' morphology, field-emission scanning electron microscopy was used (FE-SEM, JEOL JSM-7401F microscope, JEOL Ltd., Tokyo, Japan). A Brunauer–Emmett–Teller (BET) analysis was performed using N_2 adsorption/desorption isotherms at -195°C employing a S-BET Autosorb iQ2 (Quantachrome Instruments, Boynton Beach, FL, USA). Before the adsorption/desorption test, each membrane was treated at 80°C in a vacuum for 1 h.

2.3.4. Thermal Analysis

The thermal properties of hydrogels were studied by thermogravimetric analysis (TGA) and differential scanning calorimetry (DSC) using a DSC-TGA Q600 (TA Instruments, New Castle, DE, USA). Nitrogen was employed as the purge gas. The temperature range used was from 25 to 800°C with a heating rate of $10^\circ\text{C min}^{-1}$.

2.3.5. Electrochemical Measurements

To evaluate the electrochemical behavior of the hydrogels, potential electrochemical impedance spectroscopy (PEIS) was performed using a VIONIC instrument (Metrohm model, Ecuador). The frequency range for the PEIS varied from 100 kHz to 1 Hz, and the cell configuration used was Pt/hydrogel/Pt, with a 1 cm^2 area Pt blocking the electrodes. The conductivity at different temperatures was examined in the range of 0 to 60°C with $\pm 1^\circ\text{C}$ precision using a Julabo circulator Polyscience (-40°C , 15 L). Four measurements were performed for each hydrogel and temperature. The system was stabilized after each temperature drop for 5 min before taking the resistance measurement. The ionic conductivity (σ) was calculated using Equation (2):

$$\sigma = \frac{l}{A \times R_b} \quad (2)$$

where l is the film thickness, A is the Pt electrode area, and R_b is the bulk resistance obtained from the intersections of the impedance curve with the x -axis. Four impedance measurements were carried out for each membrane. To determine the activation energy (E_a) of each electrolyte, the Arrhenius Equation (3) was used with a linear fitting by plotting a logarithmic relationship between $\ln(\sigma)$ and $1000/T$:

$$\sigma = \sigma_0 \exp\left(-\frac{E_a}{K_b \times (T)}\right) \quad (3)$$

where K_b is the Boltzmann's constant, T is the absolute temperature, and σ_0 is a pre-exponential factor [46].

The linear sweep voltammetry (LSV) staircase of the hydrogels was registered between 0.0 and +4.0 V using a Zn/hydrogel/Pt cell. Pt was used as the working electrode, and a Zn disc served both as the counter electrode and the reference electrode. The measurements were performed at a speed of 1 mV/s. Cyclic voltammetry (CV) was performed to evaluate the electrochemical behavior of the hydrogels. The CV studies were carried out using a Zn/hydrogel/Zn symmetric two-electrode cell with Zn electrodes of 0.5 cm^2 and a scanning speed of $50\text{ mV}\cdot\text{s}^{-1}$ in a symmetric potential window from -1.5 to $+1.5\text{ V}$.

2.4. Battery Tests

The battery tests were conducted in an AMETEK® VersaSTAT 3 potentiostat/galvanostat (Princeton Applied Research, Berwyn, IL, USA). The anode consisted of a piece of polished high-purity Zn foil ($15 \times 10\text{ mm}$ length and width, 0.2 mm in depth, purity 99.9%, Yun-

express Inc., Shenzhen, China). SIGRACET® 39 B slides (15 × 10 mm length and width, 0.4 mm in depth) impregnated with commercial catalytic ink and Pt/C (20% wt.%) were used as a cathode. The catalyst mass loading was 1 mg cm⁻². For the battery assembly, the hydrogels were placed between the two electrodes. The discharge current density was −3 mA cm⁻², and the cut-off voltage was 0.2 V. The specific capacitance was determined through the zinc weight loss after discharging the Zn–air battery at 1.98 mA cm⁻².

3. Results

3.1. Formation Reaction of the Hydrogels

The CMC in an anionic polyelectrolyte form reacts with chitosan (cationic polyelectrolyte) by ionic interactions/crosslinking to form CMC–CS [47], leading to intra- and interchange compensation (Figure 1a). However, with the introduction of CA, in addition to the ionic interaction, there is a reaction of esterification [48] because of the –OH and –COOH groups added to the system, resulting in the formation of hydrogels (Figure 1b). The primary –OH group of the carboxylic acid present in CA is known to be more reactive than the –OH group formed in the CMC–CS uncrosslinked membrane, assuring the esterification reaction with the CA. The crosslinking reaction seeks to increase the number of –OH and –COOH, functional groups desired in a polymer host for ionic conduction systems.

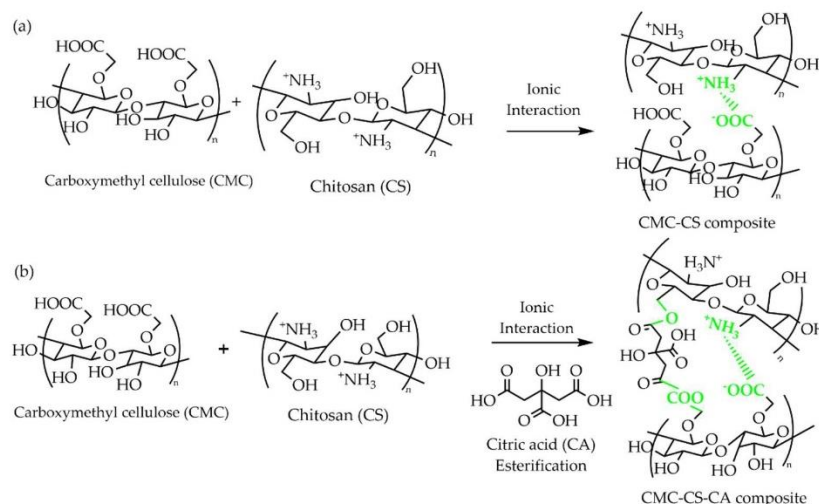


Figure 1. Proposed reaction for the formation of the (a) CMC–CS and (b) CMC–CS–CA hydrogels.

3.2. Swelling Behavior

The SR of the soaked membranes was calculated, using Equation (1), by the KOH uptake in the hydrogels (Figure 2). It was observed that the noncrosslinked membrane exhibited the highest KOH uptake and volume change (288.68 ± 26.49 wt.%, 37.5 vol.%). In the case of the crosslinked hydrogels, a decrease in the SR was observed as the proportion of CA increased. This behavior agrees with that reported by Fekete et al. [49], who noticed a lower degree of swelling when a higher crosslink density was achieved. However, it is noteworthy that the CA50 membrane, which swelled the least, absorbed approximately 1.5 times its weight with a very low volume change (Figure 2) pointing to a higher swelling capacity in contrast to other polymeric blends [50,51]. In the synthesized hydrogels, the KOH plays the role of an electrolyte ionic species donor to increase the ionic conductivity of the system. In addition, it has been reported that KOH is able to enter the polymer backbone causing conformational changes [52]. Additionally, the thickness of the hydrogels ranged between 0.28 and 0.36 cm (Table S1).

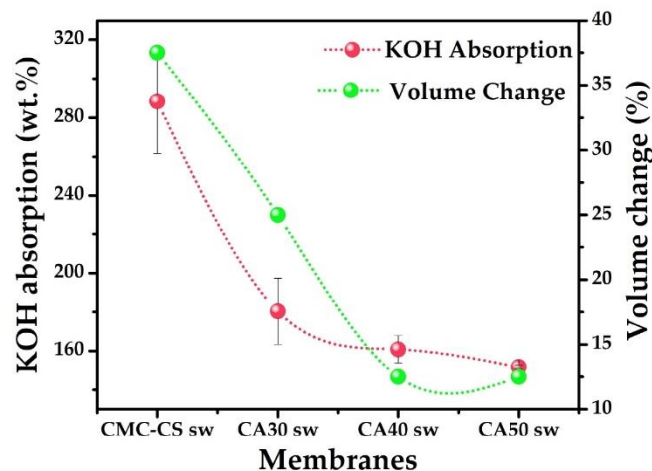


Figure 2. Swelling behavior in mass percentage and volume change of the CMC-CS sw hydrogels at different CA proportions.

3.3. Structural Characterization

3.3.1. ATR-FTIR Analysis

The ATR-FTIR spectral data (Figure 3a) of the CS and CMC polymers showed typical spectral bands. For the pure CS film, the spectrum showed a band in the region between 3100 and 3500 cm^{-1} , assigned to the -OH/NH stretching vibrations [53]. The band at 2920 cm^{-1} corresponded to the C-H bond of the methylene group attached to the primary alcohol. In addition, two peaks observed at 2869 and 2857 cm^{-1} were related to the asymmetric and symmetric C-H stretching vibration of the N-acetyl group. The band at 1610 cm^{-1} was related to the carbonyl assigned to the stretching vibrations of the acetylated amino groups (amide I) and 1541 cm^{-1} for the N-H bending vibration of the primary amine (amide II), as reported previously [54]. The bands of the glycosidic bonds of the skeletal polysaccharides at 1150 and 1063 cm^{-1} were again related to the stretching of the asymmetric C-O bridge, while the peak at 1016 cm^{-1} was assigned to the vibration of the C-O-C pyranose ring and the β -glycosidic bond, giving rise to bands similar to those reported by Corazzari et al. [55]. In the spectrum obtained for the pure CMC film, a fundamental band at 3209 cm^{-1} , attributable to the -OH stretching vibration, was observed. On the other hand, there was a band at 1585 cm^{-1} assigned to the symmetric stretching vibration of the carbonyl [56]. The bands observed at 1425 and 1375 cm^{-1} were assigned to the -CH_2 stretching and -OH bending vibration of the CMC [57], while those at 1114 and 1024 cm^{-1} were characteristic of the C-O stretching of the polysaccharide backbone [58].

In the case of the CMC-CS membrane, along with the fundamental bands that are characteristic for both polymers, a band at 1578 cm^{-1} was observed, which was associated with the symmetric stretching vibrations of the COO- groups for the CMC (1584 cm^{-1}) and to the N-H bending vibration (1563 cm^{-1}) of the -NH_2 groups in chitosan. However, this band has shifted to 1578 cm^{-1} , suggesting ionic interactions and/or hydrogen bonds between the CS and the CMC [59]. There is evidence that hydrogen bridge bonds between the chitosan and the CMC could also be a factor in this shift [39]. The band shift to low/high wavenumbers either weakened/strengthened, indicating crosslinking and the extent of the linkage between the biopolymer backbone and the crosslinker [60].

As for the CA30, CA40, and CA50 spectra, there is evidence pointing to the formation of ester bonds due to the fact of CA insertion, with the peak located at 1717 cm^{-1} , where the difference in the peak intensity between the three hydrogels was given by the degree of chemical crosslinking [39]. In the pure polymers and in the membrane without CA, this peak was absent. In addition, the peak at 1578 cm^{-1} was also present in the crosslinked

membranes. This allows us to conclude that both physical interactions and chemical bonds occurred.

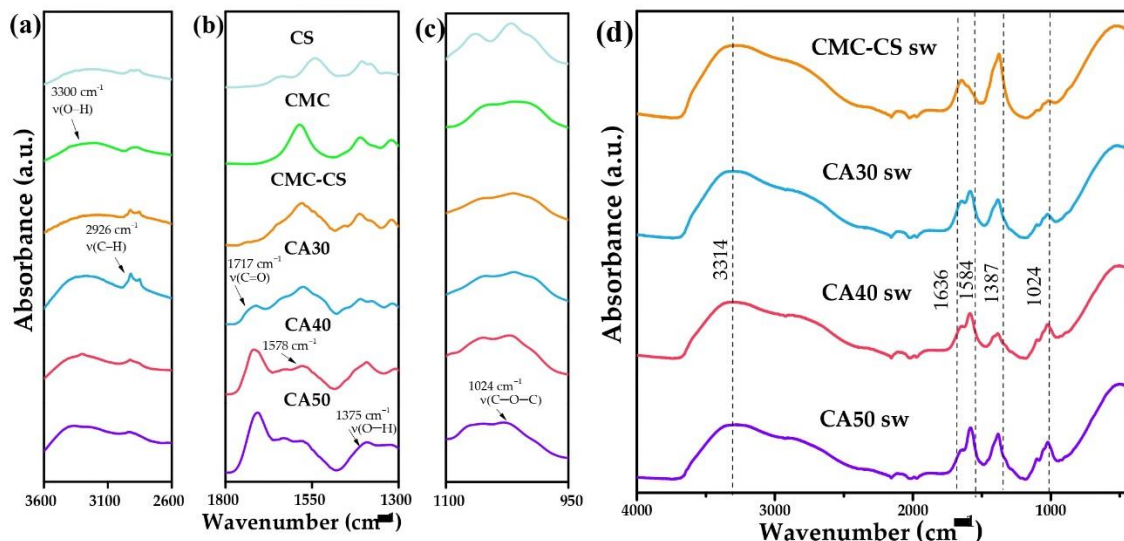


Figure 3. ATR-FTIR spectra of (a) CS, (b) CMC, (c) CMC-CS, and (d) CMC-CS sw hydrogels at different CA proportions.

As for the swollen hydrogels (Figure 3b), the first relevant observed change was in the $-OH$ and $-C-H$ region, with an increase in the broad band due to the insertion of water, pointing to a higher amount and stronger hydrogen bonds within the polymeric matrix [43]. The band at 1636 cm^{-1} mapped to the frequency of the water bending mode [61]. The characteristic $C=O$ peak shifted to 1584 cm^{-1} , probably because of an amorphous state [62] due to the presence of hydroxyl groups of the KOH. Santos et al. [41] reported that the oxygen atoms of the KOH and the $C=O$ groups of the polymer were strong electron donors due to the presence of available lone pairs of electrons, pointing to coordination of the K^+ cations, with these groups forming complexes such as $C=O \cdots K^+$ or $C-O \cdots K^+$. The fingerprint region indicated the skeletal signals of the glycosidic bonds, where the $C-O-C$ vibration of the pyramidal ring at 1024 cm^{-1} was shown to be reduced in intensity, evidencing the change in the shape and intensity of the $C-H$ and $C-O-C$ peaks [63]. This reduction can be explained by the interaction between the Lewis OH^- base and Lewis acid of the CA, with the smaller band for the membrane with less CA content, pointing to the preservation of the polysaccharide chains when more CA was added to the matrix.

3.3.2. XRD Analysis

The XRD pattern from pure CMC is reported to exhibit a diffraction peak at $2\theta = 19.59^\circ$ [64], while for CS it presents characteristic peaks at 10.18° and 20.16° . These values indicate a semicrystalline nature for the polymers [65]. In our study, the peak at 10.18° disappeared from the diffractograms, and the most relevant peak obtained was at $2\theta = 21^\circ$, exhibiting a broad shape (Figure 4). This peak points to the amorphous nature of the membranes when compared with the pure polymers [39,59]. Then, when analyzing the swollen membranes, the degree of crystallinity (X_c) decreased due to the addition of the KOH solution. The formed complex between the polysaccharide chains and the potassium cations could explain this behavior. Hence, the decrease in the crystallinity could be explained by the destruction of the hydrogen bonding in the matrix [66].

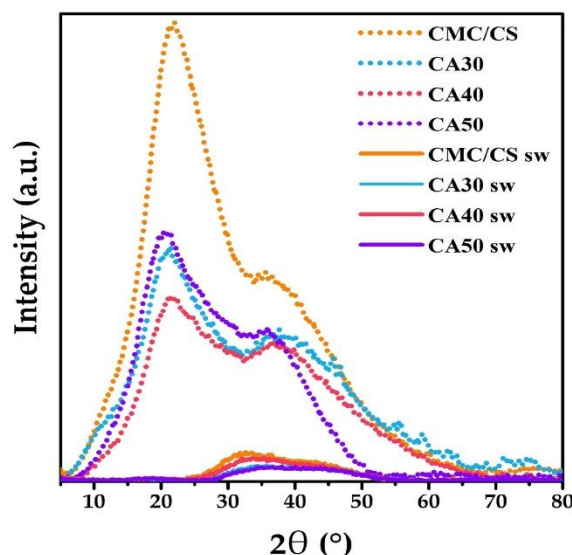


Figure 4. XRD patterns of the CMC-CS and CMC-CS sw hydrogels at different CA proportions.

The addition of the CA crosslinker increased the amorphousness of the hydrogels, obtaining 15.6% of the crystallinity in the case of the CA50 unswollen membrane (Table 2). Moreover, with the absorption of the KOH, it was observed that X_c decreased. The smallest degree of crystallinity was obtained for the CA40 sw hydrogel, reaching 4.6%, while the values for the CA30 sw and CA50 sw membranes were 5.2% and 4.7%, respectively. The degree of crystallinity is important, as it is related to the hydrogels' swelling behavior [67]. Additionally, the ionic conductivity suffered an improvement, as the crystallinity decreased since the ions have low mobility in the crystalline phases [68,69]. With the increased amorphousness, more voids were present, which is relevant to obtain higher ionic conductivity values [70].

Table 2. Crystallinity degree (X_c) calculated from the XRD patterns.

Membranes	X_c (%)
CMC-CS	17.9
CA30	15.5
CA40	14.4
CA50	15.6
CMC-CS sw	10.7
CA30 sw	5.2
CA40 sw	4.6
CA50 sw	4.7

3.3.3. SEM Micrographs and BET Analysis

For the uncrosslinked membrane CMC-CS, more smoothness and uniformity of the surface was shown, with few lumps presented on it (Figure 5a,b). This observation suggests good miscibility, homogeneity, and interaction of the polymers that form the membrane, leading to compaction of the microstructure [71]. For the crosslinked membrane CA50, a chapped surface with pleats, granules, and some orifices (macroporous) was observed. Wang et al. [72] reported similar surface structures related to the crosslinking degree achieved by polyethyleneimine/poly(vinyl alcohol) composites. Otherwise, Ritonga et al. [73] reported that the presence of uneven granules dispersed on the surface of hydrogels composed of chitosan-ethylenediaminetetraacetic acid, which has been iden-

tified as a crosslinker. The N_2 adsorption–desorption isotherms for the hydrogels were obtained (Figure S1). A mix of type II and type III isotherms was observed, with a low superficial area ranging from $3.3 \text{ m}^2/\text{g}$ for the CMC-CS membrane to $2.0 \text{ m}^2/\text{g}$ for the CA50 membrane. The herein obtained results suggest the obtention of nonporous or macroporous materials with a low relationship between the adsorbent and adsorbate. Hence, the swelling behavior when the membranes were hydrated with KOH solutions can be explained by a phenomenon of absorption rather than adsorption, indeed related to the crosslinking degree [39].

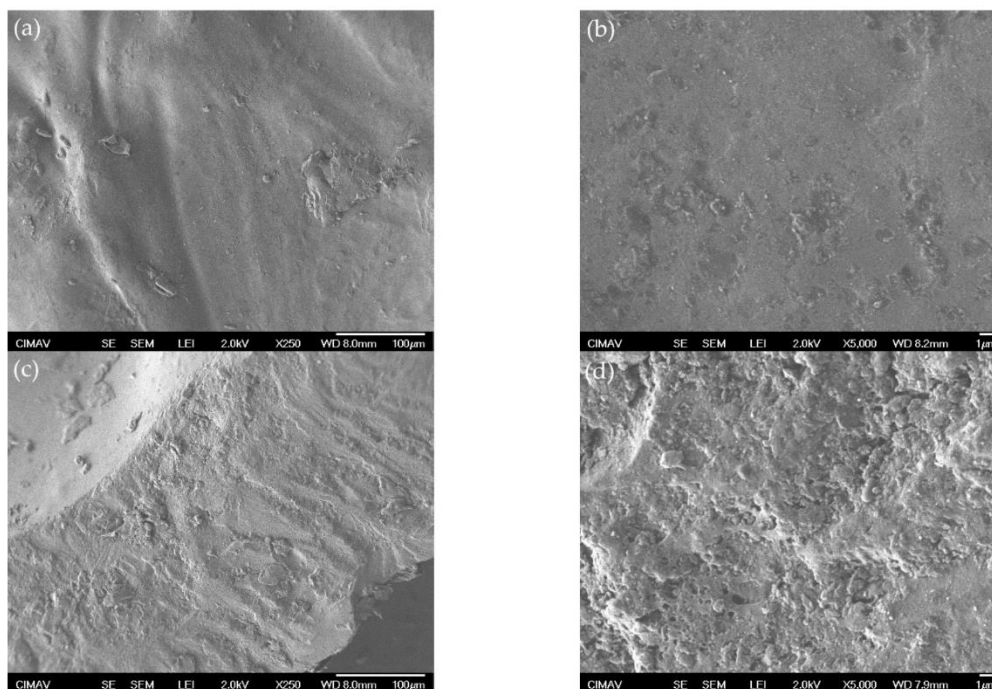


Figure 5. SEM micrographs of the CMC-CS membrane at (a) 250 \times and (b) 5000 \times and the CA50 membrane at (c) 250 \times and (d) 5000 \times .

3.4. Thermal Characterization

The CMC-CS membrane shows three degradation regions starting at 40, 130, and 330 $^{\circ}\text{C}$ (Figure 6). The first loss (17.8 wt.%) was attributed to the internal loss of water that the polymeric matrix undergoes. The second and third losses were linked to the degradation of the polymeric backbone. The second weight loss was also related to carbon formation [74,75]. Comparing our curves for the dry membranes with the curves obtained by Uyanga et al. [39] for pure polymers, it can be seen that the degradation regions coincide but in our case with an increase in the thermal stability. From $\sim 450^{\circ}\text{C}$ onwards, a stable behavior was observed, with a remaining residue of ~ 34.6 wt.% for the CMC-CS membrane and 26.4 wt.% for the CA50 membrane, suggesting an increase in the carbon yield with the increasing CA content in the hydrogel. The carbon yield is influenced by the chemical bonds and functional groups in a sample [76].

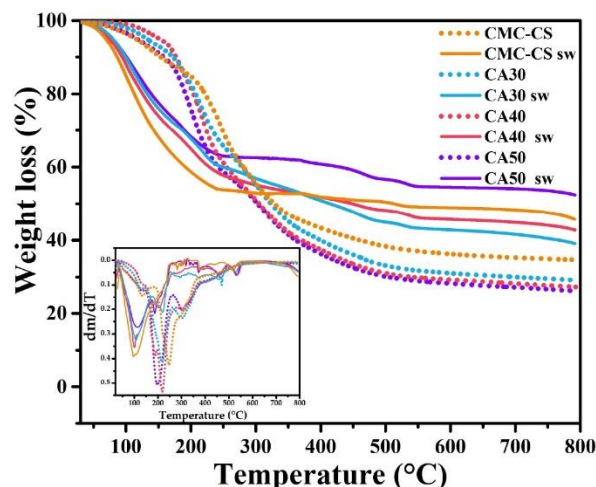


Figure 6. TGA curves of the CMC-CS and CMC-CS sw hydrogels at different CA proportions. Inset: DTGA curves of the electrolytes.

In the case of the swelled membranes in KOH solution, the loss of absorbed water by the hydrophilic groups in the polymer chains began at 47.7, 50.8, 53.6, and 56.6 °C for the CMC-CS sw, CA40 sw, CA50 sw, and CA30 sw, respectively. It was observed from the DTGA curves (Figure 6 inset) that the minimum peak shifted from 96.8 to 112.8 °C as more CA was added to the crosslinked membrane (CA50). That shift of the minimum peak is evidence of an increased thermal stability and higher water retention in the polymer matrix [62]. This can be explained by the higher degree of esterification (discussed in Section 3.1), since with the presence of more ester bonds in the polymer chain, a more reinforced structure is obtained, leading to stronger internal bonds that require more heat to undergo the regions of degradation. The next range of the matrix's degradation began at 240 °C. The weight loss was 45.9%, 41.5%, 39.64%, and 36.7% for CMC-CS sw, CA30 sw, CA40 sw, and CA50 sw, respectively. These losses originated from the degradation of the saccharide structure of the molecule [77]. The last region found from 516 to 537 °C shows the modification of the chemical structure produced by the oxygen-containing KOH molecule. The intensity of this peak was related to the KOH swelling behavior of the membranes. The higher residue percentage in the swelled hydrogels in comparison to the dried membranes could suggest the presence of potassium salts formed when KOH is decomposed [78].

The intermolecular interaction of the components could be evidenced in the DSC curves of the dried hydrogels (Figure S2a). For the CMC-CS hydrogel, it was evidenced an endothermic peak at 110 °C, attributable to heat absorption by water evaporation from the hydrogels [40]. Moreover, another endothermic peak was depicted at 204 °C, referable to the thermal degradation of the polymers [79]. However, for the CMC-CS-CA hydrogels, this peak shifted to lower values (194 °C), further confirming crosslinking. Beyond 235 °C, the last peak turned into an exothermic peak for all hydrogels. This phenomenon has been reported to be associated with CS structure debonding and the decomposition of its amine unit [80]. In terms of the soaked hydrogels, the increase in the intensity of the DSC curves (Figure S2b) points to firmer internal bonds related to the addition of CA, requiring more heat to evaporate the moisture and break the membrane bonds and, finally, leading to the thermal degradation of the structures [39].

3.5. Electrochemical Characterization

3.5.1. Influence of the CA Content on the Ionic Conductivity

The ionic conductivity (σ) was studied as a function of the temperature for all of the swollen hydrogels (Figure 7). For Arrhenius to be suitable, the plots of $\ln(\sigma)$ versus $1000/T$ should follow a linear fitting in the chosen temperature range. This linearity points to a thermally assisted conduction [81]. In this type of conduction, the energy barrier E_a needs to be surmounted for the ion to move from one site to another [82]. The highest value of E_a was obtained for the CMC-CS sw hydrogel, with 0.21 eV. Smaller values of 0.14 and 0.18 eV were obtained for the crosslinked hydrogels CA40 sw and CA30 sw, respectively (Table 3). Moreover, the Arrhenius behavior in the CMC-CS sw hydrogel was lost at 50 °C, whereas for the CMC-CS-CA sw membranes, they achieved linearity until 60 °C, suggesting an enhanced stability of the conduction process for the synthesized hydrogels.

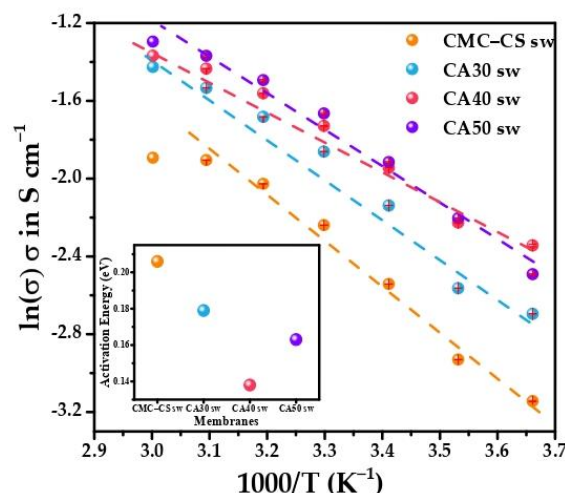


Figure 7. Ionic conductivity of the CMC-CS sw electrolytes at different temperatures. Inset: Activation energy (E_a) of the CMC-CS sw electrolytes.

Table 3. Swelling ratio and some electrochemical values obtained for the CMC-CS and CMC-CS-CA sw electrolytes. Ionic conductivity values were obtained at $T = 30$ °C.

Electrolyte	KOH Absorption (%)	E_a (eV)	σ (S·cm ^{−1})
CMC-CS sw	288.35 ± 26.64	0.21	0.11
CA30 sw	180.40 ± 17.01	0.18	0.16
CA40 sw	160.83 ± 7.10	0.14	0.18
CA50 sw	151.69 ± 1.09	0.16	0.19

The results show the swelled KOH to be inversely proportional to the increase in ionic conductivity, obtaining a maximum of 189 mS cm^{−1} for the CA50 sw hydrogel (Figure 8). This apparent contradictory behavior can be explained by the capability of the membrane to retain the swelled KOH when it is pressed between the electrodes and its further integrity. These values follow the trend of the decrease in the crystallinity caused by the KOH solution, which was already discussed in Section 3.3.2. This effect was enhanced when the temperature increased, generating a more structural relaxation of the polymer chains and expanding the free volume, causing an increase in the conductivity as evidenced in Figure 7, obtaining a conductivity of 273 mS cm^{−1} for the CA50 sw hydrogel at 60 °C. Therefore, the results agree with reports of the decrease in the crystallinity to be inversely proportional

with the increase in the ionic conductivity [83,84]. The obtained values for σ show a substantial increase from previous studies in the field, where ionic conductivities of less than $10^{-3} \text{ S}\cdot\text{cm}^{-1}$ were reported [85–89], pointing to the applicability of these membranes in electrochemical applications. Achieving a high ionic conductivity allows for more ions to pass through at a given time, improving the capacity at higher discharge rates [90], which is also important for obtaining a high energy density [91].

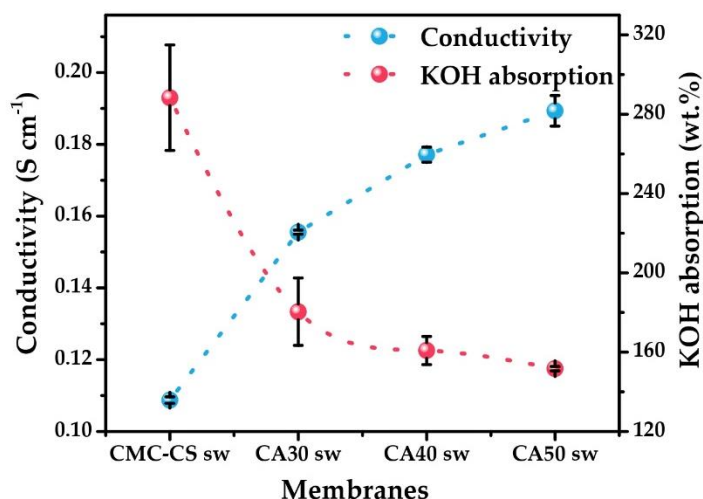
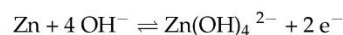


Figure 8. Comparison between the ionic conductive values and KOH absorption behavior of the CMC-CS sw hydrogels at different CA proportions.

3.5.2. Linear Sweep and Cyclic Voltammetry (CV)

It can be evidenced from the linear sweep voltammetry (LSV) studies how the electrolytes were stable in a long electrochemical potential window (Figure 9a), with the best window obtained for the CA50 membrane, which reached up to approximately +2.1 V, while the other electrolytes resulted in being also highly stable in comparison with a liquid electrolyte, for which the electrochemical window (1.23 V) is restricted due to the water electrolysis. The cyclic voltammetry (CV) studies were performed in an electrochemical stability window in the range of -1.5 to 1.5 V to study Zn^{2+} conduction and reversible equilibrium between the zinc metal and the zinc ions present inside the CMC-CS sw hydrogels, as presented in Figure 9b. When analyzing the peaks' shape, a quasi-reversible behavior for the redox processes was evidenced; the cathodic peak corresponded to the reduction process of Zn^{2+} to Zn^0 , while the anodic peak was attributed to zinc oxidation to Zn^{2+} cations [43]. The oxidation/reduction reactions were evidenced for all of the membranes according to the peaks in the CV plot as evidence of the establishment of the reversibility of the Zn/Zn^{2+} couple. Two peaks split into both anodic (a_1 and a_2) and cathodic (c_1 and c_2) branches were observed. The first peak in the anodic branch (a_1) was highly reported for alkaline electrolytes [90], being as follows:



Whereas for the second peak, a_2 , Cai et al. [92] associated it to the formation of $\text{Zn}(\text{OH})_3^-$ complexes due to the depletion of OH^- anions near the electrode surface, creating a prepassive layer at a more positive potential than a_1 . For the cathode peaks, the reverse reactions were happening. The inverse peak b' in the cathodic branch was reported to occur due to the oxidation of Zn after some dissolution of the passive film deposited

on the surface of the Zn electrode that was released during the cathodic sweep. The same occurred for peak b'' in the anodic sweep [41].

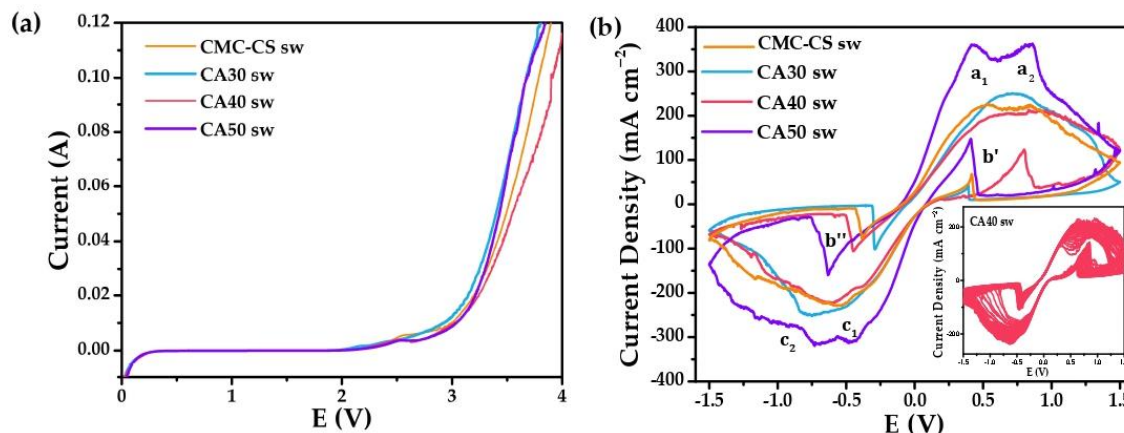


Figure 9. (a) Linear sweep voltammetry studies for the CMC–CS sw hydrogels at different CA proportions; (b) cyclic voltammograms of the swollen hydrogels at ambient temperature. Inset: 40 consecutive cycles of the CA40 sw membrane.

A maximum peak of intensity at $225 \text{ mA} \cdot \text{cm}^{-2}$ for the CMC–CS sw hydrogel was obtained, while for the CA50 sw membrane it achieved $360 \text{ mA} \cdot \text{cm}^{-2}$. The large separation in peak potentials is reported to be due to the absence of reference electrode used, typical for the evaluation of gel PEs [93,94]. For all the membranes, stability is evidenced when performing 40 consecutive cycles, pointing to a good electrochemical behavior and the reversibility of the system. The presented results indicate an improvement of the fast-ionic motion across the electrolyte matrix, since the intensity values are reported to depend on the number of electrons transferred between the redox species and the electrode, which depends on the ions' movement [43,95]. The ionic conductive behavior of these type of PEs has been reported to be due to the heteroatoms from CMC and CS donating electron pairs from s orbitals to Lewis's acids, forming a complex–transport system [41]. Thus, it points to the applicability of the hydrogels in electrochemical devices.

3.6. Zn/Hydrogel/Air Battery

The primary ZAB was constructed using a previously reported configuration [96], without the use of the reservoir, being replaced by the hydrogel electrolytes proposed in this work (Figure 10e). The open circuit potential for all of the membranes reached values of 1.46 V. The discharge and power densities displayed in Figure 10a showed clear differences between the use of the CMC–CS sw membrane and the crosslinked membranes, with double the power density for the CA50 sw membrane (85 mW cm^{-2}) compared to the noncrosslinked membrane (40 mW cm^{-2}). These results show an enhancement in the power density of the system when compared with the use of KOH 6 M as an electrolyte, where a power density of 28 mW cm^{-2} was reported by Díaz-Patiño et al. [97]. The CMC–CS sw hydrogel required the greatest electrical work at the demanding current densities in the stability tests at different current densities (Figure 10b), reflected in the higher overpotentials. In comparison, the CA50 sw membrane required lower overpotentials to provide the fixed current densities. In addition, the ZAB using the CMC–CS sw electrolyte was unable to sustain operation at current densities of $10 \text{ mA} \cdot \text{cm}^{-2}$. Table 4 shows the battery performance obtained in this work compared to other reports that used polymers in their electrolyte system.

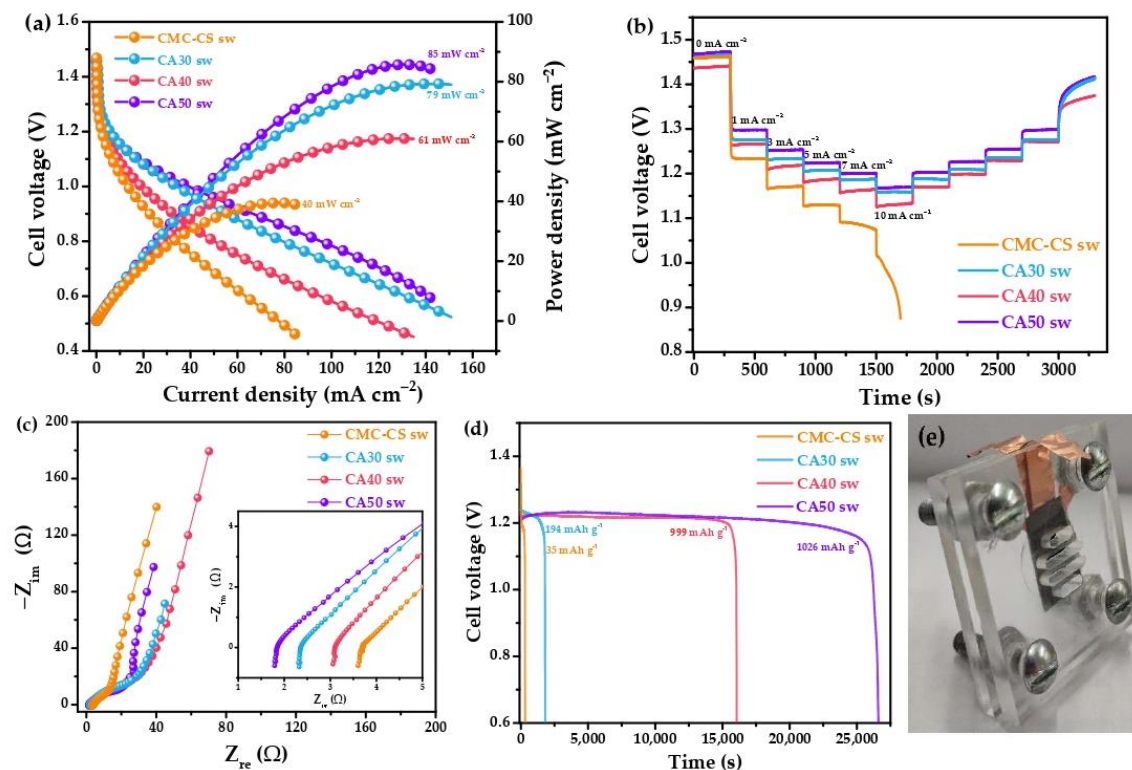


Figure 10. (a) Discharge and power density curves for the battery operated with the Zn foil as an anode and Pt/C as a cathode and the synthesized hydrogels; (b) discharge tests at selected current densities; (c) potential electrochemical impedance spectroscopy studies; (d) discharge performance at 3 mA cm⁻²; (e) photograph of the assembled device.

Table 4. Battery performance of some Zinc–air batteries with polymer electrolytes.

Electrolyte	Ionic Conductivity (S cm ⁻¹)	Bulk Resistance (Ω)	Specific Capacitance (mA · h g ⁻¹)	Power Density (mW cm ⁻²)	Reference
Chitosan-PDDA-GA KOH	0.02	~1.00	-	48.9	[98]
QA-functionalized nanocellulose-GO-KOH	0.04	-	-	44.1	[99]
PVA-PEG-SiO ₂ KOH	0.06	~1.30	720.6	62.6	[100]
PVA-NH ₄ Cl-ZnCl	0.07	2.16	-	~8	[101]
CS-PVA KOH	0.11	1.06	221.6	-	[102]
CMC-CS-CA KOH	0.19	1.85	1026	85	This work

In terms of the bulk resistances (R_b) of the ZABs (Figure 10c), values of 3.65 Ω for the CMC-CS sw membrane and 1.85 Ω for the CA50 sw membrane were obtained. This decreasing pattern of R_b was due to the increasing of the charge carriers and the OH⁻ ions with an increased SR [103]. The discharge time of the battery using the CA50 sw reached a 7.4 h set time for the discharge process (Figure 10d), while for the CMC-CS sw membrane, it only took 4 min to finish discharging. The average nominal voltages at the flat plateau region ranged from 1.23 V for the CA50 sw hydrogel to 1.20 V for the CMC-CS sw hydrogel before hitting cutoff voltages of 1.19 and 1.18 V, respectively. The voltage values decreased

slightly in the plateau region, possibly due to the concentration polarization caused by salt depletion or accumulation within the cell [104]. The maximum specific capacitance obtained was $1026 \text{ mA} \cdot \text{h} \cdot \text{g}^{-1}$ for the battery assembled with the CA50 sw electrolyte.

4. Conclusions

The esterification/crosslinking reaction for the CMC-CS-CA hydrogels was achieved through the synthesis proposed in this work, confirmed by ATR-FTIR. The swelling behavior of the noncrosslinked hydrogel had a higher swelling ratio than its counterparts with citric acid. However, this higher capacity came along with low structural integrity when used in battery assemblies. With the addition of CA, a superior structural stability of the membranes was obtained. The structural characterization carried out suggested a higher thermal stability and a decrease in the degree of crystallinity of the crosslinked membranes. The absorption and nonadsorption mechanism was confirmed through the study of N_2 adsorption/desorption processes.

The values of the ionic conductivity and current improved with the proposed hydrogels compared to the noncrosslinked electrolyte, confirmed by the electrochemical characterization by electrochemical impedance spectroscopy and cyclic voltammetry. Arrhenius behavior was confirmed in the range of 0 to 60°C for the crosslinked membranes, and a maximum value of $0.19 \text{ S} \cdot \text{cm}^{-1}$ was found at 30°C . In addition, the cyclic voltammetry studies confirmed a quasi-reversible behavior, with maximum intensity peaks of $360 \text{ mA} \cdot \text{cm}^{-2}$, as evidence of the high ionic transfer achieved by the CA50 sw hydrogel. The synthesized hydrogels were finally tested in a zinc–air battery, with high performance in terms of power densities, bulk resistances, and discharge times. The obtained results show that these hydrogels are suitable candidates for use in energy storage devices.

Supplementary Materials: The following supporting information can be downloaded at: <https://www.mdpi.com/article/10.3390/batteries8120265/s1>, Figure S1: Nitrogen adsorption/desorption isotherms for the synthesized hydrogels; Figure S2: DSC curves for (a) dried hydrogels and (b) swollen hydrogels. Table S1. Average electrolytes' thickness used for ionic conductivity calculations.

Author Contributions: Conceptualization, methodology, formal analysis, data curation, investigation, and writing—original draft preparation, M.F.B.-C.; writing—review and editing, A.D.D., V.M.C., J.B., N.A., L.Á.-C. and J.P.T.; conceptualization, methodology, and supervision, N.A., L.Á.-C., L.D.L. and J.P.T.; project administration, L.Á.-C. and J.P.T.; funding acquisition, L.Á.-C. All authors have read and agreed to the published version of the manuscript.

Funding: CONACYT “Ciencia Básica y/o Ciencia de Frontera Modalidad: Paradigmas y Controversias de la Ciencia 2022” (grant: 319645) and Centro de Investigación en Materiales Avanzados S.C., for supporting through the internal project PI-22-10.

Data Availability Statement: Data sharing is not applicable to this article.

Acknowledgments: The authors gratefully acknowledge the Mexican Council of Science and Technology (CONACYT) for supporting this work through the project CONACYT “Ciencia Básica y/o Ciencia de Frontera Modalidad: Paradigmas y Controversias de la Ciencia 2022” (grant: 319645) and to Centro de Investigación en Materiales Avanzados S.C. for support through the internal project PI-22-10. The authors gratefully acknowledge the Grupo de Investigación Aplicada en Materiales y Procesos (GIAMP) and the School of Physical Sciences and Nanotechnology, Yachay Tech University for their collaboration through some of the necessary equipment for this research work. The authors acknowledge the technical support of Luis de la Torre Saenz and César Cutberto Leyva Porras for the physicochemical characterization.

Conflicts of Interest: The authors declare no conflict of interest.

References

1. Liu, F.; Chen, Z.; Fang, G.; Wang, Z.; Cai, Y.; Tang, B.; Zhou, J.; Liang, S. V₂O₅ Nanospheres with Mixed Vanadium Valences as High Electrochemically Active Aqueous Zinc-Ion Battery Cathode. *Nano-Micro Lett.* **2019**, *11*, 1–11. [CrossRef]
2. Deivanayagam, R.; Ingram, B.J.; Shahbazian-Yassar, R. Progress in development of electrolytes for magnesium batteries. *Energy Storage Mater.* **2019**, *21*, 136–153. [CrossRef]

3. Wang, F.; Borodin, O.; Gao, T.; Fan, X.; Sun, W.; Han, F.; Faraone, A.; Dura, J.A.; Xu, K.; Wang, C. Highly reversible zinc metal anode for aqueous batteries. *Nat. Mater.* **2018**, *17*, 543–549. [[CrossRef](#)] [[PubMed](#)]
4. Boaretto, N.; Meabe, L.; Martinez-Ibañez, M.; Armand, M.; Zhang, H. Review—Polymer Electrolytes for Rechargeable Batteries: From Nanocomposite to Nanohybrid. *J. Electrochem. Soc.* **2020**, *167*, 070524. [[CrossRef](#)]
5. Fang, G.; Zhu, C.; Chen, M.; Zhou, J.; Tang, B.; Cao, X.; Zheng, X.; Pan, A.; Liang, S. Suppressing Manganese Dissolution in Potassium Manganate with Rich Oxygen Defects Engaged High-Energy-Density and Durable Aqueous Zinc-Ion Battery. *Adv. Funct. Mater.* **2019**, *29*, 1808375. [[CrossRef](#)]
6. Kundu, D.; Adams, B.D.; Duffort, V.; Vajargah, S.H.; Nazar, L.F. A high-capacity and long-life aqueous rechargeable zinc battery using a metal oxide intercalation cathode. *Nat. Energy* **2016**, *1*, 16119. [[CrossRef](#)]
7. Pan, H.; Shao, Y.; Yan, P.; Cheng, Y.; Han, K.S.; Nie, Z.; Wang, C.; Yang, J.; Li, X.; Bhattacharya, P.; et al. Reversible aqueous zinc/manganese oxide energy storage from conversion reactions. *Nat. Energy* **2016**, *1*, 16039. [[CrossRef](#)]
8. Zhang, Y.; Liu, Y.; Liu, Z.; Wu, X.; Wen, Y.; Chen, H.; Ni, X.; Liu, G.; Huang, J.; Peng, S. MnO₂ cathode materials with the improved stability via nitrogen doping for aqueous zinc-ion batteries. *J. Energy Chem.* **2022**, *64*, 23–32. [[CrossRef](#)]
9. Li, Y.; Dai, H. Recent advances in zinc-air batteries. *Chem. Soc. Rev.* **2014**, *43*, 5257–5275. [[CrossRef](#)] [[PubMed](#)]
10. Li, S.; Guo, H.; He, S.; Yang, H.; Liu, K.; Duan, G.; Jiang, S. Advanced electrospun nanofibers as bifunctional electrocatalysts for flexible metal-air (O₂) batteries: Opportunities and challenges. *Mater. Des.* **2022**, *214*, 110406. [[CrossRef](#)]
11. Li, D.; Lv, Q.; Zhang, C.; Zhou, W.; Guo, H.; Jiang, S.; Li, Z. The Effect of Electrode Thickness on the High-Current Discharge and Long-Term Cycle Performance of a Lithium-Ion Battery. *Batteries* **2022**, *8*, 101. [[CrossRef](#)]
12. Zaghbi, K.; Song, S.-W.; Singh, K.; Yao, Y.; Ichikawa, T.; Jain, A.; Singh, R. Zinc as a Promising Anodic Material for All-Solid-State Lithium-Ion Batteries. *Batteries* **2022**, *8*, 113. [[CrossRef](#)]
13. Lu, C.-T.; Zhu, Z.-Y.; Chen, S.-W.; Chang, Y.-L.; Hsueh, K.-L. Effects of Cell Design Parameters on Zinc-Air Battery Performance. *Batteries* **2022**, *8*, 92. [[CrossRef](#)]
14. Parveen, N.; Ansari, S.A.; Ansari, M.Z.; Ansari, M.O. Manganese oxide as an effective electrode material for energy storage: A review. *Environ. Chem. Lett.* **2021**, *20*, 283–309. [[CrossRef](#)]
15. He, W.; Zuo, S.; Xu, X.; Zeng, L.; Liu, L.; Zhao, W.; Liu, J. Challenges and strategies of zinc anode for aqueous zinc-ion batteries. *Mater. Chem. Front.* **2021**, *5*, 2201–2217. [[CrossRef](#)]
16. Ye, T.; Li, L.; Zhang, Y. Recent Progress in Solid Electrolytes for Energy Storage Devices. *Adv. Funct. Mater.* **2020**, *30*, 2000077. [[CrossRef](#)]
17. Zhao, C.; Liu, L.; Qi, X.; Lu, Y.; Wu, F.; Zhao, J.; Yu, Y.; Hu, Y.-S.; Chen, L. Solid-State Sodium Batteries. *Adv. Energy Mater.* **2018**, *8*, 1703012. [[CrossRef](#)]
18. Xu, Z.; Wu, M. Toward Dendrite-Free Deposition in Zinc-Based Flow Batteries: Status and Prospects. *Batteries* **2022**, *8*, 117. [[CrossRef](#)]
19. Wood, K.N.; Kazyak, E.; Chadwick, A.F.; Chen, K.-H.; Zhang, J.-G.; Thornton, K.; Dasgupta, N.P. Dendrites and Pits: Untangling the Complex Behavior of Lithium Metal Anodes through Operando Video Microscopy. *ACS Cent. Sci.* **2016**, *2*, 790–801. [[CrossRef](#)]
20. Wu, F.; Yuan, Y.-X.; Cheng, X.-B.; Bai, Y.; Li, Y.; Wu, C.; Zhang, Q. Perspectives for restraining harsh lithium dendrite growth: Towards robust lithium metal anodes. *Energy Storage Mater.* **2018**, *15*, 148–170. [[CrossRef](#)]
21. Zhang, H.; Li, C.; Piszcz, M.; Coya, E.; Rojo, T.; Rodriguez-Martinez, L.M.; Armand, M.; Zhou, Z. Single lithium-ion conducting solid polymer electrolytes: Advances and perspectives. *Chem. Soc. Rev.* **2017**, *46*, 797–815. [[CrossRef](#)] [[PubMed](#)]
22. Hallinan, D.T.; Villaluenga, I.; Balsara, N.P. Polymer and composite electrolytes. *MRS Bull.* **2018**, *43*, 775–781. [[CrossRef](#)]
23. Mindemark, J.; Lacey, M.J.; Bowden, T.; Brandell, D. Beyond PEO—Alternative host materials for Li⁺-conducting solid polymer electrolytes. *Prog. Polym. Sci.* **2018**, *81*, 114–143. [[CrossRef](#)]
24. Bósquez-Cáceres, M.F.; Hidalgo-Bonilla, S.; Córdova, V.M.; Michell, R.M.; Tafur, J.P. Nanocomposite Polymer Electrolytes for Zinc and Magnesium Batteries: From Synthetic to Biopolymers. *Polymers* **2021**, *13*, 4284. [[CrossRef](#)]
25. Mo, F.; Guo, B.; Ling, W.; Wei, J.; Chen, L.; Yu, S.; Liang, G. Recent Progress and Challenges of Flexible Zn-Based Batteries with Polymer Electrolyte. *Batteries* **2022**, *8*, 59. [[CrossRef](#)]
26. Wu, K.; Huang, J.; Yi, J.; Liu, X.; Liu, Y.; Wang, Y.; Zhang, J.; Xia, Y. Recent Advances in Polymer Electrolytes for Zinc Ion Batteries: Mechanisms, Properties, and Perspectives. *Adv. Energy Mater.* **2020**, *10*, 209–216. [[CrossRef](#)]
27. Lorca, S.; Santos, F.; Fernández Romero, A.J. A Review of the Use of GPEs in Zinc-Based Batteries. A Step Closer to Wearable Electronic Gadgets and Smart Textiles. *Polymers* **2020**, *12*, 2812. [[CrossRef](#)]
28. Mohamed, N.S.; Subban, R.H.Y.; Arof, A.K. Polymer batteries fabricated from lithium complexed acetylated chitosan. *J. Power Sources* **1995**, *56*, 153–156. [[CrossRef](#)]
29. Saad, E.M.; Elshaarawy, R.F.; Mahmoud, S.A.; El-Moselhy, K.M. New Ulva lactuca Algae Based Chitosan Bio-composites for Bioremediation of Cd(II) Ions. *J. Bioresour. Bioprod.* **2021**, *6*, 223–242. [[CrossRef](#)]
30. Madni, A.; Kousar, R.; Naeem, N.; Wahid, F. Recent advancements in applications of chitosan-based biomaterials for skin tissue engineering. *J. Bioresour. Bioprod.* **2021**, *6*, 11–25. [[CrossRef](#)]
31. Rosca, C.; Popa, M.I.; Lisa, G.; Chitanu, G.C. Interaction of chitosan with natural or synthetic anionic polyelectrolytes. 1. The chitosan-carboxymethylcellulose complex. *Carbohydr. Polym.* **2005**, *62*, 35–41. [[CrossRef](#)]
32. Shang, J.; Shao, Z.; Chen, X. Electrical Behavior of a Natural Polyelectrolyte Hydrogel: Chitosan/Carboxymethylcellulose Hydrogel. *Biomacromolecules* **2008**, *9*, 1208–1213. [[CrossRef](#)] [[PubMed](#)]

33. Bakar, N.Y.; Isa, M.I.N. Potential of Ionic Conductivity and Transport Properties Solid Biopolymer Electrolytes Based Carboxy Methylcellulose/Chitosan Polymer Blend Doped with Dodecyltrimethyl Ammonium Bromide. *Res. J. Recent Sci.* **2014**, *3*, 74.
34. Rani, M.S.A.; Mohamed, N.S.; Isa, M.I.N. Investigation of the Ionic Conduction Mechanism in Carboxymethyl Cellulose/Chitosan Biopolymer Blend Electrolyte Impregnated with Ammonium Nitrate. *Int. J. Polym. Anal. Charact.* **2015**, *20*, 491–503. [\[CrossRef\]](#)
35. Wang, Z.; Li, H.; Tang, Z.; Liu, Z.; Ruan, Z.; Ma, L.; Yang, Q.; Wang, D.; Zhi, C.; Wang, Z.F.; et al. Hydrogel Electrolytes for Flexible Aqueous Energy Storage Devices. *Adv. Funct. Mater.* **2018**, *28*, 1804560. [\[CrossRef\]](#)
36. Liu, J.; Ahmed, S.; Khanam, Z.; Wang, T.; Song, S. Ionic Liquid-Incorporated Zn-Ion Conducting Polymer Electrolyte Membranes. *Polymers* **2020**, *12*, 1755. [\[CrossRef\]](#)
37. Manzoor, K.; Ahmad, M.; Ahmad, S.; Ikram, S. Removal of Pb(ii) and Cd(ii) from wastewater using arginine cross-linked chitosan-carboxymethyl cellulose beads as green adsorbent. *RSC Adv.* **2019**, *9*, 7890–7902. [\[CrossRef\]](#)
38. Salama, H.E.; Abdel Aziz, M.S.; Alsehlhi, M. Carboxymethyl cellulose/sodium alginate/chitosan biguanidine hydrochloride ternary system for edible coatings. *Int. J. Biol. Macromol.* **2019**, *139*, 614–620. [\[CrossRef\]](#)
39. Uyanga, K.A.; Daoud, W.A. Green and sustainable carboxymethyl cellulose-chitosan composite hydrogels: Effect of crosslinker on microstructure. *Cellulose* **2021**, *28*, 5493–5512. [\[CrossRef\]](#)
40. Uyanga, K.A.; Daoud, W.A. Carboxymethyl cellulose-chitosan composite hydrogel: Modelling and experimental study of the effect of composition on microstructure and swelling response. *Int. J. Biol. Macromol.* **2021**, *181*, 1010–1022. [\[CrossRef\]](#)
41. Santos, F.; Tafur, J.P.; Abad, J.; Fernández Romero, A.J. Structural modifications and ionic transport of PVA-KOH hydrogels applied in Zn/Air batteries. *J. Electroanal. Chem.* **2019**, *850*, 113380. [\[CrossRef\]](#)
42. Lewandowski, A.; Skorupska, K.; Malinska, J. Novel poly(vinyl alcohol)–KOH–H₂O alkaline polymer electrolyte. *Solid State Ion.* **2000**, *133*, 265–271. [\[CrossRef\]](#)
43. Velez, A.A.I.; Reyes, E.; Diaz-Barrios, A.; Santos, F.; Fernández Romero, A.J.; Tafur, J.P. Properties of the PVA-VA/TD KOH Blend as a Gel Polymer Electrolyte for Zinc Batteries. *Gels* **2021**, *7*, 256. [\[CrossRef\]](#)
44. Calderón Salas, L.A.; De Lima Eljuri, L.; Caetano Sousa, M. *Synthesis and Characterization of Chemically Crosslinked Carboxymethyl Cellulose/Chitosan Composite Hydrogels*; Universidad de Investigación de Tecnología Experimental Yachay: Urcuqui, Ecuador, 2021.
45. Putz, H.; Brandenburg, K. Match!—Phase Analysis Using Powder Diffraction. Available online: <https://www.crystalimpact.de/match> (accessed on 16 August 2022).
46. Nuernberg, R.B. Numerical comparison of usual Arrhenius-type equations for modeling ionic transport in solids. *Ionics* **2020**, *26*, 2405–2412. [\[CrossRef\]](#)
47. Chandra Roy, J.; Ferri, A.; Giraud, S.; Jinping, G.; Salaün, F. Chitosan–Carboxymethylcellulose-Based Polyelectrolyte Complexation and Microcapsule Shell Formulation. *Int. J. Mol. Sci.* **2018**, *19*, 2521. [\[CrossRef\]](#)
48. Seki, Y.; Altinisik, A.; Demircioğlu, B.; Tetik, C. Carboxymethylcellulose (CMC)–hydroxyethylcellulose (HEC) based hydrogels: Synthesis and characterization. *Cellulose* **2014**, *21*, 1689–1698. [\[CrossRef\]](#)
49. Fekete, T.; Borsa, J.; Takács, E.; Wojnárovits, L. Synthesis of carboxymethylcellulose/acrylic acid hydrogels with superabsorbent properties by radiation-initiated crosslinking. *Radiat. Phys. Chem.* **2016**, *124*, 135–139. [\[CrossRef\]](#)
50. Bajpai, J.; Mishra, S.; Bajpai, A.K. Dynamics of controlled release of potassium nitrate from a highly swelling binary polymeric blend of alginate and carboxymethyl cellulose. *J. Appl. Polym. Sci.* **2007**, *106*, 961–972. [\[CrossRef\]](#)
51. Johns, J.; Rao, V. Mechanical Properties and Swelling Behavior of Cross-Linked Natural Rubber/Chitosan Blends. *Int. J. Polym. Anal. Charact.* **2009**, *14*, 508–526. [\[CrossRef\]](#)
52. Zhang, P.; Wang, K.; Pei, P.; Zuo, Y.; Wei, M.; Liu, X.; Xiao, Y.; Xiong, J. Selection of hydrogel electrolytes for flexible zinc–air batteries. *Mater. Today Chem.* **2021**, *21*, 100538. [\[CrossRef\]](#)
53. Pavia, D.L.; Lampman, G.M.; Kriz, G.S.; Vyvyan, J.R. *Introduction to Spectroscopy*, 5th ed.; Cengage Learning: Boston, MA, USA, 2013.
54. Kadir, M.F.Z.; Aspanut, Z.; Majid, S.R.; Arof, A.K. FTIR studies of plasticized poly(vinyl alcohol)–chitosan blend doped with NH₄NO₃ polymer electrolyte membrane. *Spectrochim. Acta Part A Mol. Biomol. Spectrosc.* **2011**, *78*, 1068–1074. [\[CrossRef\]](#) [\[PubMed\]](#)
55. Corazzari, I.; Nisticò, R.; Turci, F.; Faga, M.G.; Franzoso, F.; Tabasso, S.; Magnacca, G. Advanced physico-chemical characterization of chitosan by means of TGA coupled on-line with FTIR and GCMS: Thermal degradation and water adsorption capacity. *Polym. Degrad. Stab.* **2015**, *112*, 1–9. [\[CrossRef\]](#)
56. He, X.; Xu, H.; Li, H. Cr(VI) Removal from Aqueous Solution by Chitosan/Carboxymethyl Cellulose/Silica Hybrid Membrane. *World J. Eng. Technol.* **2015**, *3*, 234–240. [\[CrossRef\]](#)
57. Biswal, D.R.; Singh, R.P. Characterisation of carboxymethyl cellulose and polyacrylamide graft copolymer. *Carbohydr. Polym.* **2004**, *57*, 379–387. [\[CrossRef\]](#)
58. Samsudin, A.S.; Kuan, E.C.H.; Isa, M.I.N. Investigation of the Potential of Proton-Conducting Biopolymer Electrolytes Based Methyl Cellulose-Glycolic Acid. *Int. J. Polym. Anal. Charact.* **2011**, *16*, 477–485. [\[CrossRef\]](#)
59. Rani, M.S.A.; Mohamed, N.S.; Isa, M.I.N. Characterization of Proton Conducting Carboxymethyl Cellulose/Chitosan Dual-Blend Based Biopolymer Electrolytes. *Mater. Sci. Forum* **2016**, *846*, 539–544. [\[CrossRef\]](#)
60. Harish Prashanth, K.V.; Kittur, F.S.; Tharanathan, R.N. Solid state structure of chitosan prepared under different N-deacetylating conditions. *Carbohydr. Polym.* **2002**, *50*, 27–33. [\[CrossRef\]](#)

61. Seki, T.; Chiang, K.-Y.; Yu, C.-C.; Yu, X.; Okuno, M.; Hunger, J.; Nagata, Y.; Bonn, M. The Bending Mode of Water: A Powerful Probe for Hydrogen Bond Structure of Aqueous Systems. *J. Phys. Chem. Lett.* **2020**, *11*, 8459–8469. [\[CrossRef\]](#)
62. Farinha, I.; Freitas, F. Chemically modified chitin, chitosan, and chitinous polymers as biomaterials. *Handb. Chitin Chitosan* **2020**, 43–69. [\[CrossRef\]](#)
63. Yu, M.; Li, J.; Wang, L. KOH-activated carbon aerogels derived from sodium carboxymethyl cellulose for high-performance supercapacitors and dye adsorption. *Chem. Eng. J.* **2017**, *310*, 300–306. [\[CrossRef\]](#)
64. Son, Y.-R.; Rhee, K.Y.; Park, S.-J. Influence of reduced graphene oxide on mechanical behaviors of sodium carboxymethyl cellulose. *Compos. Part B Eng.* **2015**, *83*, 36–42. [\[CrossRef\]](#)
65. Wang, Z.; Zheng, L.; Li, C.; Zhang, D.; Xiao, Y.; Guan, G.; Zhu, W. Modification of chitosan with monomethyl fumaric acid in an ionic liquid solution. *Carbohydr. Polym.* **2015**, *117*, 973–979. [\[CrossRef\]](#) [\[PubMed\]](#)
66. Aziz, S.B.; Abidin, Z.H.Z. Ion-transport study in nanocomposite solid polymer electrolytes based on chitosan: Electrical and dielectric analysis. *J. Appl. Polym. Sci.* **2015**, *132*, 41774. [\[CrossRef\]](#)
67. Zhang, J.; Wang, Y.; Zhang, L.; Zhang, R.; Liu, G.; Cheng, G. Understanding changes in cellulose crystalline structure of lignocellulosic biomass during ionic liquid pretreatment by XRD. *Bioresour. Technol.* **2014**, *151*, 402–405. [\[CrossRef\]](#)
68. Abdullah, O.G.H.; Hanna, R.R.; Salman, Y.A.K. Structural and electrical conductivity of CH:MC bio-poly-blend films: Optimize the perfect composition of the blend system. *Bull. Mater. Sci.* **2019**, *42*, 64. [\[CrossRef\]](#)
69. Saeed, M.A.M.; Gh Abdullah, O. Membranes. Effect of High Ammonium Salt Concentration and Temperature on the Structure, Morphology, and Ionic Conductivity of Proton-Conductor Solid Polymer Electrolytes Based PVA. *Membranes* **2020**, *10*, 262. [\[CrossRef\]](#)
70. Sing Ngai, K.; Ramesh, S.; Ramesh, K.; Ching Juan, J. A review of polymer electrolytes: Fundamental, approaches and applications. *Ionics* **2016**, *22*, 1259–1279. [\[CrossRef\]](#)
71. Grover, C.N.; Gwynne, J.H.; Pugh, N.; Hamaia, S.; Farndale, R.W.; Best, S.M.; Cameron, R.E. Crosslinking and composition influence the surface properties, mechanical stiffness and cell reactivity of collagen-based films. *Acta Biomater.* **2012**, *8*, 3080–3090. [\[CrossRef\]](#)
72. Wang, L.; Yang, X.; Daoud, W.A. High power-output mechanical energy harvester based on flexible and transparent Au nanoparticle-embedded polymer matrix. *Nano Energy* **2019**, *55*, 433–440. [\[CrossRef\]](#)
73. Ritonga, H.; Nurfadillah, A.; Rembon, F.S.; Ramadhan, L.O.A.N.; Nurdin, M. Preparation of Chitosan-EDTA hydrogel as soil conditioner for soybean plant (*Glycine max*). *Groundw. Sustain. Dev.* **2019**, *9*, 100277. [\[CrossRef\]](#)
74. Suppiah, K.; Leng, T.P.; Husseinayah, S.; Rahman, R.; Keat, Y.C.; Heng, C.W. Thermal properties of carboxymethyl cellulose (CMC) filled halloysite nanotube (HNT) bio-nanocomposite films. *Mater. Today Proc.* **2019**, *16*, 1611–1616. [\[CrossRef\]](#)
75. Rana, V.K.; Pandey, A.K.; Singh, R.P.; Kumar, B.; Mishra, S.; Ha, C.-S. Enhancement of thermal stability and phase relaxation behavior of chitosan dissolved in aqueous l-lactic acid: Using ‘silver nanoparticles’ as nano filler. *Macromol. Res.* **2010**, *18*, 713–720. [\[CrossRef\]](#)
76. Werner, K.; Pommer, L.; Broström, M. Thermal decomposition of hemicelluloses. *J. Anal. Appl. Pyrolysis* **2014**, *110*, 130–137. [\[CrossRef\]](#)
77. Paulino, A.T.; Simionato, J.I.; Garcia, J.C.; Nozaki, J. Characterization of chitosan and chitin produced from silkworm crysalides. *Carbohydr. Polym.* **2006**, *64*, 98–103. [\[CrossRef\]](#)
78. Strydom, C.A.; Collins, A.C.; Bunt, J.R. The influence of various potassium compound additions on the plasticity of a high-swelling South African coal under pyrolyzing conditions. *J. Anal. Appl. Pyrolysis* **2015**, *112*, 221–229. [\[CrossRef\]](#)
79. Wang, K.; Du, L.; Zhang, C.; Lu, Z.; Lu, F.; Zhao, H. Preparation of chitosan/curdlan/carboxymethyl cellulose blended film and its characterization. *J. Food Sci. Technol.* **2019**, *56*, 5396–5404. [\[CrossRef\]](#)
80. Ferrero, F.; Periolatto, M. Antimicrobial finish of textiles by chitosan UV-curing. *J. Nanosci. Nanotechnol.* **2012**, *12*, 4803–4810. [\[CrossRef\]](#)
81. Hatta, F.F.; Yahya, M.Z.A.; Ali, A.M.M.; Subban, R.H.Y.; Harun, M.K.; Mohamad, A.A. Electrical conductivity studies on PVA/PVP-KOH alkaline solid polymer blend electrolyte. *Ionics* **2005**, *11*, 418–422. [\[CrossRef\]](#)
82. Petrowsky, M.; Frech, R. Application of the Compensated Arrhenius Formalism to Self-Diffusion: Implications for Ionic Conductivity and Dielectric Relaxation. *J. Phys. Chem. B* **2011**, *114*, 8600–8605. [\[CrossRef\]](#)
83. Pandey, G.P.; Agrawal, R.C.; Hashmi, S.A. Magnesium ion-conducting gel polymer electrolytes dispersed with fumed silica for rechargeable magnesium battery application. *J. Solid State Electrochem.* **2010**, *15*, 2253–2264. [\[CrossRef\]](#)
84. Maheshwaran, C.; Mishra, K.; Kanchan, D.K.; Kumar, D. Mg²⁺ conducting polymer gel electrolytes: Physical and electrochemical investigations. *Ionics* **2020**, *26*, 2969–2980. [\[CrossRef\]](#)
85. Rahman, N.A.; Hanifah, S.A.; Mobarak, N.N.; Ahmad, A.; Ludin, N.A.; Bella, F.; Su’Ait, M.S. Chitosan as a paradigm for biopolymer electrolytes in solid-state dye-sensitized solar cells. *Polymer* **2021**, *230*, 124092. [\[CrossRef\]](#)
86. Dannoun, E.M.A.; Aziz, S.B.; Brza, M.A.; Nofal, M.M.; Asnawi, A.S.F.M.; Yusof, Y.M.; Al-Zangana, S.; Hamsan, M.H.; Kadir, M.F.Z.; Woo, H.J. The Study of Plasticized Solid Polymer Blend Electrolytes Based on Natural Polymers and Their Application for Energy Storage EDLC Devices. *Polymers* **2020**, *12*, 2531. [\[CrossRef\]](#) [\[PubMed\]](#)
87. Ikram, S.; Ahmed, S.; Wazed Ali, S.; Agarwal, H. Chitosan-based polymer electrolyte membranes for fuel cell applications. *Org. Compos. Polym. Electrolyte Membr. Prep. Prop. Fuel Cell Appl.* **2017**, 381–398. [\[CrossRef\]](#)

88. Xu, T.; Liu, K.; Sheng, N.; Zhang, M.; Liu, W.; Liu, H.; Dai, L.; Zhang, X.; Si, C.; Du, H.; et al. Biopolymer-based hydrogel electrolytes for advanced energy storage/conversion devices: Properties, applications, and perspectives. *Energy Storage Mater.* **2022**, *48*, 244–262. [\[CrossRef\]](#)
89. Hung, C.-L.; Chen, M.; Sohaimy, M.I.H.; Isa, M.I.N. Proton-Conducting Biopolymer Electrolytes Based on Carboxymethyl Cellulose Doped with Ammonium Formate. *Polymers* **2022**, *14*, 3019. [\[CrossRef\]](#)
90. Liu, X.; Fan, X.; Liu, B.; Ding, J.; Deng, Y.; Han, X.; Zhong, C.; Hu, W. Mapping the Design of Electrolyte Materials for Electrically Rechargeable Zinc–Air Batteries. *Adv. Mater.* **2021**, *33*, 2006461. [\[CrossRef\]](#)
91. Munaoka, T.; Yan, X.; Lopez, J.; To, J.W.F.; Park, J.; Tok, J.B.H.; Cui, Y.; Bao, Z. Ionically Conductive Self-Healing Binder for Low Cost Si Microparticles Anodes in Li-Ion Batteries. *Adv. Energy Mater.* **2018**, *8*, 1703138. [\[CrossRef\]](#)
92. Cai, M.; Park, S. Spectroelectrochemical Studies on Dissolution and Passivation of Zinc Electrodes in Alkaline Solutions. *J. Electrochem. Soc.* **1996**, *143*, 2125–2131. [\[CrossRef\]](#)
93. Kumar, G.G.; Sampath, S. Electrochemical characterization of poly(vinylidene fluoride)-zinc triflate gel polymer electrolyte and its application in solid-state zinc batteries. *Solid State Ion.* **2003**, *160*, 289–300. [\[CrossRef\]](#)
94. Girish Kumar, G.; Sampath, S. Electrochemical and spectroscopic investigations of a gel polymer electrolyte of poly(methylmethacrylate) and zinc triflate. *Solid State Ion.* **2005**, *176*, 773–780. [\[CrossRef\]](#)
95. Tafur, J.P.; Romero, A.J.F. Interaction between Zn²⁺ cations and n-methyl-2-pyrrolidone in ionic liquid-based Gel Polymer Electrolytes for Zn batteries. *Electrochim. Acta* **2015**, *176*, 1447–1453. [\[CrossRef\]](#)
96. Béjar, J.; Álvarez-Contreras, L.; Ledesma-García, J.; Arjona, N.; Arriaga, L.G. An advanced three-dimensionally ordered macroporous NiCo₂O₄ spinel as a bifunctional electrocatalyst for rechargeable Zn–air batteries. *J. Mater. Chem. A* **2020**, *8*, 8554–8565. [\[CrossRef\]](#)
97. Díaz-Patiño, L.; Béjar, J.; Ortiz-Ortega, E.; Trejo, G.; Guerra-Balcázar, M.; Arjona, N.; Álvarez-Contreras, L. Zinc-Air Battery Operated with Modified-Zinc Electrodes/Gel Polymer Electrolytes. *ChemElectroChem* **2022**, *9*, e202200222. [\[CrossRef\]](#)
98. Wei, Y.; Wang, M.; Xu, N.; Peng, L.; Mao, J.; Gong, Q.; Qiao, J. Alkaline Exchange Polymer Membrane Electrolyte for High Performance of All-Solid-State Electrochemical Devices. *ACS Appl. Mater. Interfaces* **2018**, *10*, 29593–29598. [\[CrossRef\]](#)
99. Zhang, J.; Fu, J.; Song, X.; Jiang, G.; Zarrin, H.; Xu, P.; Li, K.; Yu, A.; Chen, Z. Laminated Cross-Linked Nanocellulose/Graphene Oxide Electrolyte for Flexible Rechargeable Zinc–Air Batteries. *Adv. Energy Mater.* **2016**, *6*, 1600476. [\[CrossRef\]](#)
100. Fan, X.; Liu, J.; Song, Z.; Han, X.; Deng, Y.; Zhong, C.; Hu, W. Porous nanocomposite gel polymer electrolyte with high ionic conductivity and superior electrolyte retention capability for long-cycle-life flexible zinc–air batteries. *Nano Energy* **2019**, *56*, 454–462. [\[CrossRef\]](#)
101. Li, Y.; Fan, X.; Liu, X.; Qu, S.; Liu, J.; Ding, J.; Han, X.; Deng, Y.; Hu, W.; Zhong, C. Long-battery-life flexible zinc–air battery with near-neutral polymer electrolyte and nanoporous integrated air electrode. *J. Mater. Chem. A* **2019**, *7*, 25449–25457. [\[CrossRef\]](#)
102. Poosapati, A.; Negrete, K.; Thorpe, M.; Hutchison, J.; Zupan, M.; Lan, Y.; Madan, D. Safe and flexible chitosan-based polymer gel as an electrolyte for use in zinc-alkaline based chemistries. *J. Appl. Polym. Sci.* **2021**, *138*, 50813. [\[CrossRef\]](#)
103. Song, W.; Wang, Y.; Deng, H. Ion-conducting polymer gels of polyacrylamide embedded with K₂CO₃. *J. Appl. Polym. Sci.* **2004**, *92*, 2076–2081. [\[CrossRef\]](#)
104. Ng, P.L.; Jamaludin, A.; Alias, Y.; Basirun, W.J.; Ahmad, Z.A.; Mohamad, A.A. Effect of KOH concentration in the gel polymer electrolyte for direct borohydride fuel cell. *J. Appl. Polym. Sci.* **2012**, *123*, 2662–2666. [\[CrossRef\]](#)

Supporting Information

Table S1. Average electrolytes' thickness used for ionic conductivity calculations.

Electrolyte	Thickness (cm)
CMC-CS sw	0.28 ± 0.09
CA30 sw	0.31 ± 0.0001
CA40 sw	0.36 ± 0.05
CA50 sw	0.35 ± 0.05

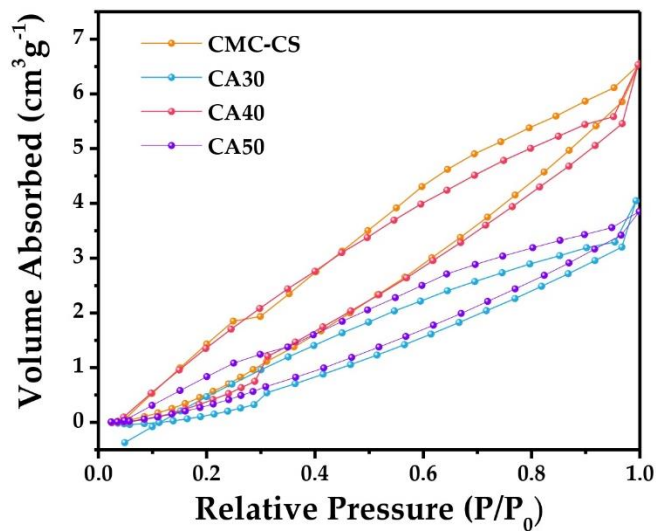


Figure S1. Nitrogen adsorption/desorption isotherms for the synthesized hydrogels.

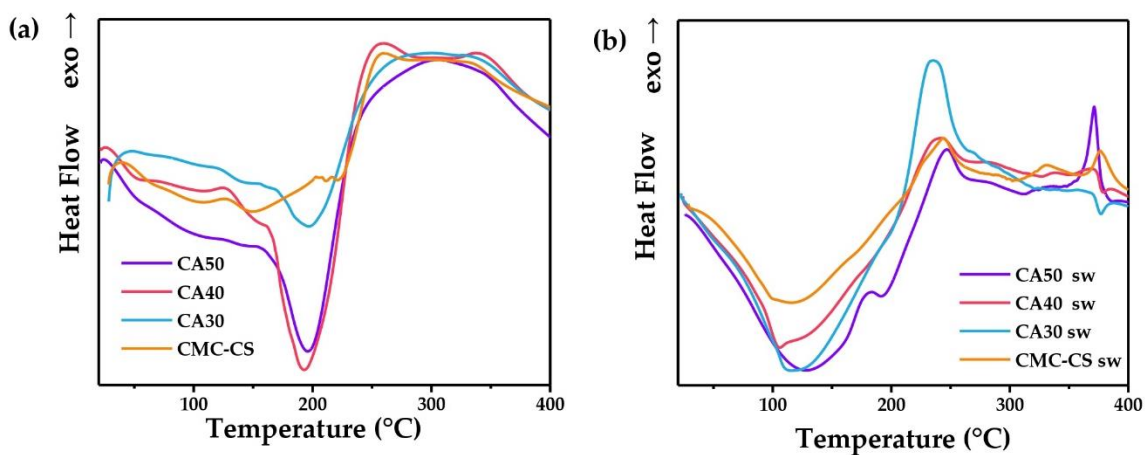


Figure S2. DSC curves for (a) dried hydrogels and (b) swollen hydrogels.

2.3. Article published in the *Journal of the Electrochemical Society* “Enhancing Electrochemical Performance of Zinc-Air Batteries using Freeze Crosslinked Carboxymethylcellulose-Chitosan Hydrogels as Electrolytes.”

The third and last work of this thesis is proposed based on a modification to the synthesis performed in the second article, where the method of drying the polymer membranes by conventional casting technique was used. Thus, this step is modified through five freeze-thawing cycles, followed by a final freeze-drying process. The subsequent effects of the proposed drying strategies are overviewed.

The structural characterization by ATR-FTIR demonstrated similar bands to those reported in the previous work. The band at 1021 cm^{-1} corresponding to the C–O–C ether pyranose ring presented a higher intensity compared to the homologous casting-dried counterparts, suggesting that the physical crosslinking originated from the F-T processes and preserved the polymeric chains in the system. All the other bands showed no differences, suggesting that this drying approach does not affect other chemical interactions between the two biopolymers.

The most important modification in the system was evidenced by the SEM micrographs, obtaining a highly porous morphology. Hence, the drying strategies play a significant role in the pore size and shape of the hydrogels. This morphology was related to the more KOH uptake of the membranes. EDX characterization exhibited a better uniform dispersion of potassium in the chemically crosslinked hydrogel.

The swelling behavior was greatly enhanced, since the membranes were capable of absorbing six-seven times their own weight, with a non-significant volume change. The hydrogel's biodegradability was analyzed and confirmed by burying the membranes in soil, obtaining a final weight remanent of 22.73% on day 39. Besides, the CA50L sw electrolyte was folded and released, preserving its initial shape without breakage, as a demonstration of the flexible nature of the membranes. Moreover, the hydrogel's flammability was proved, since when exposed to fire the membrane only shrugged, without explosions.

Arrhenius conduction mechanism was demonstrated from $0\text{ }^{\circ}\text{C}$ to $70\text{ }^{\circ}\text{C}$, suggesting superior thermal stability. The electrolyte exhibited an enhanced ionic conductivity of $0.39\text{ S}\cdot\text{cm}^{-1}$. This enhancement can be explained in terms of the pores and channels generated by the drying strategies since this obtained morphology provides paths for the ions to move more easily in the system.

In terms of the battery tests, a maximum power density of $117\text{ mW}\cdot\text{cm}^{-2}$ was achieved with the CA50L sw electrolyte, besides a specific capacity of $1899\text{ mA}\cdot\text{h g}^{-1}$. Altogether, these results demonstrate the great effects obtained in dependence of the drying technique chosen for the synthesis procedure.

OPEN ACCESS

Enhancing Electrochemical Performance of Zinc-Air Batteries Using Freeze Crosslinked Carboxymethylcellulose-Chitosan Hydrogels as Electrolytes

To cite this article: María Fernanda Bósquez-Cáceres *et al* 2023 *J. Electrochem. Soc.* **170** 060502

View the [article online](#) for updates and enhancements.

You may also like

- [Effects of local distortion on the electrical properties of lead free perovskite-type electro-ceramics \$\text{Ba}_{1-x}\text{Ca}_x\text{Ti}_{0.8}\text{Zr}_{0.2}\text{O}_3\$](#)
G Herrera-Pérez, A Reyes-Montero, J Canche-Tello et al.
- [Janus-Typed Integrated Bifunctional Air Electrode with \$\text{MnO}_2\$ -NiFe LDH/Ni Foam for Rechargeable Zinc-Air Batteries](#)
Lei Wan, Peican Wang, Yuqun Lin et al.
- [Aquatic Colloidal Graphene Gel Polymer Electrolyte for Flexible Rechargeable Zinc Air Batteries](#)
Xingliang Jia, Jingling Ma, Liangliang Zhang et al.



Enhancing Electrochemical Performance of Zinc-Air Batteries Using Freeze Crosslinked Carboxymethylcellulose-Chitosan Hydrogels as Electrolytes

María Fernanda Bósquez-Cáceres,^{1,*} José Bejar,² Lorena Álvarez-Contreras,² and Juan P. Tafur^{1,✉}

¹Grupo de Investigación Aplicada en Materiales y Procesos (GIAMP), School of Chemical Sciences & Engineering, Yachay Tech University, Urcuquí 100115, Ecuador

²Centro de Investigación en Materiales Avanzados S.C. (CIMAV), Miguel de Cervantes No. 120, Complejo Industrial Chihuahua, Chihuahua 31136, Mexico

Zinc-air batteries (ZABs) are devices of great interest as a replacement option for subsequent technologies to lithium-ion batteries. Still, the need for suitable electrolyte materials limits their application in commercial devices. In this study, a green hydrogel composed of chitosan and carboxymethylcellulose was synthesized with the use of citric acid as a chemical crosslinker, physical freezing-thawing, and freezing-drying strategies. Physicochemical, thermal, and electrochemical characterizations were performed to study the effects of the proposed synthesis on the performance of the hydrogels for the desired application. The obtained hydrogels showed a porous morphology that was doped with a 12 M KOH solution. Adequate complexation of K^+ cations and the polymer chains was observed. The resulting membranes showed an enhanced ionic conductivity of 0.39 S cm^{-1} , attributed to the pores and channels generated by the crosslinking strategies, contributing to the pathways for ions to move easily. In addition, the temperature dependence of the conduction mechanism was confirmed in the temperature range of 0°C to 70°C . The electrolytes were employed in ZABs prototypes, achieving a maximum power density of 117 mW cm^{-2} and a specific capacitance of 1899 mAh g^{-1} . The presented results show the promising properties of these hydrogels as electrolytes for green storage devices.

© 2023 The Author(s). Published on behalf of The Electrochemical Society by IOP Publishing Limited. This is an open access article distributed under the terms of the Creative Commons Attribution Non-Commercial No Derivatives 4.0 License (CC BY-NC-ND, <http://creativecommons.org/licenses/by-nc-nd/4.0/>), which permits non-commercial reuse, distribution, and reproduction in any medium, provided the original work is not changed in any way and is properly cited. For permission for commercial reuse, please email: permissions@iopublishing.org. [DOI: 10.1149/1945-7111/acd876]



Manuscript submitted March 9, 2023; revised manuscript received April 29, 2023. Published June 1, 2023.

Supplementary material for this article is available online

Zinc-air batteries (ZABs) have attracted considerable interest as an energy storage device for a wide range of applications. These batteries employ zinc as the negative metal electrode and an air-breathing positive electrode, and the advantages of this metal include inherent safety, low cost, and availability.¹ To develop a suitable ZAB prototype that can be scalable to commercial use, it is essential to have an appropriate electrolyte to connect both electrodes. Polymer electrolytes (PEs) are an important and promising technology for energy storage devices applications. These materials are a type of solid-state or gel-based matrix employed as the electrolyte component of a battery. PEs are known to be less volatile and non-flammable, leading to safer cells than conventional liquid electrolytes, avoiding some undesired reactions that provoke internal shorting, electrolyte leakage, and production of harmful gases.²

Several polymer matrices designed to retain plasticizers or liquid electrolytes have been researched to improve their performance in ZABs.³ Electrolytes made of biopolymers have shown comparable ion conduction and electrochemical properties than the traditional fossil-based polymer matrices.^{4–6} Their abundance, low cost, and easier processing ability make biopolymer electrolytes expected to be the next generation of green energy technologies. Among the available biopolymers, carboxymethylcellulose (CMC), and chitosan (CS) have been reported to form intermolecular complexes through strong electrostatic and hydrogen bonding interactions.^{7,8} CMC-CS hydrogels can be synthesized through chemical and physical crosslinking. Chemical crosslinking has been the focus of our previous work employing citric acid (CA) as a chemical crosslinker,⁹ which allowed us to obtain better structural integrity, higher thermal stability, and enhanced electrochemical properties. A maximum ionic conductivity value of 0.19 S cm^{-1} at 30°C was achieved, along with a power density of 85 mW cm^{-2} .

Physically crosslinked hydrogels are synthesized by different strategies that lead to ionic interactions between the polymers, crystallization (freezing strategies), the formation of hydrophobic polysaccharide stereocomplexes, protein interaction, and hydrogen bonding.¹⁰ Physical hydrogels can be obtained by repeated freeze-thaw (F-T) cycles from a concentrated aqueous solution containing polymers capable of forming physical crosslinks through weak interactions.¹¹ During freezing, the formed ice crystals organize the polymer chains around themselves. Then, during the thawing of the cycle, the ice crystals melt, giving rise to a microporous structure.¹² The stability of hydrogels obtained by this method increases with the number of F-T cycles.¹³ From the works reported to date, in which chitosan hydrogels are synthesized by this technique, a decrease in pore size and an increase in elastic modulus and tensile strength are evidenced.^{14–16}

On the other hand, freeze-drying through lyophilization is another inexpensive physical crosslinking method in which the sublimation process at low temperatures and under vacuum conditions produces homogeneous porous polymeric membranes with reduced shrinkage and high mechanical strength.¹⁷ Zhong et al.¹⁸ designed a porous methyl cellulose-based gel polymer electrolyte fabricated through freeze-drying that exhibited high ionic conductivity, low interface impedance, and low activation energy for Li^+ migration due to the presence of micropores in the matrix, capable of retaining large volumes of liquid electrolyte.

In the present study, membranes were synthesized from CS, CMC, and CA by freezing-thawing and posterior freeze-drying procedures. The synthesized membranes were doped with a 12 M KOH electrolyte solution. The physicochemical, thermal, and electrochemical properties of the hydrogels were determined to analyze the effect of the chemical and physical crosslinking strategies employed and to evaluate the applicability of the material as an electrolyte in ZABs. Then, a cell prototype was constructed with each membrane to perform primary battery tests to investigate the bulk resistance, the power and current densities, and the specific capacity of the cell prototypes with the designed materials.

*Electrochemical Society Student Member.

✉E-mail: jtafur@yachaytech.edu.ec

Experimental

Chemicals and materials.—Carboxymethyl cellulose sodium salt (high molecular weight, high viscosity grade, sodium glycolate max. 0.4%), and anhydrous citric acid (CA) (purity 99.5%) were purchased from Loba Chemie. 90.6% deacetylated¹⁹ chitosan food grade (low molecular weight, purity 100%, BioFitnest). Anhydrous glacial acetic acid for analysis (purity 100%) and potassium hydroxide pellets (purity $\geq 85.00\%$) were purchased from Sigma Aldrich. All chemicals were used directly without further purification, and distilled water was used to prepare all the aqueous solutions. For electrochemical testing, Zn discs (99.99%) and Pt plates (99.97%) were acquired from Goodfellow. For the battery prototype, the anode was built of a piece of polished high-purity Zn foil of 0.2 mm thick, 10×15 mm width and length (purity 99.9%, Yunexpress Inc., Shenzhen). SIGRACET[®] 39 B slides of 0.4 mm thick, 10×15 mm width and length, impregnated with a catalyst mass loading of 1 mg cm^{-2} commercial catalytic ink and Pt/C (20% wt%) were designed as the cathode.

Preparation of the Frozen-Thawed CMC-CS-CA hydrogels.—Hydrogels were prepared by solution polymerization/crosslinking methods, following a procedure similar to the one previously reported by our research group,⁹ and modified in this new work. We added 5 freeze-thawing cycles along with a freeze-drying step. Briefly, homogenous solutions of 2 wt% of CMC, 4 wt% of CA and 2 wt% of CS (in 1 wt% of acetic acid) were prepared separately. First, 90 ml CMC solution was mixed with 30 ml CS solution to form CMC-CSL solution. Then, varying amounts of the CA solution were added to form hydrogels named CA30L, CA40L, and CA50L (Table SI). The solutions were homogenized with an immersion blender for 3 min. Subsequently, the solutions were sonicated at 40 kHz at 60 °C for 1 h. The mixtures were then dried in an oven at 80 °C for 1 h. Excess liquid was removed starting the freezing-thawing cycle process. The solutions were frozen at -80 °C for 16 h, followed by thawing (room temperature for 8 h) for up to 5 repeated cycles. Finally, all hydrogels were freeze-dried for 48 h at -55 °C, 76 mmHg in a lyophilizer (Gperon), and stored in a desiccator for characterization. One set of membranes was immersed in a 12 M KOH solution for 48 h for testing. The synthesis procedure is shown in Figure 1. Hydrated membranes are labeled with “sw” next to the names of the hydrogel (Table SI).

Physicochemical characterization.—X-ray diffractograms were obtained using a computer-controlled Rigaku Mini-flex-600 with a D/tex Ultra 2 detector 26 (Rigaku, Tokyo, Japan) operated at 40 kV and 15 mA in a sealed tube with a Ni-filtered Cu K α radiation source ($\lambda = 0.15418 \text{ nm}$). The studied angular region was $2\theta = 5^\circ$ – 80° with a step width of 0.01° . Match! Software (Crystal Impact, Bonn, Germany) was used to quantify the crystallinity degree (CD) of the hydrogels.²⁰ Fourier transform-infrared (FTIR) was used to analyze the chemical bands of the hydrogels. IR spectra were obtained using a Cary 630 spectrophotometer equipped with a 1-bounce diamond ATR accessory (Agilent Technologies Inc.). The spectra were registered with 64 scans in the range of 4000 – 400 cm^{-1} , with a resolution of 4 cm^{-1} . Surface and cross-sectional scanning electron microscopy (SEM) micrographs were acquired with a JEOL JSM-6010/LV microscope (JEOL Ltd). Elemental mapping was performed on the swelled and used membranes by energy-dispersive X-ray spectroscopy (EDX) using an EDX TEAM analysis system integrated into the SEM. Thermogravimetric analysis was performed by a TGA SDT Q600 (TA Instruments), with a nitrogen flow from ambient to 800 °C using a heating ramp of 10 °C·min⁻¹. KOH swelling retention tests were carried out by weighing the membranes before and after 48 h of being immersed in the 12 M KOH solution, and the swelling ratio (SR) calculations were performed using Eq. 1:

$$\text{SR} = ((W_T - W_0)/W_0) \times 100\% \quad [1]$$

where W is weight or volume, and the subindexes T and 0 represent the swollen membrane and the initial membrane, respectively. The initial and final volume of the hydrogels was measured by obtaining the length, width, and height of the sample with the use of a micrometer and multiplying these measurements to calculate the volume of a box-shaped figure.

A biodegradation study in composted soil was conducted using commercial soil employed for cultivation, following a similar method as the one reported by Michelle et al.²¹ Membranes of 1.0 cm^2 and $\sim 0.5 \text{ cm}$ were interred in the soil at room temperature in triplicate. Soil was watered every 3 d. Samples weights were registered at different time intervals after vacuum drying for 24 h.

Electrochemical measurements.—Electrochemical assays were performed using a VIONIC instrument (Metrohm model). Cyclic voltammograms (CV) were obtained at a sweep rate of 50 mV s^{-1} in a symmetrical potential window from -1.5 to $+1.5 \text{ V}$ using a symmetrical two-electrode Zn/hydrogel/Zn cell with 0.5 cm^2 non-blocking Zn electrodes. Potential electrochemical impedance spectroscopies (EIS) of the swollen hydrogels were obtained in the frequency range from 100 kHz to 1 Hz using a Pt/hydrogel/Pt cell configuration with 1 cm^2 Pt blocking electrodes. Impedance was measured over a temperature range from 0 °C to 70 °C with an accuracy of ± 1 °C using a Julabo Polyscience circulator (-40 °C, 15 L) to calculate the ionic conductivity with Eq. 2:

$$\sigma = l/(A \times R_b) \quad [2]$$

where A is the Pt electrode area, l is the film thickness, and R_b is the bulk resistance, obtained from the intersection of the impedance curve with the x-axis. Four measurements were performed for each membrane and temperature. The activation energy (E_a) was determined with Arrhenius Eq. 3 fitted linearly by plotting the logarithmic relationship between $\ln(\sigma)$ and $1000/T$:

$$\sigma = \sigma_0 \times (-E_a/(T \times K_b)) \quad [3]$$

where T is the absolute temperature, σ_0 is a pre-exponential factor, and K_b is the Boltzmann's constant.²²

Zn-air battery tests.—The battery prototype tests were performed in an AMETEK[®] VersaSTAT 3 potentiostat/galvanostat (Princeton Applied Research). The hydrogels were placed between the Zn-Pt/C electrodes using the previously reported configuration,²³ without the use of the reservoir. Firstly, EIS spectra were obtained at the open circuit potential in a frequency range of 100 kHz to 0.1 Hz . Then, ZAB experiments like polarization and power density curves were performed for each membrane. The discharge current density for the polarization curves was 20 mV s^{-1} , and the cut-off voltage was 0.2 V . Additionally, the battery was discharged using different current densities maintained for 300 s. Finally, specific capacity was determined by applying a constant current density of 3 mA cm^{-2} , the zinc mass loss from this test, and the previously reported equation.²⁴

Results and Discussion

Structural characterization.—XRD and FTIR studies In the obtained diffractograms, the peak at 10.2° , reported to be assigned to the amine I “ $-\text{N}-\text{CO}-\text{CH}_3$ ” of chitosan,²⁵ had almost disappeared from the XRD patterns. The most prominent peak appeared at $2\theta = 21.3^\circ$, with a broader shape compared to that of the pure polymers (Fig. 2), which is an indication of amorphization. The shift in this peak indicated the pairing of the CMC and CS chains by ionic interaction between the carboxyl groups from CMC and the amine groups from CS. It was reported that $2\theta = 20.01^\circ$ was assigned to the amine II ($-\text{NH}_2$) and to crystallographic planes (020), (110) and (120).²⁶ The shift presented towards higher theta values indicates a decrease in interchain spacing, typical of enhanced crosslinking.²⁷

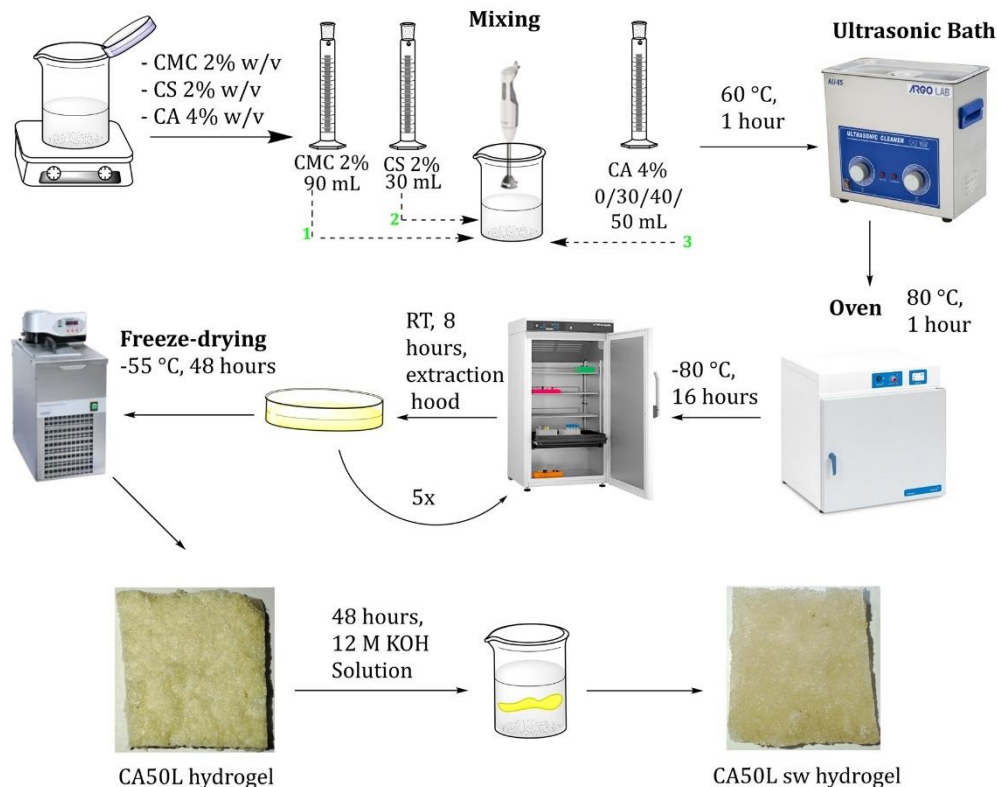


Figure 1. Scheme of the synthesis process of the CMC-CSL membranes as hydrogels for electrolytes.

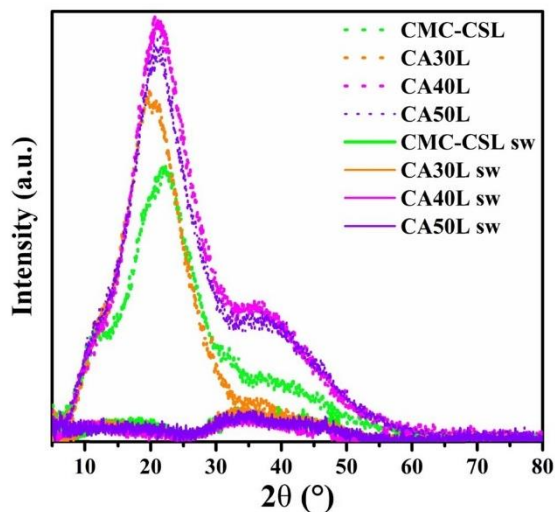


Figure 2. XRD patterns of the CMC-CSL and CMC-CSL sw hydrogels at different CA proportions.

The CA crosslinked membranes demonstrated an increase in the peak intensity for $2\theta = 21.3^\circ$, and when compared to the CA-free hydrogel, an increase in the material's crystalline degree is evidenced, confirmed quantitatively with the CD obtained with Match!

Software,²⁰ with values from 18.6% for the membrane without CA, up to a value of 24.2% for the CA50L membrane (Table I). This increase was especially evident in the peak $2\theta = 36.7^\circ$ in the CA40L and CA50L membranes. The obtained XRD patterns are congruent with those published in the literature for similar polymeric matrices and pure polymers.^{28,29} In terms of the hydrated hydrogels, the CD decreased due to the addition of KOH molecules to the matrix, since the K^+ cations form complexes with the polymer chains, breaking some of the hydrogen bonding in the system.³⁰

Among the identified bands in the FTIR spectra, the CMC-CSL membrane depicted the characteristic bands for both polymers in the IR spectrum at 3200 and 3300 cm^{-1} , assigned to the $-\text{OH}/\text{NH}$ stretching vibrations of CMC/CS, respectively (Fig. 3a).²⁸ The peaks observed at 2880 and 2857 cm^{-1} correspond to asymmetric and symmetric C-H stretching vibration of the N- acetyl group.³¹ The band at 1021 cm^{-1} is related to the C-O-C vibration of the pyranose ring.³² The most significant change in the spectrum of this hydrogel compared to pure polymers is that the amide group (1655 cm^{-1}) of CS and the carbonyl group (1596 cm^{-1}) of CMC interact to form a band at 1574 cm^{-1} , which suggests the complexation of CMC-CS by ionic interaction between the COO^- group of CMC and NH_3^+ group of CS.³³

In the case of the CA crosslinked membranes, the ester bond formation reported for the reaction mechanism⁹ was also confirmed for the proposed synthesis, with the band located at 1711 cm^{-1} , with the band observed at lower frequency compared to the casting dried membranes. The intensity of the band among the three samples is also an indicator of chemical cross-linking degree. The band corresponding to the C-O-C shifted to lower wavenumbers (1015 cm^{-1}), but with an increase in intensity, which is attributed to physical crosslinking caused by the F-T cycles.³⁴

Table I. Crystallinity degree (CD) calculated from the XRD patterns.

Hydrogels	CD(%)
CMC-CSL	18.6
CA30L	19.6
CA40L	23.5
CA50L	24.2
CMC-CSL sw	9.6
CA30L sw	6.8
CA40L sw	6.4
CA50L sw	7.6

As for the hydrated membranes (Fig. 3b), the bands related to the O–H region showed changes, principally with an increase in the band at 3306 cm^{-1} due to the water insertion, confirmed also by the band at 1636 cm^{-1} , assigned to the O–H bending mode of water.³⁵ The carbonyl band shifted to 1596 cm^{-1} , due to the formation of complexes with K^+ originated from KOH insertion.³⁶ The band at 1021 cm^{-1} corresponding to the C–O–C ether pyranose ring presented a higher intensity compared to the homologous casting-dried counterparts,⁹ which suggests that the physical crosslinking originated from the F–T processes preserves the polymeric chains in the system. Besides these differences in intensity of ester and ether bands, all the other bands between cast-dried and F–T dried membranes showed no differences, as an indicator of how this drying method does not affect other interactions that occur between both polymers.

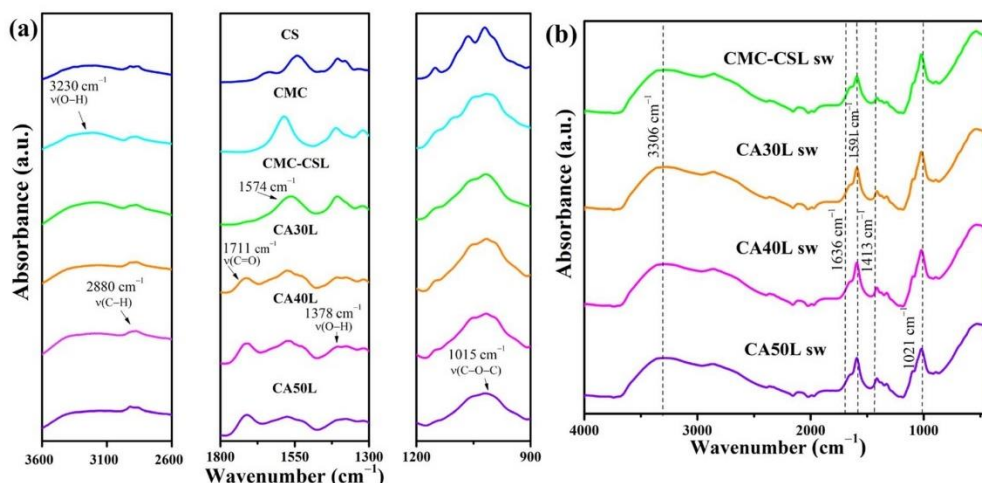
SEM micrographs and EDX characterization.—Surface and cross-section micrographs of the CMC-CSL (Fig. 4a) presented an irregular morphology, with disordered pores and a smoother surface. Granules were also identified on the surface. The CA40L membranes (Fig. 4b), a highly porous and more distributed structure, was observed pointing towards efficient miscibility between the employed biopolymers and CA. Concerning its casting counterpart,⁹ the morphology obtained in this work showed smaller and denser pores, attributed to the physical crosslinking of the hydrogels due to the repetitive F–T cycles.³⁴ These results suggest that the crosslinking methods used play a significant role in the pore size and shape of the membranes, as previously reported.³⁷ This morphology is related to

the more KOH solution absorption capability of the hydrogels, with the expanding of the pores in the matrix. The micrograph of the CA40L sw membrane (Fig. 4bIII) exhibited granules all over the matrix, due to the absorbed ionic salt solution. These granules evidenced the KOH dispersion throughout the membrane, and the complexation of the electrolyte components. In the case of the CMC-CSL sw hydrogel (Fig. 4aIII) the system showed some granules present, but a more tubular morphology was obtained.

After the discharge test, EDX mapping was performed on the hydrogels (Fig. 5), where the material composition expressed as weight percentage was obtained (Table II). For both membranes, some Zn deposition was evidenced, with higher metal residue in the case of the CMC-CSL sw membrane, and the appearance of dendrites (Fig. S1), that are originated by heterogeneous nucleation and growth of the electrodeposited Zn during the discharge process. These dendrites could cause perforations in the system, leading to safety issues.¹⁸ Better uniform dispersion of potassium was observed in the chemically crosslinked membrane.

Swelling behavior, volume changes and biodegradability.—To know the KOH absorption in hydrogels, the swelling ratio and volume changes of the hydrated membranes were obtained with Eq. 1. The largest change was presented for the CA-free hydrogel ($1342 \pm 105\text{ wt\%}$, $63.61 \pm 0.07\text{ vol\%}$) (Table III). As the hydrogel was prepared with more CA, a decrease in the SR was obtained. This is in agreement with what is expected when a higher crosslinking density is achieved,³⁸ with the same trend for the cast-dried membranes. Nevertheless, the physically crosslinked hydrogels absorbed at least 6 times its weight (CA50L sw membrane) with a non-significant volume change ($657 \pm 42\text{ wt\%}$, $16.69 \pm 1.30\text{ vol\%}$). The volume change is a critical evaluation parameter since it affects the design of the final battery prototype.

To study the changes in the liquid content of the hydrogels, the weight percentage was recorded over time at room temperature. Figure 6a displays these changes over 56 d. A period of weight gain attributed to the hygroscopic nature of chitosan and CMC was evidenced due to the absorption of moisture from the environment.^{39,40} The hydrogels underwent a dehydration process after 25 d, reaching a maximum weight percentage of 28.6% for the CA50L sw hydrogel. Moreover, the CA50L sw electrolyte was folded (Fig. 6b) and released, preserving its initial shape without breakage, as a demonstration of the flexible nature of the membranes. The hydrogels biodegradability was analyzed by burying the membranes in soil for 39 d (Figs. 6c–6e). During the study time, the

**Figure 3.** ATR-FTIR spectra of (a) CMC-CSL, and (b) CMC-CSL sw hydrogels at different CA proportions.

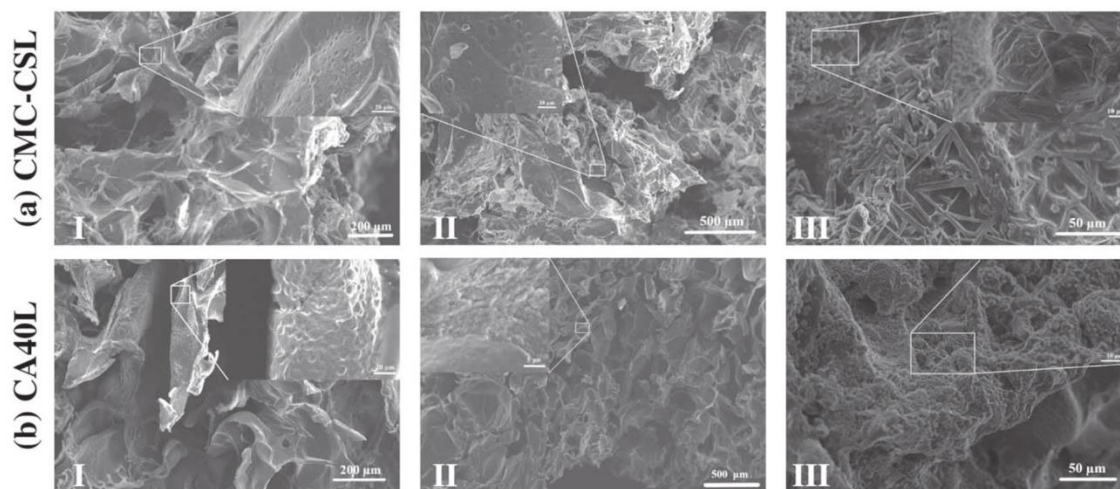


Figure 4. SEM micrographs of the dried (a) CMC-CSL and (b) CA40L hydrogel. Micrograph of the (I) surface, (II) cross section and (III) swollen in 12 M KOH.

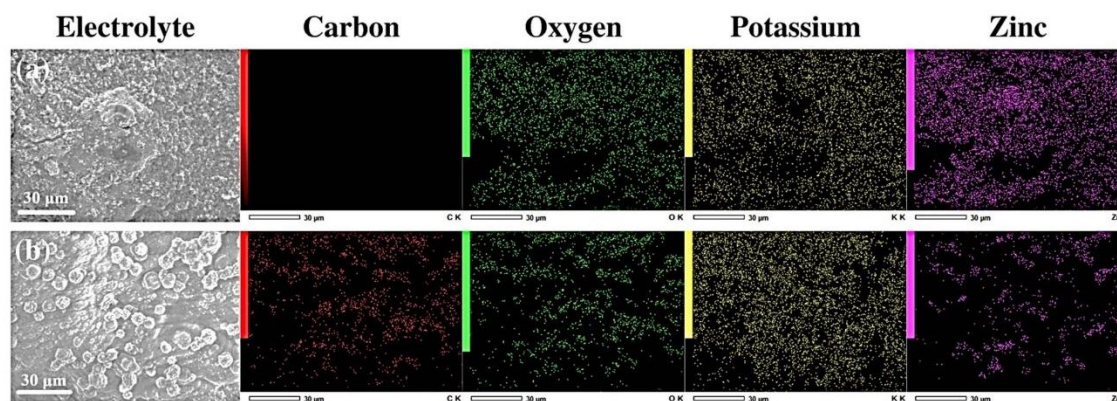


Figure 5. SEM images and EDX maps of (a) CMC-CSL sw and (b) CA40L sw in the cathode-facing side after discharging the Zn-air battery.

Table II. Material composition expressed as percentage by weight of the CMC-CSL sw and CA40L sw hydrogels in the cathode-facing side after discharging the Zinc-air battery.

Membrane	Material composition (Weight %)			
	Carbon	Oxygen	Potassium	Zinc
CMC-CSL sw	25.81	36.93	22.79	14.47
CA40L sw	26.35	32.52	38.08	3.06

Table III. Swelling behavior in mass percentage and volume change percentage of the synthesized membranes.

Electrolyte	Swelling Ratio (%)	Volume Change (%)
CMC-CSL sw	1342 ± 105	63.61 ± 0.07
CA30L sw	797 ± 38	18.77 ± 5.17
CA40L sw	743 ± 13	16.90 ± 4.56
CA50L sw	657 ± 42	16.69 ± 1.30

hydrogel started to degrade and became more malleable, and some mildew arose. By the weight retention measurements as a function of buried time (Fig. S2), the CA50L hydrogel lost 54.50% of its initial weight during the first 30 d of testing. A final remnant of 22.73% of weight was registered on day 39, where dirt got stuck on the membrane, making it difficult to assure an appropriate measurement after that. Moreover, the hydrogel's flammability was proved (Figs. 6e–6g), which demonstrates that when exposed to fire the membrane only shrugged, without explosions. This behavior is attributed to the non-flammable components employed for the hydrogel's fabrication.⁴¹ The results indicate that these electrolytes are an option for developing green ZABs.

Thermal studies.—For the dry hydrogels, three degradation stages were identified (Fig. 7a). The first region, from 40 °C to 240 °C, corresponds to the process of loss of internal water. The weight of the hydrogel matrices only decreased by up to 15.1% between 30 °C and 200 °C. The second loss, up to 360 °C, is attributed to the degradation of the polymeric matrix and char formation. The considerable weight loss between 240 °C to 400 °C was related to the partial degradation of CS, decarboxylation of CMC, and decomposition of CA.⁴² The last region represents the complete decomposition of the organic components of the

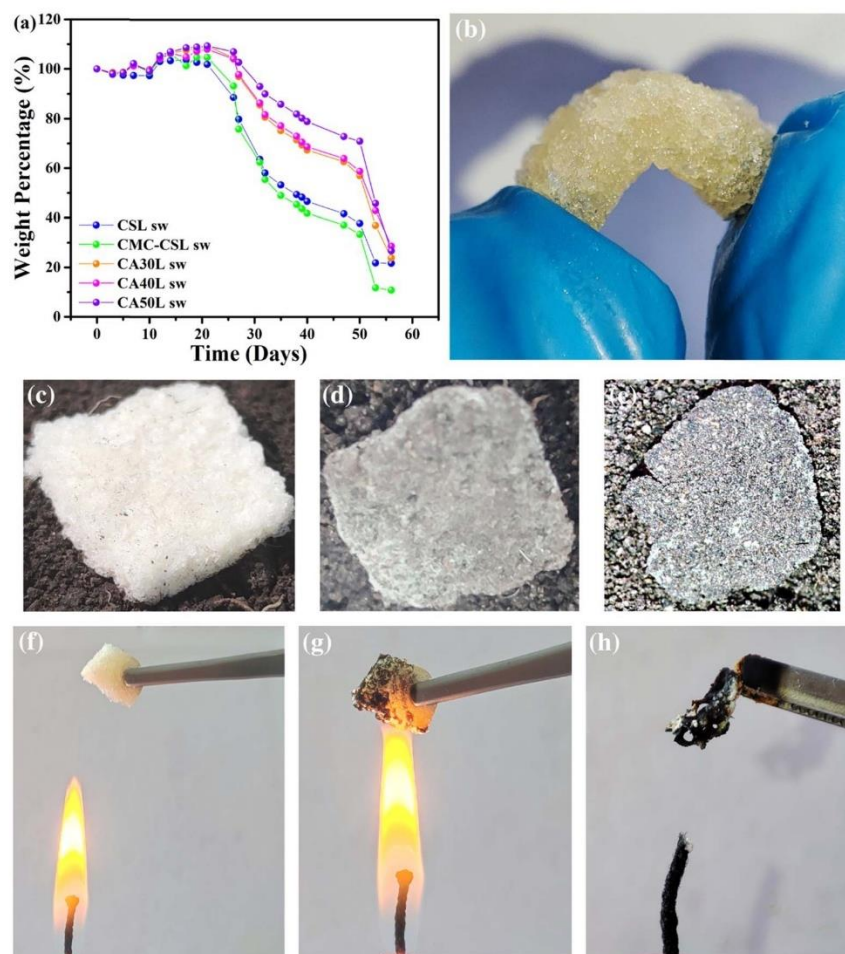


Figure 6. (a) Relation between the swollen membranes' changes with the storage time at ambient temperature. (b) Photograph of the CA50L sw hydrogel being bent to show its flexibility. Photographs of the CA50L electrolyte (c) fresh, buried in soil for (d) 30 d and (e) 39 d. (f) Photograph of the CA50L sw electrolyte prior to burning, (g) the CA50L sw electrolyte exposed to the flame, and (h) the hydrogel remanent after burning.

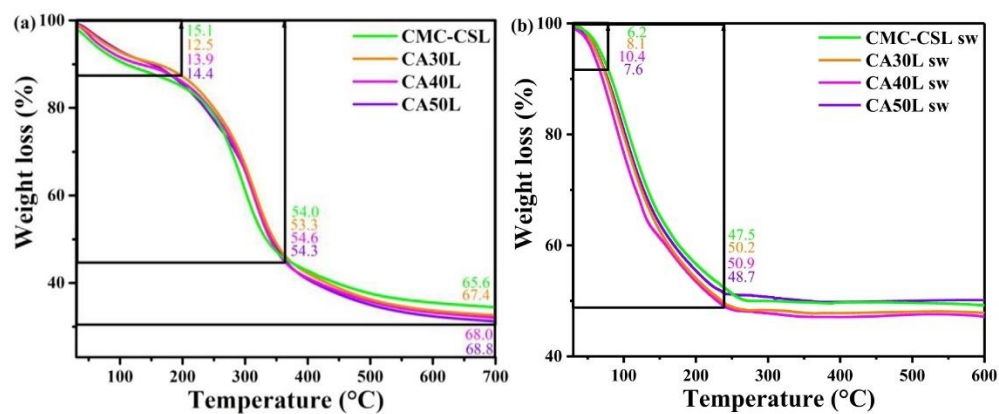


Figure 7. Thermogravimetric analysis curves of the (a) CMC-CSL and (b) CMC-CSL sw hydrogels.

hydrogels, with a stable weight from $\sim 550^\circ\text{C}$ onwards, with residues ranging from 34.4% for the CMC-CSL membrane to 31.6% for the CA50L hydrogel. The weight of the CA containing-membranes only decreased by less than $\sim 9\%$ at 100°C , which suggests the thermal stability of the matrices over the range of temperature applicability.

For the hydrated hydrogels, the first stage is related to the loss of water incorporated by the absorption of the KOH solution (Fig. 7b). From the DTGA curves (Fig. S3), it was evidenced that the minimum peak shifted to 101.1°C for the most crosslinked membrane CA50L sw, increasing the thermal stability and water retention of the crosslinked biopolymeric membrane.⁴³ Nevertheless, this shift is smaller than the one previously obtained for its casting-dried counterpart.⁹ The second region was found at 231.7°C , 233.3°C , 235.9°C , 236.4°C and 256.6°C for the CA40L sw, CMC-CSL sw, CA30L sw, and CA50L sw, respectively, which corresponds to the degradation of the polysaccharide structure of the membrane.⁴⁴

In the casting-dried hydrogels, there was an extra region at $\sim 537^\circ\text{C}$ that is absent in the TGA results presented. This step is related to the modification of the chemical structure by the oxygen-containing KOH molecule, which apparently does not occur in the proposed membranes. The hydrated membranes presented a higher residue percentage when compared to the dried membranes and were stable from $\sim 250^\circ\text{C}$ to the final test temperature, with the lowest loss of 47.5% for the CA30L sw hydrogel.

The DSC results (Fig. S4a) showed the apparition of an endothermic peak that increases in the range of 206°C to 220°C with the increase in the CA content, attributable to the heat absorption by thermal degradation of the polymers. Above 250°C , the last peak becomes exothermic for all hydrogels, and becomes sharper as the CA content increases. The CA50L membrane showed the most endothermic nature, pointing to an enhancement of thermal stability, as a result of strong intermolecular interactions.⁴⁵ Swollen hydrogels (Fig. S4b) showed an increase in the intensity of the endothermic curve at 110°C , indicating the formation of stronger internal bonds, implying that more heat is required to evaporate the absorbed water molecules. An exothermic peak was displayed at 250°C , which could be associated with the decomposition of CS and of the amine unit.²⁹

Electrochemical characterization.—Ion-conducting polymer electrolytes are characterized by the dissolving of salts in polar polymer matrices, as KOH complexed the synthesized membranes. In this context, the formed cations are expected to be responsible for ionic conductivity. Several models have been discussed to explain the conductive mechanism of these systems: Williams-Landel-Ferry (WLF) equation, Arrhenius equation, Effective Medium Theory (EMT), and Vogel-Tammann-Fulcher (VTF) equation.⁴⁶ Among them, Arrhenius's theory was confirmed by analyzing the relationship between the temperature and the ionic conductivity for all the hydrated membranes (Fig. 8a). The resulting cation transport mechanism is associated with the ions jumping to the nearest vacant sites, as occurs in ionic crystals, which results in a thermally assisted ionic conductivity mechanism.⁴⁷ The electrolyte membranes maintained the Arrhenius behavior until 70°C , as an upgrade in contrast to the casting-dried membranes that lost it at 60°C .⁹ From the linear-fit equation, the activation energy (E_a) was calculated (Table IV), and an average of 0.12 eV was obtained, required by the ion so that it gets to move from one site to another in the conduction process.⁴⁸

The ionic conductivity results have been analyzed in comparison to the SR (Fig. 8b), and the obtained values confirmed that KOH plays an imperative role in the system as it acts as the ionic species donor, increasing the ionic conductivity of the system when more KOH is present in the matrix. The highest ionic conductivity for the CA crosslinked membranes was 0.39 S cm^{-1} for the CA40L sw hydrogel. The obtained ionic conductivity values at 30°C double the values reported in our previous study for the casting-dried membranes (0.19 S cm^{-1}),⁹ even much higher than related reported works in the field, (less than 10^{-3} S cm^{-1}).^{49–51} The enhancement

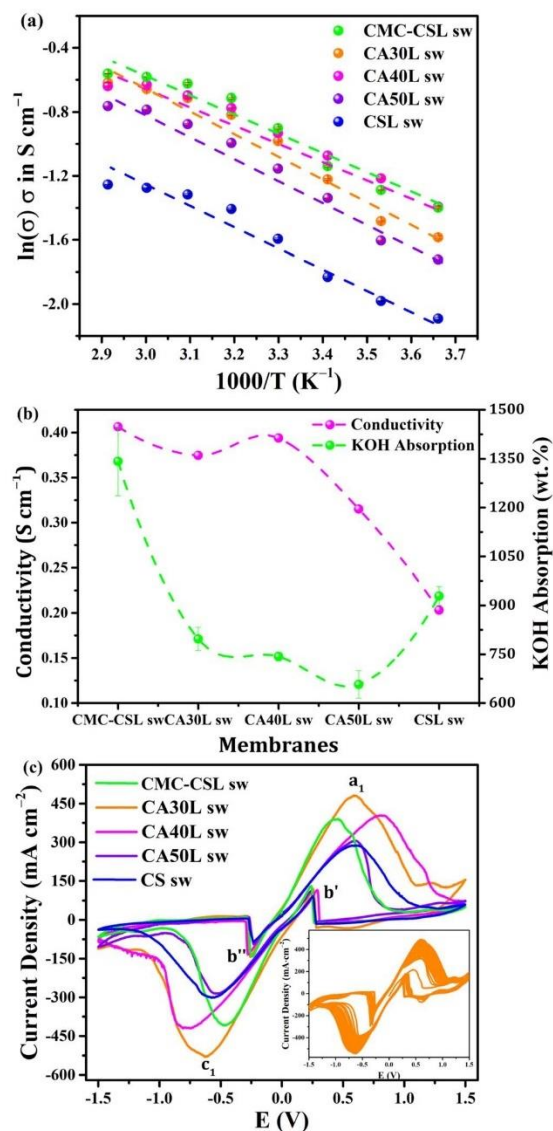


Figure 8. (a) Ionic conductivity of the CMC-CSL sw hydrogels at different temperatures. (b) Comparison between the ionic conductive values and swelling degree of the CMC-CSL sw hydrogels at different CA proportions. (c) Cyclic voltammograms of the swollen hydrogels at ambient temperature. Inset: 50 consecutive cycles of the CA30L sw hydrogels.

in the σ can also be explained in terms of the pores and channels generated by the physical crosslinking strategies since this obtained morphology provides paths for the ions to move more easily in the system.⁵² In alkaline systems, as the one proposed, it is known that OH^- is the specie that contributes to the ionic transport in the system. The pore sizes formed in the polymer matrix and the KOH concentration are the factors reported to be dependent on the anion transport.⁵³

The cyclic voltammetry (CV) technique was used to analyze the electrochemical stability of the membranes, with a potential sweep in the range $+1.5$ to -1.5 volts. Figure 8c compares the voltammograms registered for the swollen hydrogels, where CA30L sw

Table IV. Electrochemical properties and battery performance for the hydrated hydrogels.

Electrolyte	E_a (eV)	σ (S cm ⁻¹)	ΔE_p (V)	Bulk resistance (Ω)	Specific capacitance (mAh g ⁻¹)	Power density (mW cm ⁻²)
CMC-CSL sw	0.12	0.40	0.91	1.6	3.8	58
CA30L sw	0.13	0.37	1.21	1.5	1111	60
CA40L sw	0.10	0.39	1.59	2.0	1436	65
CA50L sw	0.13	0.32	1.14	1.4	1899	117

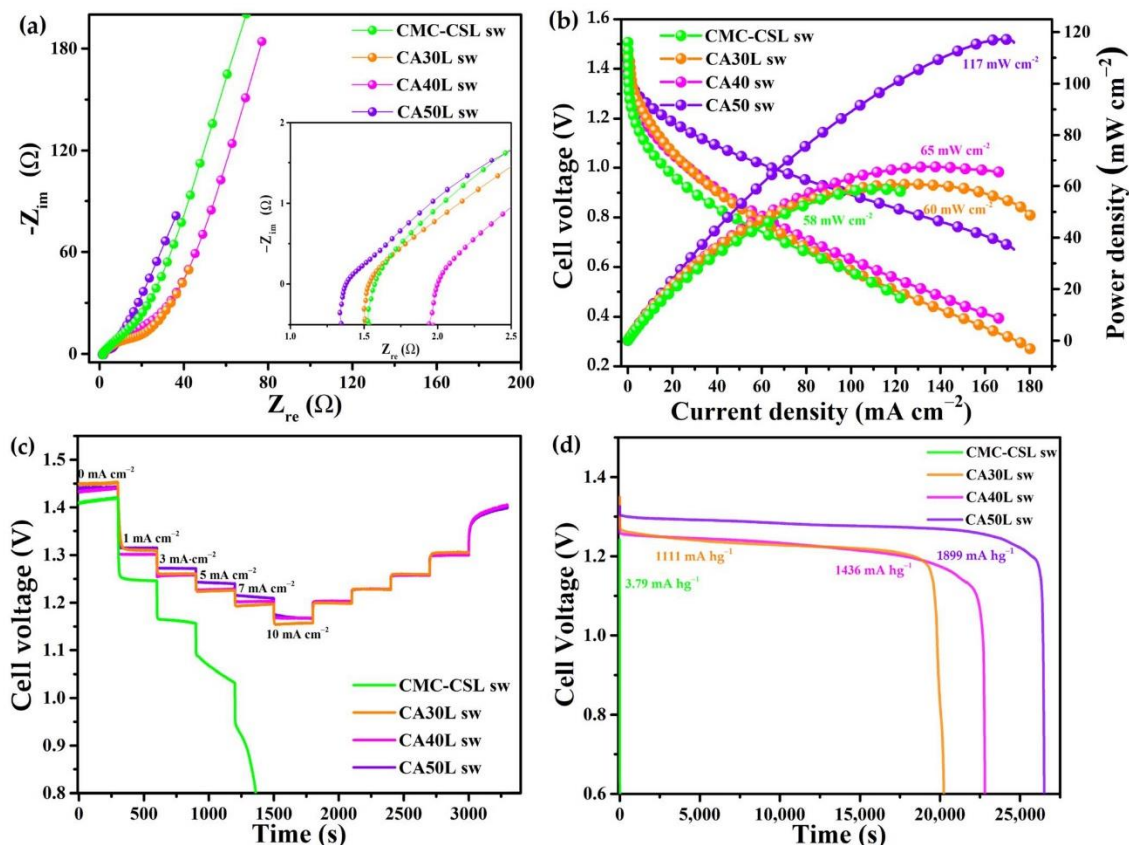


Figure 9. (a) Nyquist plot from PEIS studies (b) Polarization curves: discharge and power density profiles for the battery prototype and the synthesized hydrogels; (c) discharge tests at selected current densities; (C); (d) discharge curves at 3 mA cm⁻².

hydrogel presented the highest peak currents, with intensities higher than 450 mA cm⁻² obtained. The reference electrode was connected in short-circuit to the counter electrode, with a large separation of the peak potentials due to this configuration. The anodic peak (a_1) is related to the zinc oxidation to Zn²⁺ cations in alkaline media, with the formation of Zn(OH)₄²⁻, while the cathodic peak corresponded to the reduction process of this specie to solid Zn.^{54,55} The b' inverse peak in the cathodic branch has been previously reported to appear in the cathodic sweep due to the Zn oxidation after the dissolution of some of the passive film formed on the Zn's electrode surface, with the equivalent process in the anodic sweep for the peak b' .³⁶ The potential difference (ΔE_p) was calculated to be in the range of 0.91 V to 1.59 V for the CMC-CSL sw and CA40L sw hydrogels, respectively (Table IV). From the 50 consecutive cycles (inset Fig. 8c), stability was evidenced by the peaks' shape with a quasi-reversible behavior. This tendency confirmed that the hydrogels are capable of Zn dissolution into the membranes, an essential step for

the ions' mobility in battery applications, corroborating the applicability of the synthesized hydrogels in energy devices.

Battery prototype testing.—For practical applications, the swollen hydrogels were tested as electrolyte in a ZAB prototype. Figure 9a exhibits the Nyquist plots, obtaining bulk resistances (R_b) values in the range of 1.4 Ω to 2.0 Ω (inset), which suggests a good electrical contact between electrodes across the synthesized membranes. Concerning the polarization curves (Fig. 9b), it is possible to distinguish the superior performance displayed by CA50L sw membrane, since it reached a current and maximum power densities of 172 mA cm⁻² and 117 mW cm⁻², respectively. This superior performance obtained for the CA50L sw hydrogel could be explained by the higher chemical crosslinking degree achieved, and subsequent more density of functional groups in the structure of CA50L sw. The latter favors the intermolecular interactions with the liquid electrolyte, through the establishment of hydrogen bonds. These interactions lead to a greater stability of the

KOH solution in the polymer matrix, as discussed in the structural characterization section. Hence, this phenomenon is directly related to the higher ionic mass transport during the test process. Regarding the discharge at different demanded current densities (Fig. 9c), the CA50L sw electrolyte required the lowest overpotentials to deliver the fixed current, in addition to possessing an excellent recovery capability, because no significative changes were observed during the inverse process. Comparatively, the prototype with the CMC-CSL sw was only capable of supplying values of less than 7 mA cm^{-2} . Finally, the specific capacity test results are displayed in Fig. 9d, where the best result was obtained for the CA50L sw hydrogel with a capacitance of 1899 mAh g^{-1} . This value exceeded that reported for similar polymeric electrolyte systems. Poosapati et al.⁵⁶ obtained a maximum of 221.6 mAh g^{-1} for a gel-based polymer electrolyte composed of CS, polyvinyl alcohol (PVA) and KOH. The battery fabricated with the CMC-CSL sw hydrogel was not able to maintain performance during the discharge process. This collapse is attributed to the rapid formation of dendrites in this electrolyte (Fig. S1). It is suggested that these Zn dendrites were responsible for the early loss of the electrical connection with the Zn foil, leading to the early and severe loss of capacity of the prototype battery fabricated with the CMC-CSL sw membrane. In contrast, the CA-crosslinked membranes showed larger operation times, indicating their potential applicability in ZAB devices.

Conclusions

The design of a chemically and physically crosslinked CMC-CS hydrogel electrolyte doped with a 12 M KOH solution demonstrates its applicability of use in ZABs. The reticulation process was confirmed by ATR-FTIR, while the obtained XRD patterns pointed to the crystallinity changes that show the complexes formation between the K^+ cations and the polymer chains. SEM micrographs showed the porous morphology of the hydrogels and the appropriate complexation of the matrix with the doping salt. The hydrogel was fabricated with the proper combination of chemical and physical crosslinking techniques, resulting in a matrix with an enhanced ionic conductivity of 0.39 S cm^{-1} . The physical crosslinking achieved by the proposed freezing strategies is also enhancing the performance during the discharge process, attributed to the pores and channels generated, that contribute to the paths for the ions to be transported more easily. Arrhenius conduction mechanism was demonstrated from 0°C to 70°C . The high ionic transfer was confirmed by the CV studies, where the highest intensity peak of 480 mA cm^{-2} was obtained. A maximum power density of 117 mW cm^{-2} was achieved with the ZAB prototype assembled, besides a specific capacitance of 1899 mA h g^{-1} . These results demonstrate the potential of biopolymer hydrogels as electrolytes for green storage devices.

Acknowledgments

The authors gratefully thank the Mexican Council of Science and Technology for supporting this work through the project Ciencia de Frontera grant # CF-2019 39569 and to the Centro de Investigación en Materiales Avanzados S.C "CIMAV," for the financial support granted for the development of this research through project PI-22-05/2022 and grant# PI-23-10. Also, the authors are grateful for the technical support of PhD. Anabel de la Cruz from CIMAV. The authors are grateful for the suggestions during the writing process made by PhD. Vivian Morera Córdova of Yachay Tech University. The support of Andrew Nelson (English instructor at Yachay Tech University) is also appreciated. The authors are thankful to the School of Physical Sciences and Nanotechnology and the Grupo de Investigación Aplicada en Materiales y Procesos (GIAMP), Yachay Tech University for their collaboration through some of the necessary equipment for this research project.

ORCID

Juan P. Tafur  <https://orcid.org/0000-0002-8944-2723>

References

1. E. Davari and D. G. Ivey, *Sustain. Energy Fuels*, **2**, 39 (2017).
2. R. C. Agrawal and G. P. Pandey, *J. Phys. D: Appl. Phys.*, **41**, 223001 (2008).
3. F. Mo et al., *Batteries*, **8**, 59 (2022).
4. M. F. Bósquez-Cáceres, S. Hidalgo-Bonilla, V. M. Córdova, R. M. Mitchell, and J. P. Tafur, *Polymers (Basel)*, **13**, 4284 (2021).
5. S. Lorca, F. Santos, and A. J. Fernández Romero, *Polymers (Basel)*, **12**, 1 (2020).
6. M. Rayung et al., *Materials (Basel)*, **13**, 838 (2020).
7. N. Y. Bakar and M. I. N. Isa, *Res. J. Recent Sci.*, **3**, 74 (2014).
8. M. S. A. Rani, N. S. Mohamed, and M. I. N. Isa, *Int. J. Polym. Anal. Charact.*, **20**, 491 (2015).
9. M. F. Bósquez-Cáceres et al., *Batteries*, **8**, 265 (2022).
10. M. F. Akhtar, M. Hanif, and N. M. Ranjha, *Saudi Pharm. J.*, **24**, 554 (2016).
11. E. S. Dragan and M. V. Dinu, *React. Funct. Polym.*, **146**, 104372 (2020).
12. H. Zhang, F. Zhang, and J. Wu, *React. Funct. Polym.*, **73**, 923 (2013).
13. Y. Guan, J. Bian, F. Peng, X. M. Zhang, and R. C. Sun, *Carbohydr. Polym.*, **101**, 272 (2014).
14. M. T. Khorasani, A. Joorabloo, H. Adeli, Z. Mansoori-Moghadam, and A. Moghaddam, *Carbohydr. Polym.*, **207**, 542 (2018).
15. S. Noori, M. Kokabi, and Z. M. Hassan, *J. Appl. Polym. Sci.*, **135**, 46311 (2018).
16. M. T. Khorasani, A. Joorabloo, A. Moghaddam, H. Shamsi, and Z. Mansoori-Moghadam, *Int. J. Biol. Macromol.*, **114**, 1203 (2018).
17. L. Hu, R. He, Z. Lu, K. Zhang, and X. Bai, *RSC Adv.*, **9**, 9931 (2019).
18. G. Zhong et al., *Appl. Mater. Today*, **30**, 101705 (2023).
19. L. A. Calderón Salas, L. De Lima Eljuri, and M. Caetano Sousa, *Thesis*, Universidad de Investigación de Tecnología Experimental Yachay (Urcuqui) (2021).
20. H. Putz and K. Brandenburg, <https://crystalimpact.de/match>.
21. R. M. Michelle et al., *Macromolecules*, **42**, 6671 (2009).
22. R. B. Nuernberg, *Ionics (Kiel)*, **26**, 2405 (2020).
23. J. Béjar, L. Álvarez-Contreras, J. Ledesma-García, N. Arjona, and L. G. Arriaga, *J. Mater. Chem. A*, **8**, 8554 (2020).
24. J. Béjar et al., *Carbon N. Y.*, **204**, 411 (2023).
25. Y. Jampafuang, A. Tongta, and Y. Waiphib, *Polymers (Basel)*, **11**, 2010 (2019).
26. H. E. Salama, M. S. Abdel Aziz, and M. W. Sabaa, *Int. J. Biol. Macromol.*, **139**, 1162 (2019).
27. M. K. Jaiswal et al., *ACS Nano*, **10**, 246 (2016).
28. K. A. Uyanga, O. P. Okpozo, O. S. Onyekwere, and W. A. Daoud, *React. Funct. Polym.*, **154**, 104682 (2020).
29. K. A. Uyanga and W. A. Daoud, *Cellulose*, **28**, 5493 (2021).
30. A. A. Iles Velez et al., *Gels*, **7**, 256 (2021).
31. K. A. Uyanga and W. A. Daoud, *Int. J. Biol. Macromol.*, **181**, 1010 (2021).
32. Y. Zhang et al., *Chem. Eng. J.*, **353**, 225 (2018).
33. S. Benhanem, A. Chetouani, M. Elkolli, M. Bounekhel, and D. Benachour, *Biocybern. Biomed. Eng.*, **37**, 94 (2017).
34. C. Chang, A. Lue, and L. Zhang, *Macromol. Chem. Phys.*, **209**, 1266 (2008).
35. T. Seki et al., *J. Phys. Chem. Lett.*, **11**, 8459 (2020).
36. F. Santos, J. P. Tafur, J. Abad, and A. J. Fernández Romero, *J. Electroanal. Chem.*, **850**, 113380 (2019).
37. A. Autissier, C. Le Visage, C. Pouzet, F. Chaubet, and D. Letourneur, *Acta Biomater.*, **6**, 3640 (2010).
38. T. Fekete, J. Borsa, E. Takács, and L. Wojnárovits, *Radiat. Phys. Chem.*, **124**, 135 (2016).
39. E. Szymańska and K. Winnicka, *Mar. Drugs*, **13**, 1819 (2015).
40. M. D. Torres, R. Moreira, F. Chenlo, and M. J. Vázquez, *Carbohydr. Polym.*, **89**, 592 (2012).
41. M. Wu et al., *Matter*, **5**, 3402 (2022).
42. K. Dharmalingam and R. Anandalakshmi, *Int. J. Biol. Macromol.*, **134**, 815 (2019).
43. I. Farinha and F. Freitas, *Handb. Chitin Chitosan*, **3**, 43 (2020).
44. L. Song, F. Liu, C. Zhu, and A. Li, *Chem. Eng. J.*, **369**, 641 (2019).
45. K. Wang et al., *J. Food Sci. Technol.*, **56**, 5396 (2019).
46. G. Dlubek, D. Kilburn, and M. A. Alam, *Electrochim. Acta*, **49**, 5241 (2004).
47. S. B. Aziz, T. J. Woo, M. F. Z. Kadir, and H. M. Ahmed, *J. Sci. Adv. Mater. Devices*, **3**, 1 (2018).
48. M. Petrowsky and R. Frech, *J. Phys. Chem. B*, **114**, 8600 (2010).
49. T. Xu et al., *Energy Storage Mater.*, **48**, 244 (2022).
50. C.-L. Hung, M. Chen, M. I. H. Sohaimy, and M. I. N. Isa, *Polymers (Basel)*, **14**, 3019 (2022).
51. K. Jayalakshmi et al., *J. Phys. Chem. Solids*, **173**, 111119 (2023).
52. L. Cao et al., *Chem. Soc. Rev.*, **46**, 6725 (2017).
53. K. N. Grew and W. K. S. Chiu, *J. Electrochem. Soc.*, **157**, B327 (2010).
54. X. Liu et al., *Adv. Mater.*, **33**, 2006461 (2021).
55. J. Abad et al., *J. Power Sources*, **363**, 199 (2017).
56. A. Poosapati et al., *J. Appl. Polym. Sci.*, **138**, 50813 (2021).

Enhancing Electrochemical Performance of Zinc-Air Batteries using Freeze Crosslinked Carboxymethylcellulose- Chitosan Hydrogels as Electrolytes

María Fernanda Bósquez-Cáceres,^{1,*} José Bejar,² Lorena Álvarez-Contreras,² and Juan P. Tafur^{1,z}

¹ *Grupo de Investigación Aplicada en Materiales y Procesos (GLAMP), School of Chemical Sciences & Engineering, Yachay Tech University, Urcuquí 100115, Ecuador. Email: jtafur@yachaytech.edu.ec*

² *Centro de Investigación en Materiales Avanzados S.C. (CIMAV), Miguel de Cervantes No. 120, Complejo Industrial Chihuahua, Chihuahua 31136, México*

^zE-mail: jtafur@yachaytech.edu.ec

*Electrochemical Society Student Member

Table S1. Hydrogel names used in this work for different biopolymer compositions.

Electrolyte	Hydrogel Code
CMC90/CS30	CMC-CSL
CMC90/CS30/CA30	CA30L
CMC90/CS30/CA40	CA40L
CMC90/CS30/CA50	CA50L
CMC90/CS30 'sw'	CMC-CSL sw
CMC90/CS30/CA30 'sw'	CA30L sw
CMC90/CS30/CA40 'sw'	CA40L sw
CMC90/CS30/CA50 'sw'	CA50L sw

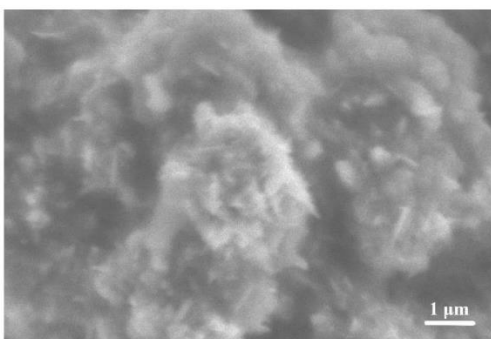


Figure S1. SEM image of the CMC-CSL sw in the cathode-facing side after discharging the Zinc-air battery.

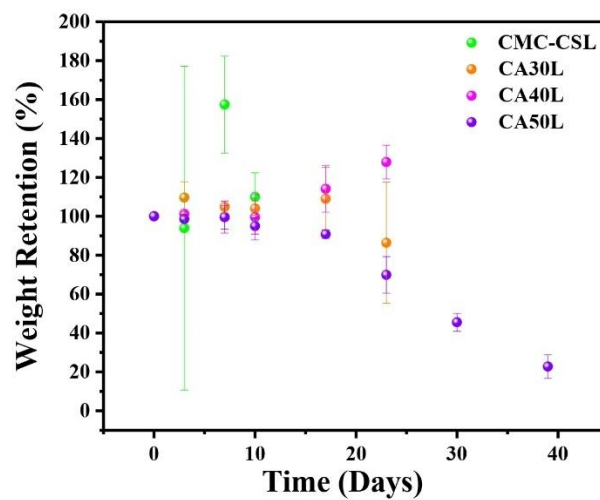


Fig. S2 Biodegradation results for the dried hydrogels in composted soil. Weight retention in the samples as a function of exposure time.

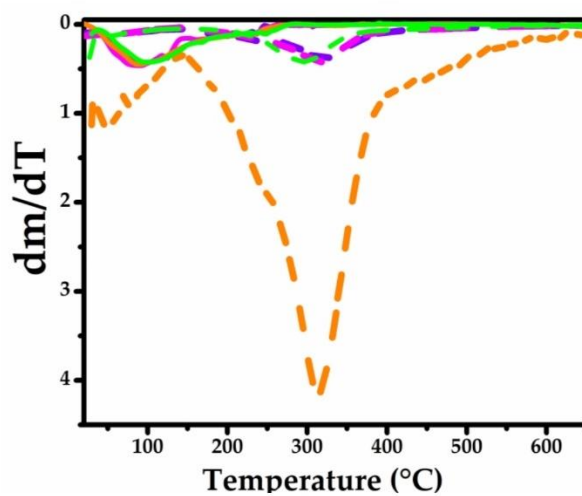


Fig. S3 DTGA curves of the hydrogel electrolytes.

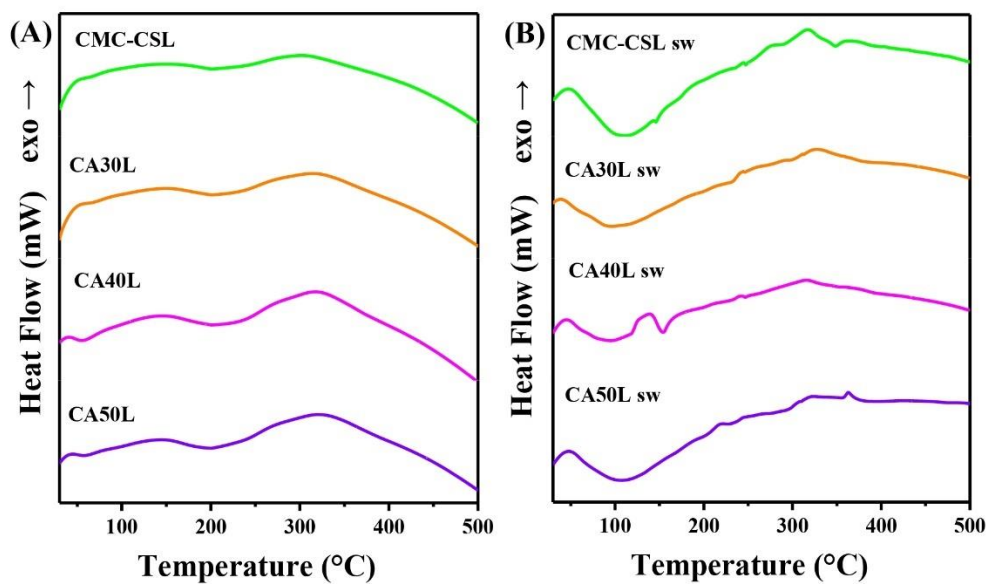


Fig. S4 DSC curves for (A) dried hydrogels and (B) swollen hydrogels.

3. Conclusions

Once the results of the work carried out in this project have been presented, this chapter will be devoted to the main conclusions that can be drawn from each of the articles that make up this thesis. In general, it can be concluded that several polymeric hydrogel systems were successfully developed, designed, and prepared using CMC and CS biopolymers, through different crosslinking strategies and doping of the medium with 12 M KOH solutions. The resulting materials have demonstrated adequate structural and thermal properties. In addition, they have obtained remarkable ionic conductivity values and current intensities, which point to their possible application in zinc-air batteries.

- I. From the first work, which reviewed the state-of-the-art publications on NCPEs for zinc and magnesium batteries, the following conclusions can be drawn:
 - In general, for polymer electrolyte systems, the addition of nanoparticles (ZnO, MgO, TiO₂, Al₂O₃, SnO₂) has been proved to enhance the electrical conductivity by, in the least of the cases, one order of magnitude. Not only conductivity is improved, but cationic species' electrochemical properties, mechanical strength, and transport properties are.
 - The improved electrochemical results in terms of ionic conductivity obtained for PEs along with the addition of nanofillers, provoke a space-charge region, understood by the existence of free electrons at the surface of the nanocomposite, facilitating the new kinetic path for ionic transport and polymer segmental motion. This mechanism ensures the electrolyte is capable of ion transference.
 - Improved high ionic conductivity and better thermal and mechanical stability compared to liquid electrolyte systems have been confirmed. Moreover, when a specific percentage of nanofiller is reached, a decrease in ionic conductivity is observed. Excessive fillers could provoke this in the NCPE that may trigger the formation of ion pairs and ion aggregation, such as the non-conducting phase presented as an electrically inert component blocking ion transport.
 - When deciding which state is better for the electrolyte, between making it a solid or a gel, it is paramount to consider the device's application. Gel polymer electrolytes have been shown to be capable of being employed in conditions where flexibility is well appreciated. However, they currently rely on mobile liquid phases to perform the conduction process, and the current ones present concerns in terms of safety and stability. Consequently, the search for more benign and environmentally friendly mobile liquids is a current issue to increase the expectation of developing batteries based on sustainable components.

- In terms of the biopolymer electrolytes, they have shown comparable ion conduction and electrochemical properties compared to the traditional synthetic polymer electrolytes. However, the state-of-the-art is still lacking in terms of the development of NCPEs based on biopolymers. The few investigations overviewed so far set a precedent for the demand for further research with this specific approach.
- II. Regarding the second article, which reported the synthesis and characterization of hydrogels based on CMC, CS, and different amounts of CA, dried by the conventional solution casting technique, the following remarks can be stated:
- The esterification reaction / chemical crosslinking approach for the CMC-CS-CA hydrogels was achieved through the synthesis proposed in this work, confirmed by the ATR-FTIR analysis. The modification of the chemical structure in the polymer system was evaluated, and conformational changes were presented along with a decrease in the crystallinity degree of the membranes.
 - The swelling degree of the CA-free hydrogel obtained a higher value than its counterparts with citric acid. Nevertheless, this higher capacity came along with low structural integrity when used in battery assemblies.
 - In terms of the electrochemical characterization, Arrhenius behavior was confirmed in the range of 0 to 60 °C for the crosslinked membranes, suggesting the thermal stability and operability of the electrolytes when these temperature ranges are required.
 - A maximum ionic conductivity value of $0.19 \text{ S}\cdot\text{cm}^{-1}$ was found at 30 °C. Moreover, the cyclic voltammetry studies confirmed a quasi-reversible behavior, with maximum intensity peaks of $360 \text{ mA}\cdot\text{cm}^{-2}$, as evidence of the high ionic transfer achieved by the designed hydrogels.
 - The battery prototype tests showed a high performance in terms of power densities, bulk resistances, and discharge times., A maximum specific capacity of $1026 \text{ mA}\cdot\text{h g}^{-1}$ for the battery assembled with the CA50 sw electrolyte was obtained, pointing to adequate performance in order to apply the proposed material in energy storage devices.
- III. In the third work, it was presented a modification of the synthesis conducted in the second article, performing five freeze-thawing cycles, followed by a final freeze-drying process. The following are the main conclusions highlighted from this publication:
- The design and characterization of a chemically and physically crosslinked CMC-CS hydrogel electrolyte doped with a 12 M KOH solution demonstrate its superior performance and further applicability of use in zinc-air batteries.

- The proposed crosslinking processes were confirmed by the ATR-FTIR studies, while the obtained XRD patterns pointed to the crystallinity changes that show the complexes formation between the K^+ cations and the polymer chains.
- A crucial effect of the modification in this work was evidenced by the SEM micrographs, where a highly porous morphology indicates the obtention of the desired effect of the drying strategy in the matrix of the membranes.
- The drying strategies were proved to used play a significant role in the pore size and shape of the membranes. The obtained morphology was related to the more KOH solution absorption capability of the hydrogels, with the expanding of the pores in the matrix.
- The swelling behavior was greatly enhanced, with the hydrogels being capable of absorbing six-seven times their own weight, while their casting-dried counterparts were able to retain two times their weight.
- Arrhenius conduction mechanism was demonstrated from 0 °C to 70 °C, suggesting an even superior thermal stability. The electrolyte exhibited an enhanced ionic conductivity of $0.39 \text{ S}\cdot\text{cm}^{-1}$.
- A maximum power density of $117 \text{ mW}\cdot\text{cm}^{-2}$ was achieved with the zinc-air prototype assembled, besides a specific capacity of $1899 \text{ mA}\cdot\text{h g}^{-1}$. These results demonstrate the potential of biopolymer hydrogels with appropriate synthesis approaches as promising electrolytes for green storage devices.

4. References

- (1) Jaschin, P. W.; Gao, Y.; Li, Y.; Bo, S. H. A Materials Perspective on Magnesium-Ion-Based Solid-State Electrolytes. *J. Mater. Chem. A* **2020**, *8* (6), 2875–2897. <https://doi.org/10.1039/c9ta11729f>.
- (2) Qiu, L.; Xiang, W.; Tian, W.; Xu, C. L.; Li, Y. C.; Wu, Z. G.; Chen, T. R.; Jia, K.; Wang, D.; He, F. R.; Guo, X. D. Polyanion and Cation Co-Doping Stabilized Ni-Rich Ni–Co–Al Material as Cathode with Enhanced Electrochemical Performance for Li-Ion Battery. *Nano Energy* **2019**, *63*, 103818. <https://doi.org/10.1016/j.nanoen.2019.06.014>.
- (3) Xu, Y. Di; Xiang, W.; Wu, Z. G.; Xu, C. L.; Li, Y. C.; Guo, X. D.; Lv, G. P.; Peng, X.; Zhong, B. H. Improving Cycling Performance and Rate Capability of Ni-Rich LiNi_{0.8}Co_{0.1}Mn_{0.1}O₂ Cathode Materials by Li₄Ti₅O₁₂ Coating. *Electrochim. Acta* **2018**, *268*, 358–365. <https://doi.org/10.1016/j.electacta.2018.02.049>.
- (4) Etacheri, V.; Marom, R.; Elazari, R.; Salitra, G.; Aurbach, D. Challenges in the Development of Advanced Li-Ion Batteries: A Review. *Energy Environ. Sci.* **2011**, *4* (9), 3243–3262. <https://doi.org/10.1039/c1ee01598b>.
- (5) Wang, Y.; Yi, J.; Xia, Y. Recent Progress in Aqueous Lithium-Ion Batteries. *Adv. Energy Mater.* **2012**, *2* (7), 830–840. <https://doi.org/10.1002/aenm.201200065>.
- (6) Kim, H.; Hong, J.; Park, K. Y.; Kim, H.; Kim, S. W.; Kang, K. Aqueous Rechargeable Li and Na Ion Batteries. *Chem. Rev.* **2014**, *114* (23), 11788–11827. <https://doi.org/10.1021/cr500232y>.
- (7) Wu, K.; Huang, J.; Yi, J.; Liu, X.; Liu, Y.; Wang, Y.; Zhang, J.; Xia, Y. Recent Advances in Polymer Electrolytes for Zinc Ion Batteries: Mechanisms, Properties, and Perspectives. *Adv. Energy Mater.* **2020**, *10* (12), 1903977. <https://doi.org/10.1002/aenm.201903977>.
- (8) He, W.; Zuo, S.; Xu, X.; Zeng, L.; Liu, L.; Zhao, W.; Liu, J. Challenges and Strategies of Zinc Anode for Aqueous Zinc-Ion Batteries. *Mater. Chem. Front.* **2021**, *5* (5), 2201–2217. <https://doi.org/10.1039/d0qm00693a>.
- (9) Ye, T.; Li, L.; Zhang, Y. Recent Progress in Solid Electrolytes for Energy Storage Devices. *Adv. Funct. Mater.* **2020**, *30* (29), 1–20. <https://doi.org/10.1002/adfm.202000077>.
- (10) Zhao, C.; Liu, L.; Qi, X.; Lu, Y.; Wu, F.; Zhao, J.; Yu, Y.; Hu, Y. S.; Chen, L. Solid-State Sodium Batteries. *Adv. Energy Mater.* **2018**, *8* (17), 1703012. <https://doi.org/10.1002/aenm.201703012>.
- (11) Wu, F.; Yuan, Y. X.; Cheng, X. B.; Bai, Y.; Li, Y.; Wu, C.; Zhang, Q. Perspectives for Restraining Harsh Lithium Dendrite Growth: Towards Robust Lithium Metal Anodes. *Energy Storage Mater.* **2018**, *15*, 148–170. <https://doi.org/10.1016/j.ensm.2018.03.024>.
- (12) Wood, K. N.; Kazyak, E.; Chadwick, A. F.; Chen, K.-H.; Zhang, J.-G.; Thornton, K.; Dasgupta, N. P. Dendrites and Pits: Untangling the Complex Behavior of Li Metal Anodes through Operando Video Microscopy. *ECS Meet. Abstr.* **2017**, *MA2017-01* (5), 518. <https://doi.org/10.1149/ma2017-01/5/518>.
- (13) Zhang, H.; Li, C.; Piszcz, M.; Coya, E.; Rojo, T.; Rodriguez-Martinez, L. M.; Armand, M.; Zhou, Z. Single Lithium-Ion Conducting Solid Polymer Electrolytes: Advances and Perspectives. *Chem. Soc. Rev.* **2017**, *46* (3), 797–815. <https://doi.org/10.1039/c6cs00491a>.
- (14) Hallinan, D. T.; Villaluenga, I.; Balsara, N. P. Polymer and Composite Electrolytes. *MRS Bull.* **2018**, *43* (10), 775–781. <https://doi.org/10.1557/mrs.2018.212>.
- (15) Mindemark, J.; Lacey, M. J.; Bowden, T.; Brandell, D. Beyond PEO—Alternative Host Materials for Li⁺-Conducting Solid Polymer Electrolytes. *Prog. Polym. Sci.* **2018**, *81*, 114–143. <https://doi.org/10.1016/j.progpolymsci.2017.12.004>.
- (16) Kundu, D.; Adams, B. D.; Duffort, V.; Vajargah, S. H.; Nazar, L. F. A High-Capacity and Long-Life Aqueous Rechargeable Zinc Battery Using a Metal Oxide Intercalation Cathode. *Nat. Energy* **2016**, *1* (10), 16119. <https://doi.org/10.1038/nenergy.2016.119>.
- (17) Pan, H.; Shao, Y.; Yan, P.; Cheng, Y.; Han, K. S.; Nie, Z.; Wang, C.; Yang, J.; Li, X.; Bhattacharya, P.; Mueller, K. T.; Liu, J. Reversible Aqueous Zinc/Manganese Oxide Energy

- Storage from Conversion Reactions. *Nat. Energy* **2016**, *1* (5), 16039. <https://doi.org/10.1038/nenergy.2016.39>.
- (18) Liu, F.; Chen, Z.; Fang, G.; Wang, Z.; Cai, Y.; Tang, B.; Zhou, J.; Liang, S. V2O5 Nanospheres with Mixed Vanadium Valences as High Electrochemically Active Aqueous Zinc-Ion Battery Cathode. *Nano-Micro Lett.* **2019**, *11* (1), 1–11. <https://doi.org/10.1007/s40820-019-0256-2>.
 - (19) Deivanayagam, R.; Ingram, B. J.; Shahbazian-Yassar, R. Progress in Development of Electrolytes for Magnesium Batteries. *Energy Storage Mater.* **2019**, *21*, 136–153. <https://doi.org/10.1016/j.ensm.2019.05.028>.
 - (20) Wang, F.; Borodin, O.; Gao, T.; Fan, X.; Sun, W.; Han, F.; Faraone, A.; Dura, J. A.; Xu, K.; Wang, C. Highly Reversible Zinc Metal Anode for Aqueous Batteries. *Nat. Mater.* **2018**, *17* (6), 543–549. <https://doi.org/10.1038/s41563-018-0063-z>.
 - (21) Boaretto, N.; Meabe, L.; Martinez-Ibañez, M.; Armand, M.; Zhang, H. Review—Polymer Electrolytes for Rechargeable Batteries: From Nanocomposite to Nanohybrid. *J. Electrochem. Soc.* **2020**, *167* (7), 070524. <https://doi.org/10.1149/1945-7111/ab7221>.
 - (22) Fang, G.; Zhu, C.; Chen, M.; Zhou, J.; Tang, B.; Cao, X.; Zheng, X.; Pan, A.; Liang, S. Suppressing Manganese Dissolution in Potassium Manganate with Rich Oxygen Defects Engaged High-Energy-Density and Durable Aqueous Zinc-Ion Battery. *Adv. Funct. Mater.* **2019**, *29* (15). <https://doi.org/10.1002/adfm.201808375>.
 - (23) Peter, S.; Lyczko, N.; Gopakumar, D.; Maria, H. J.; Nzihou, A.; Thomas, S. Chitin and Chitosan Based Composites for Energy and Environmental Applications: A Review. *Waste Biomass Valorization* **2020**, *129* **2020**, *12* (9), 4777–4804. <https://doi.org/10.1007/S12649-020-01244-6>.
 - (24) Muhmed, S. A.; Nor, N. A. M.; Jaafar, J.; Ismail, A. F.; Othman, M. H. D.; Rahman, M. A.; Aziz, F.; Yusof, N. Emerging Chitosan and Cellulose Green Materials for Ion Exchange Membrane Fuel Cell: A Review. *Energy, Ecol. Environ.* **2019**, *52* **2019**, *5* (2), 85–107. <https://doi.org/10.1007/S40974-019-00127-4>.
 - (25) Yahya, M. Z. A.; Arof, A. K. Effect of Oleic Acid Plasticizer on Chitosan-Lithium Acetate Solid Polymer Electrolytes. *Eur. Polym. J.* **2003**, *39* (5), 897–902. [https://doi.org/10.1016/S0014-3057\(02\)00355-5](https://doi.org/10.1016/S0014-3057(02)00355-5).
 - (26) Yang, R.; Li, H.; Huang, M.; Yang, H.; Li, A. A Review on Chitosan-Based Flocculants and Their Applications in Water Treatment. *Water Res.* **2016**, *95*, 59–89. <https://doi.org/10.1016/j.watres.2016.02.068>.
 - (27) Mohamed, N. S.; Subban, R. H. Y.; Arof, A. K. Polymer Batteries Fabricated from Lithium Complexed Acetylated Chitosan. *J. Power Sources* **1995**, *56* (2), 153–156. [https://doi.org/10.1016/0378-7753\(95\)80027-E](https://doi.org/10.1016/0378-7753(95)80027-E).
 - (28) Saberi Riseh, R.; Gholizadeh Vazvani, M.; Hassanisaadi, M.; Skorik, Y. A. Micro-/Nano-Carboxymethyl Cellulose as a Promising Biopolymer with Prospects in the Agriculture Sector: A Review. *Polymers (Basel)*. **2023**, *15* (2), 440. <https://doi.org/10.3390/POLYM15020440>.
 - (29) Rosca, C.; Popa, M. I.; Lisa, G.; Chitanu, G. C. Interaction of Chitosan with Natural or Synthetic Anionic Polyelectrolytes. 1. The Chitosan-Carboxymethylcellulose Complex. *Carbohydr. Polym.* **2005**, *62*, 35–41. <https://doi.org/10.1016/j.carbpol.2005.07.004>.
 - (30) Shang, J.; Shao, Z.; Chen, X. Electrical Behavior of a Natural Polyelectrolyte Hydrogel: Chitosan/Carboxymethylcellulose Hydrogel. *Biomacromolecules* **2008**, *9* (4), 1208–1213. <https://doi.org/10.1021/bm701204j>.
 - (31) Bratskaya, S.; Privar, Y.; Nesterov, D.; Modin, E.; Kodess, M.; Slobodyuk, A.; Marinin, D.; Pestov, A. Chitosan Gels and Cryogels Cross-Linked with Diglycidyl Ethers of Ethylene Glycol and Polyethylene Glycol in Acidic Media. *Biomacromolecules* **2019**, *20* (4), 1635–1643. <https://doi.org/10.1021/ACS.BIOMAC.8B01817>.
 - (32) Mittal, H.; Ray, S. S.; Kaith, B. S.; Bhatia, J. K.; Sukriti; Sharma, J.; Alhassan, S. M. Recent Progress in the Structural Modification of Chitosan for Applications in Diversified Biomedical Fields. *Eur. Polym. J.* **2018**, *109*, 402–434. <https://doi.org/10.1016/J.EURPOLYMJ.2018.10.013>.
 - (33) Thakur, V. K.; Thakur, M. K. Recent Advances in Graft Copolymerization and Applications of

- Chitosan: A Review. *ACS Sustain. Chem. Eng.* **2014**, 2 (12), 2637–2652. <https://doi.org/10.1021/SC500634P>.
- (34) Uyanga, K. A.; Daoud, W. A. Carboxymethyl Cellulose-Chitosan Composite Hydrogel: Modelling and Experimental Study of the Effect of Composition on Microstructure and Swelling Response. *Int. J. Biol. Macromol.* **2021**, 181, 1010–1022. <https://doi.org/10.1016/J.IJBIOMAC.2021.04.117>.
 - (35) Akhtar, M. F.; Hanif, M.; Ranjha, N. M. Methods of Synthesis of Hydrogels ... A Review. *Saudi Pharm. J.* **2016**, 24 (5), 554–559. <https://doi.org/10.1016/J.JSPS.2015.03.022>.
 - (36) Dragan, E. S.; Dinu, M. V. Advances in Porous Chitosan-Based Composite Hydrogels: Synthesis and Applications. *React. Funct. Polym.* **2020**, 146, 104372. <https://doi.org/10.1016/J.REACTFUNCTPOLYM.2019.104372>.
 - (37) Zhang, H.; Zhang, F.; Wu, J. Physically Crosslinked Hydrogels from Polysaccharides Prepared by Freeze–Thaw Technique. *React. Funct. Polym.* **2013**, 73 (7), 923–928. <https://doi.org/10.1016/J.REACTFUNCTPOLYM.2012.12.014>.
 - (38) Guan, Y.; Bian, J.; Peng, F.; Zhang, X. M.; Sun, R. C. High Strength of Hemicelluloses Based Hydrogels by Freeze/Thaw Technique. *Carbohydr. Polym.* **2014**, 101 (1), 272–280. <https://doi.org/10.1016/J.CARBPOL.2013.08.085>.
 - (39) Khorasani, M. T.; Joorabloo, A.; Adeli, H.; Mansoori-Moghadam, Z.; Moghaddam, A. Design and Optimization of Process Parameters of Polyvinyl (Alcohol)/ Chitosan/Nano Zinc Oxide Hydrogels as Wound Healing Materials. *Carbohydr. Polym.* **2018**, 207, 542–554. <https://doi.org/10.1016/j.carbpol.2018.12.021>.
 - (40) Noori, S.; Kokabi, M.; Hassan, Z. M. Poly(Vinyl Alcohol)/Chitosan/Honey/Clay Responsive Nanocomposite Hydrogel Wound Dressing. *J. Appl. Polym. Sci.* **2018**, 135 (21), 46311. <https://doi.org/10.1002/APP.46311>.
 - (41) Khorasani, M. T.; Joorabloo, A.; Moghaddam, A.; Shamsi, H.; MansooriMoghadam, Z. Incorporation of ZnO Nanoparticles into Heparinised Polyvinyl Alcohol/Chitosan Hydrogels for Wound Dressing Application. *Int. J. Biol. Macromol.* **2018**, 114, 1203–1215. <https://doi.org/10.1016/J.IJBIOMAC.2018.04.010>.
 - (42) Maitra, J.; Shukla, V. K.; Kumar Shukla, V. Cross-Linking in Hydrogels-a Review. *Am. J. Polym. Sci.* **2014**, 2014 (2), 25–31. <https://doi.org/10.5923/j.ajps.20140402.01>.

5. Appendixes

5.1. Notifications of acceptance of the articles.

5.1.1. Article published in the Journal *Polymers*

[Polymers] Manuscript ID: polymers-1486469 - Accepted for Publication

1 message

Polymers Editorial Office <polymers@mdpi.com> Sun, Nov 28, 2021 at 4:19 AM
Reply-To: Logan Sheng <logan.sheng@mdpi.com>, Polymers Editorial Office <polymers@mdpi.com>
To: Juan Pablo Tafur <jtafur@yachaytech.edu.ec>
Cc: "M. Fernanda Bósquez-Cáceres" <maria.bosquez@yachaytech.edu.ec>, Sandra Hidalgo-Bonilla <sahidalgo@yachaytech.edu.ec>, Vivian Morera Córdova <vmorera@yachaytech.edu.ec>, "Rose M. Michell" <rmichell@yachaytech.edu.ec>, Polymers Editorial Office <polymers@mdpi.com>, Logan Sheng <logan.sheng@mdpi.com>

Dear Dr. Tafur,

Congratulations on the acceptance of your manuscript, and thank you for your interest in submitting your work to *Polymers*:

Manuscript ID: polymers-1486469
Type of manuscript: Review
Title: Nanocomposite Polymer Electrolytes for Zinc and Magnesium Batteries: from synthetic to biopolymers
Authors: M. Fernanda Bósquez-Cáceres, Sandra Hidalgo-Bonilla, Vivian Morera Córdova, Rose M. Michell, Juan P. Tafur *
Received: 14 November 2021
E-mails: maria.bosquez@yachaytech.edu.ec, sahidalgo@yachaytech.edu.ec, vmorera@yachaytech.edu.ec, rmichell@yachaytech.edu.ec, jtafur@yachaytech.edu.ec
Submitted to section: Polymer Composites and Nanocomposites, https://www.mdpi.com/journal/polymers/sections/polymer_composites_nanocomposites
Advanced Polymer Nanocomposites II
https://www.mdpi.com/journal/polymers/special_issues/Advanced_Polymer_NanocompositesII
https://susy.mdpi.com/user/manuscripts/review_info/6f2b765bee6274f708fb3c4798eb0877

We will now edit and finalize your paper, which will then be returned to you for your approval. Within the next couple of days, an invoice concerning the article processing charge (APC) for publication in this open access journal will be sent by email from the Editorial Office in Basel, Switzerland.

If, however, extensive English edits are required to your manuscript, we will need to return the paper requesting improvements throughout.

We encourage you to set up your profile at SciProfiles.com, MDPI's researcher network platform. Articles you publish with MDPI will be linked to your SciProfiles page, where colleagues and peers will be able to see all of your publications, citations, as well as other academic contributions.

We also invite you to contribute to Encyclopedia (<https://encyclopedia.pub>), a scholarly platform providing accurate information about the latest research results. You can adapt parts of your paper to provide valuable reference information, via Encyclopedia, for others both within the field and beyond.

Kind regards,
Ms. Claire Zhang
Section Managing Editor
of Section "Polymer Physics and Theory"
Polymers Editorial Office

5.1.2. Article published in the Journal *Batteries*

[Batteries] Manuscript ID: batteries-2011018 - Accepted for Publication

Batteries Editorial Office <batteries@mdpi.com>

Fri, Nov 25, 2022 at 1:59 AM

Reply-To: Andy Wu <andy.wu@mdpi.com>, Batteries Editorial Office <batteries@mdpi.com>

To: Lorena Alvarez-Contreras <lorena.alvarez@cimav.edu.mx>

Cc: María Fernanda Bósquez-Cáceres <maria.bosquez@yachaytech.edu.ec>, Lola de Lima <ldelima@yachaytech.edu.ec>, Vivian Morera Córdova <vmorera@yachaytech.edu.ec>, "Anabel D. Delgado" <anabel.delacruz@cimav.edu.mx>, José Béjar <eduardo.garcia@cimav.edu.mx>, Noé Arjona <wvelazquez@cidetec.mx>, "Juan P. Tafur" <jtafur@yachaytech.edu.ec>, Batteries Editorial Office <batteries@mdpi.com>, Andy Wu <andy.wu@mdpi.com>

Dear Dr. Álvarez-Contreras,

Congratulations on the acceptance of your manuscript, and thank you for submitting your work to Batteries:

Manuscript ID: batteries-2011018

Type of manuscript: Article

Title: Chitosan-Carboxymethylcellulose Hydrogels as Electrolytes for Zinc-Air Batteries: An Approach to the Transition Towards Renewable Energy Storage Devices

Authors: María Fernanda Bósquez-Cáceres, Lola de Lima, Vivian Morera Córdova, Anabel D. Delgado, José Béjar, Noé Arjona, Lorena Álvarez-Contreras *, Juan P. Tafur *

Received: 20 October 2022

E-mails: maria.bosquez@yachaytech.edu.ec, ldelima@yachaytech.edu.ec, vmorera@yachaytech.edu.ec, anabel.delacruz@cimav.edu.mx, eduardo.garcia@cimav.edu.mx, wvelazquez@cidetec.mx, lorena.alvarez@cimav.edu.mx, jtafur@yachaytech.edu.ec

Submitted to section: Battery Materials and Interfaces: Anode, Cathode, Separators and Electrolytes or Others,

https://www.mdpi.com/journal/batteries/sections/battery_materials_and_interfaces_anode_cathode_separators_and_electrolytes_or_others

Zn-Ion and Zn–Air Batteries: Materials, Mechanisms and Applications

https://www.mdpi.com/journal/batteries/special_issues/Zn_Batteries_Materials_Mechanisms_Applications

https://susy.mdpi.com/user/manuscripts/review_info/5f631d55c3c1f9f2152563f380f15a7f

We will now edit and finalize your paper, which will then be returned to you for your approval. Within the next couple of days, an invoice concerning the article processing charge (APC) for publication in this open access journal will be sent by email from the Editorial Office in Basel, Switzerland.

If, however, extensive English edits are required to your manuscript, we will need to return the paper requesting improvements throughout.

We encourage you to set up your profile at SciProfiles.com, MDPI's researcher network platform. Articles you publish with MDPI will be linked to your SciProfiles page, where colleagues and peers will be able to see all of your publications, citations, as well as other academic contributions.

We also invite you to contribute to Encyclopedia (<https://encyclopedia.pub>), a scholarly platform providing accurate information about the latest research results. You can adapt parts of your paper to provide valuable reference information, via Encyclopedia, for others both within the field and beyond.

Kind regards,

Mr. Andy Wu

E-Mail: andy.wu@mdpi.com

5.1.3. Article published in the *Journal of the Electrochemical Society*

Fwd: Journal of The Electrochemical Society - Decision on Manuscript ID JES-109865.R1

1 message

Juan Pablo Tafur Guisao <jtafur@yachaytech.edu.ec>
To: María Fernanda Bósquez Cáceres <maria.bosquez@yachaytech.edu.ec>

Mon, May 29, 2023 at 11:29 AM

----- Forwarded message -----

De: **Scott Donne** <onbehalf@manuscriptcentral.com>
Date: mié, 24 may 2023 a las 15:14
Subject: Journal of The Electrochemical Society - Decision on Manuscript ID JES-109865.R1
To: <jtafur@yachaytech.edu.ec>, <tafur8652@gmail.com>
Cc: <scott.donne@newcastle.edu.au>

24-May-2023

Dear Dr. Tafur:

We have checked the manuscript record for your paper entitled "Enhancing Electrochemical Performance of Zinc-Air Batteries Using Freeze Crosslinked Carboxymethylcellulose-Chitosan Hydrogels as Electrolytes" and have confirmed that everything required to publish the paper in the Journal of The Electrochemical Society is in place.

Thank you for your fine contribution. On behalf of the Editors of the Journal of The Electrochemical Society, we look forward to your continued contributions to the Journal.

Sincerely,

andrea guenzel
Journal of The Electrochemical Society
publications@electrochem.org

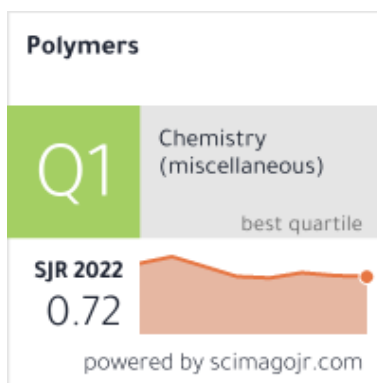
5.2. Impact Factors of Publications

- Article published in the Journal *Polymers*

Bósquez-Cáceres, M. F.; Hidalgo-Bonilla, S.; Córdova, V. M.; Michell, R. M.; Tafur, J. P. Nanocomposite Polymer Electrolytes for Zinc and Magnesium Batteries: From Synthetic to Biopolymers. *Polymers (Basel)*. **2021**, *13* (24), 4284.
<https://doi.org/doi.org/10.3390/polym13244284>.

Impact Factor: 4.967 (2021)

Citescore: 5.7

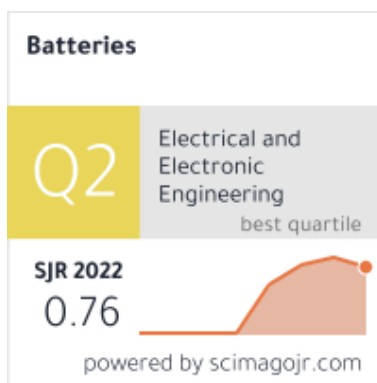


- Article published in the Journal *Batteries*

Bósquez-Cáceres, M. F.; De Lima, L.; Morera Córdova, V.; Delgado, A. D.; Béjar, J.; Arjona, N.; Álvarez-Contreras, L.; Tafur, J. P. Chitosan-Carboxymethylcellulose Hydrogels as Electrolytes for Zinc-Air Batteries: An Approach to the Transition towards Renewable Energy Storage Devices. *Batteries* **2022**, 8 (12), 265. <https://doi.org/10.3390/batteries8120265>.

Impact Factor: 5.938 (2021)

Citescore: 7.9



- Article published in the *Journal of the Electrochemical Society*

Bósquez-Cáceres, M. F.; Béjar, J.; Álvarez-Contreras, L.; Tafur, J. P. Enhancing Electrochemical Performance of Zinc-Air Batteries using Freeze Crosslinked Chitosan-Carboxymethylcellulose Hydrogels as Electrolytes. *J. Electrochem. Soc.* **2023**, 170, 060502. <https://doi.org/10.1149/1945-7111/acd876>

Impact Factor: 4.386 (2021)

Citescore: 6.6

